ROBUST AND ADAPTIVE LATERAL CONTROLLER FOR AUTONOMOUS VEHICLES

by

LUBNA S. KHASAWNEH

A dissertation submitted in partial fulfillment of the
requirements for the degree of

DOCTOR OF PHILOSOPHY IN SYSTEMS ENGINEERING

2022

Oakland University
Rochester, Michigan

Doctoral Advisory Committee:

Manohar Das, Ph.D., Chair
Ka C Cheok, Ph.D.
Meir Shilor, Ph.D.
Guangzhi, Ph.D.

to my mother and father (God rest their souls)

ACKNOWLEDGMENTS

I would like to express sincere thanks to my advisor, Prof. Manohar Das for his continuous support and insightful guidance while conducting the research presented in this thesis. I also would like to thank Prof. Ka C Cheok for his invaluable courses, resources and lecture notes that contributed a lot, not just to this research, but also to all my accomplishments in my career in the automotive industry. Further, I would like to thank Prof. Meir Shillor for his insightful advice, continuous support, and serving on my qualifying examination and defense committee. I also would like to thank Prof. Guangzhi Qu for his support and interest in my research and serving as committee member. I would like to thank Prof. Robert Loh, as I am indebted to him for all his advice and knowledge, he has inspired me more than I can write in simple words. Finaly, I would like to thank my husband and my kids for their support.

Lubna S Khasawneh

ABSTRACT

ROBUST AND ADAPTIVE LATERAL CONTROLLER FOR AUTONOMOUS VEHICLES

by

LUBNA S KHASAWNEH

Adviser: Manohar Das, Ph.D.

This thesis addresses the problem of controlling the lateral motion of an autonomous vehicle in the presence of parametric uncertainties, disturbances, and hard nonlinearities in the steering system, such as backlash in gears, stiction, hysteresis, and dead zones. The lateral motion of an autonomous vehicle is controlled by two cascaded controllers, the trajectory tracking controller and the steering angle controller. This thesis focuses on the development of both controllers using robust and adaptive control techniques.

Two control strategies are developed to control the electric power steering angle, sliding mode control and adaptive backstepping control. The limitation of sliding mode control is first addressed, which is the chattering phenomena, and then a proposed methodology is presented to solve it using variable gain sliding mode control. Self-aligning moment acts as disturbance on the steering system that the controller has to compensate for. A model-based approach to estimate it is first developed and its limitations are addressed, which is tire parameters dependemce. Two other approaches

are then developed to overcome these limitations, the first one is a sliding mode observer, and the second one is part of a backstepping controller.

Two approaches are developed to control the vehicle lateral trajectory, non-adaptive backstepping and adaptive backstepping. The extended matching design procedure is used in the adaptive backstepping controller to avoid the overestimation problem. Road curvature must be accurately known by the controller to follow the planned trajectory. It is usually measured by a camera, but the quality of the measurement is affected by environmental factors. An adaptive law is developed to estimate the road curvature online as part of an adaptive backstepping controller. Two feedforward approaches are presented to compensate for road curvature, one is derived from steady state vehicle lateral dynamics, and another is based on estimating the transfer function dynamics from road curvature to steering angle.

Road bank angle is a significant disturbance in vehicle lateral control systems. A vehicle lateral state and disturbance observer is developed to estimate the road bank angle and the vehicle side slip angle, which are expensive to measure in current road vehicles, using extended Kalman filter. The observer combines a dynamical vehicle model with two measurements from inexpensive sensors.

TABLE OF CONTENTS

TABLE OF CONTENTS—Continued

LIST OF FIGURES

LIST OF ABBREVIATIONS

ADAS	Advanced Driver Assistant Systems
AV	Autonomous Vehicles
SC	Software Component
EP	Environmental Perception
EM	Environmental Mapping
MP	Motion Planning
EPS	Electric Power Steering
TTC	Trajectory Tracking Controller
HCL	High Level Controller
LLC	Low Level Controller
SAC	Steering Angle Controller
SMC	Sliding Mode Control
KF	Kalman Filter
EKF	Extended Kalman Filter
GPS	Global Positioning System
INS	Inertial Navigation System
IMU	Inertial Measurement Unit
RLS	Recursive Least Squares
BS	Backstepping
ABS	Adaptive Backstepping
STC	Steering Torque Controller

LIST OF ABBREVIATIONS-Continued

FG	Fixed Gain
VG	Variable Gain
LQR	Linear Quaderatic Regulator
MPC	Model Predective Control
CG	Center of Gravity

CHAPTER ONE

INTRODUCTION

¶
¶
¶

1.1 Driver Assistance Systems and Autonomous Vehicles

Vehicle automation and active safety systems have gained increased research interest in the last two decades. Many advances in advanced driver assistant systems (ADAS) and active safety systems have been developed and introduced by the automotive industry, such as lane departure warning, lane keeping assist, yaw stability control, adaptive cruise control, evasive steering assist, and much more. Considering that most fatal crashes are due to human errors, these systems have the potential to remove human error and save lives of drivers, passengers, pedestrians, and bicyclists. In addition, these systems can improve efficiency, convenience, and mobility. By combining these systems, automotive manufacturers are developing self-driving cars, also called Autonomous Vehicles (AV).

Autonomous Vehicles can drive themselves with little or no human driver intervention (depending on the level of autonomy). The basic driving task of an autonomous vehicle can be divided into four subtasks. We are going to represent those subtasks by a modular software architecture, as illustrated in Figure 1.1. The basic software architecture of an AV consists of four main software components. The first Software Component (SC) is the Environmental Perception (EP) which forms the first step in performing the driving task. The car observes the environment around it using a variety of sensors (camera, lidar, radar, ultrasonic) and passes the raw sensor measurements to the EP module, which is dedicated to understanding the environment around the car. The EP module has two key responsibilities, the first one is localization, which is identifying the current vehicle position in space (position, velocity, acceleration, orientation) based on sensor measurements, such as GPS/IMU and wheel odometry. The second responsibility of the EP module is locating and classifying static and dynamic objects of the environment for the driving task, such as lane markings, other cars, pedestrians, traffic lights, road signs, curbs.

The second SC is the Environmental Mapping (EM), which creates a set of maps to locate objects in the environment around the AV for a range of different uses, such as collision avoidance and ego motion localization. Environmental maps provide several representations of the current environment around the autonomous vehicle. There are three types of maps: 1) Occupancy grid map, which is a map of all static objects in the environment surrounding the vehicle, 2) Localization map, which is used by the localization SC to improve the ego state estimation, 3) Detailed road map, which provides a map of road segments that represent the driving environment that the vehicle is driving through, and captures signs and lane markings in a manner that can be used for motion planning.

The third SC is the Motion Planning (MP), which makes the decision about what action to take and where to drive. It combines the outputs of the EP and the environmental mapping to create a safe, efficient, and comfortable path through the environment that moves the AV toward its goal. The MP module can be decomposed into three layers, 1) Mission planner, 2) Behavioral planner, 3) Local planner. The mission planner handles long term planning by defining the mission over the entire horizon of the driving task, from the current location to the destination. The behavior planner handles short term planning by establishing safe maneuvers to be executed while traveling along the mission path. It also provides a set of constraints to execute with each action. An example of a behavior planner decision is whether it is safe to make a lane change given the desired speed and the predicted behavior of the vehicles in the adjacent lanes. The local planner performs immediate or reactive planning. It is responsible for providing a safe and smooth path and velocity profile for a short period of time, given the behavior constraints from the behavior planner and the vehicle operating limits.

The fourth SC is the motion controller which takes the planned trajectory and turns it into actuation commands for the vehicle to apply. The control problem is separated into longitudinal control and lateral control. The longitudinal controller controls the longitudinal distance, longitudinal velocity, and longitudinal acceleration of the vehicle by actuating the engine and the brake. The lateral controller controls the lateral position, lateral velocity, and lateral acceleration of the vehicle by actuating the steering system. The focus of this thesis is on the lateral control of the vehicle.

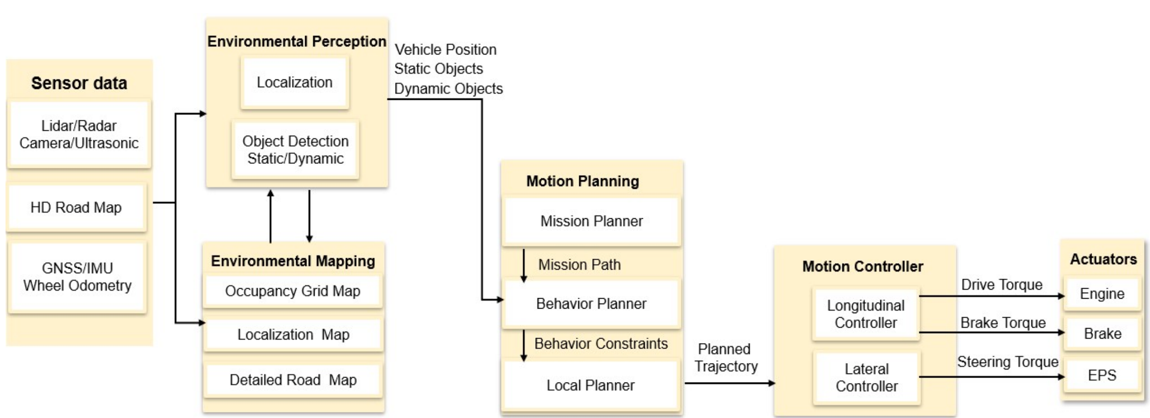

Figure 0.1 Software architecture components of self-driving cars

1.2 Vehicle Lateral Motion Controller

Since the focus of this thesis is on the lateral motion controller, we are going to describe it in more details in this section. The lateral motion controller has two levels as illustrated in Figure 1.2, the High-Level Controller (HLC), which communicates directly with the motion planner, and the Low-Level Controller (LLC) which communicates directly with the steering actuator. The steering of a vehicle is actuated by the Electric Power Steering (EPS). The HLC is the lateral Trajectory Tracking Controller (TTC), which takes in the lateral deviation and the heading angle deviation of the vehicle from the planned trajectory, and the road curvature from the motion planner to compute the steering angle required to correct the deviations of the vehicle from the desired trajectory and follow the curvature of the road. The desired steering angle is sent to the LLC, which is the Steering Angle Controller (SAC). The SAC computes the steering torque required to achieve the desired angle and actuate the EPS. This thesis focuses on the development of both controllers, the TTC and SAC.

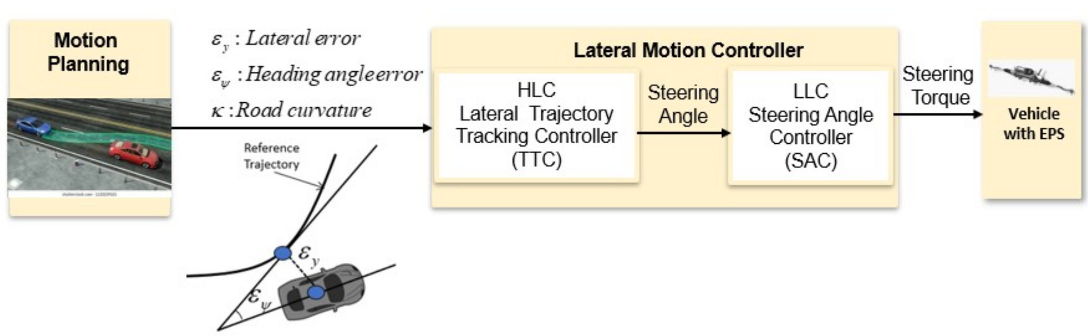

Figure 0.2 General lateral control block diagram.

1.3 Robust Control

Model imprecision can have strong adverse impact on the behavior of control systems. Therefore, these imprecisions should be addressed explicitly by any practical control design. Model imprecision can be caused by actual uncertainties in the plant such as unknown plant parameters or by simplifying the representation of the system by linearizing it or reducing its order. In general, modelling inaccuracies can be classified into two major kinds [1]: 1) structured uncertainties which corresponds to inaccuracies in the system parameters, such as inertia, damping, and friction of a mechanical system, 2) unstructured uncertainties which corresponds to unmodeled dynamics, linearization, and underestimation of a system order. One of the major approaches to dealing with model imprecision is “robust control”. A simple approach to robust control is Sliding Mode Control (SMC). SMC has been extensively studied and used in many applications due to its simplicity, tracking capabilities and robustness against parameter variations and disturbances. The typical structure of a sliding mode controller consists of a nominal part, which is simply an inverse control law, and an additional discontinuous part whose purpose is to deal with model inaccuracy and disturbances. However, this discontinuous part of the control law leads to undesired system vibrations called chattering as illustrated in figure 1.3 [1]. Chattering is undesirable in applications and might further excite high frequency dynamics that was ignored in the system modeling stage and should be eliminated to achieve smooth control performance. Several methods were investigated in the litreture to mitigate this problem. In [1] chattering was reduced by smoothing out the control discontinuity in a thin boundary layer neighboring the switching surface. This results in tracking to within a guaranteed precision rather than perfect tracking and limits the controller bandwidth. Higher-order sliding modes can mitigate the chattering effect by confining the switching control to the higher derivatives of the mechanical control variable [2]-[11]. The limitation of this approach is that it requires the existence of time derivatives of the sliding variable. This requirement could be a practical limitation in the presence of noise. In this thesis, we develop a SAC that mitigates chattering by Variable Gain (VG) SMC as will be explained in details in chapter 4.

It is worth mentioning that chattering can be acceptable in specific applications where the control input is voltage rather than mechanical force or acceleration as outlined in [1], such as control of electric motors, provided it is beyond the high frequency range of the dynamics neglected in the stage of modeling. In this case, pure SMC, without altering the control law to avoid chattering, can be extremely high-performance option.

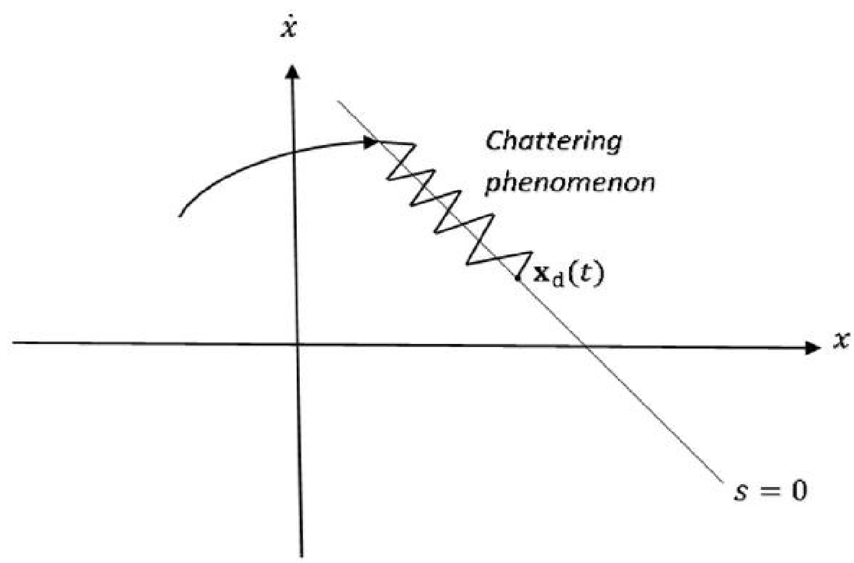

Figure 0.3 Chattering phenomenon

1.4 Adaptive Control

A second approach to dealing with model inaccuracies is Adaptive control. Adaptive control is different from ordinary control in that it has the ability to control plants with parameter uncertainties during its operation. Plant parameters may experience unpredictable variations during the control operation. Without continuous retuning or redesign of the controller parameters, the initially designed or tuned controller may not be able to control the changing plant as well as it used to initially. The objective of adaptive control is to maintain consistent behavior of the system in the presence of uncertainties or unpredictable variation in the system parameters. An adaptive controller is designed by combining a control law with a parameter estimator to estimate the unknown plant parameters. The parameters of the controller are updated during the operation of the plant. Adaptive control methods can be classified as direct and indirect. In direct adaptive control, the updated parameters are the controller parameters. In indirect adaptive control, the updated parameters are the plant parameters. Adaptive control methods can also be classified as Lyapunov-based and estimation-based [12]. In the Lyapunov-based method, the parameter estimator is part of the controller module, whereas in the estimation-based method, the parameter estimator is independent of the control module. Gradient and least squares optimization algorithms are usually used for the estimation-based method. Estimation-based adaptive control relies on the “certainty equivalence” principal [13]-[19], which means that the controller can stabilize the plant when all the parameters are known. In this thesis, adaptive backstepping method is developed for lateral control, which is considered indirect, Lyapunov-based adaptive control method based on the above classifications.

Thesis Contributions

- Development and implementation of two control strategies to control the EPS angle under model imprecision and disturbances.
    - The first approach is VG SMC, which was experimentally validated in a test vehicle to solve the problems below:
        - Significantly reduced the chattering produced by Fixed Gain (FG) SMC without affecting the tracking capability and the robustness of the controller.
        - Eliminated the need for gain scheduling because the controller automatically adjusts its gains based on the error size.
        - The controller was able to overcome the asymmetrical hysteresis behavior caused by the static friction and the backlash in gears, which is usually challenging to overcome by other methods.
    - The second approach is adaptive backstepping. This approch assumes no a priori information about the steering model mechanical parameters. Adaptive laws are developed to adjust these parameters online. Also in this approach, adaptive laws are developed to estimate the disturbances caused by self-aligning moment and static friction.
- Development of a sliding mode observer to estimate the steering model state vector and disturbances.
- Development of three approaches to estimate the self-aligning moment.
    - The first approach is model based, which depends on the relationship between lateral forces and tire slip angle. This approach also depends on tire

parameters that represent shape, stiffness, peak, and curvature, respectively. These parameters are functions of tire normal forces, and eight coefficients whose values depend on the tire type and characteristics. The dependency of these coefficients on the tire type makes this approach impractical because if the tires of the vehicle are changed to a diffrent type, this will require replacing the coefficients in the code with those of the new tire type.

  - The second approach is a sliding mode observer, which treats the self-aligning moment as disturbance and estimates it without dependency on the tire parameters. This approach is a modular design because the observer is a separate module from the controller design.
  - The third approach is part of an adaptive BS controller, which also treats the self-aligning moment as disturbance and develops adaptive laws to estimate it online with no required information about tire parameters. This approach is a non modular design because the adaptive law is part of the controller module.

- Development of a control strategy for trajectory tracking in autonomous vehicles using the adaptive backstepping method. The controller consists of a feedback control law and adaptive laws to estimate the vehicle parameters as well as the road curvature. The adaptive law for the road curvature estimation is developed using the extended matching design to avoid overparameterization. In addition, two feed forward approaches are developed to compensate for road curvature. The first one uses the steady state lateral vehicle dynamics, and the second one is based on estimating the transfer function dynamics from road curvature to road wheel steering angle based on real time data.

- Development and implementation of a lateral vehicle state and disturbance observer using EKF to estimate the vehicle sideslip angle and the road bank angle disturbance. The observer combines a vehicle dynamical model with two sensor measurements, lateral acceleration and yaw rate.

Dissertation Outline

- In chapter 2, a model of vehicle lateral dynamics is described in section 2.1, followed by development of a lateral state and disturbance observer to estimate the vehicle body sideslip angle and road bank angle disturbance in section 2.2, and then experimental validation of the observer performance in chapter 2.3.
- In chapter 3, a steering model for the electric power steering is described in section 3.2. An EPS model parameter identification algorithm is developed in section 3.2.1, followed by experimental results of the parameter identification algorithm in section 3.2.2. In section 3.3, a model based self-aligning moment estimation algorithm is designed and experimentally validated.
- In chapter 4, the steering angle controllers are derived. In section 4.2, the sliding mode controller (SMC) and the sliding mode observer are derived, followed by simulation and experimental result. In section 4.3, the adaptive backstepping steering angle controller is derived followed by simulation results.
- In chapter 5, the trajectory tracking controllers (TTCs) are developed. In section 5.2, a TTC is designed using the non-adaptive backstepping approach, and a feedforward is designed using steady state vehicle lateral dynamics. In section 5.3, a TTC is designed using the adaptive backstepping approach, and a

feedforward is designed by estimating the transfer function dynamics from road curvature to road wheel steering angle.

CHAPTER TWO

VEHICLE TIRE MODEL AND LATERAL STATE ESTIMATION

Tires provide the necessary lateral forces to change the direction of a vehicle. These forces result from the deformation of the tire at the contact patch during cornering events. During straight driving maneuvers, in the absence of lateral forces, the velocity vector of a rolling tire is in the direction of the plane of the wheel; whereas during cornering maneuvers, the tire contact patch slips to the side while the tire is rolling and the resulting velocity vector is no longer in the direction of the wheel plane. The angle between the velocity vector of the wheel and the wheel plane is called “slip angle”. The side slip of the tire generates a lateral force that acts not exactly at the contact patch, but at a distance from it, called “pneumatic trail”. This results in a moment that tends to realign the wheel in the direction of rolling. At normal cornering manauvers, the resulting lateral force is small, which results in a small lateral tire slip angle, usually does not exceed about 4 degrees. In this case, lateral forces are proportional to slip angle and the proportionality constant is called the Cornering stiffeness, in units of force/degree. In this region of the tire behavior, the vehicle lateral motion can be well described by a linear model, referred to as “single track model” or “bycicle model”. This model will be described in details in section 2.1.

At large slip angles, lateral force increases and reaches a maximum as the tire begins to slide, until it reaches a constant level. In this case, we enter the nonlinear region of the tire and lateral forces will not only depend on slip angle, but also will depend on normal tire load, tire road friction coefficient, and longitudinal tire force. The bicycle model is no longer valid in this case and we need a more complicated tire model that takes into account the effect of these variables. There exist several tire models that describe the full range of the tire behavior beyond the linear region, such as Pacejka, Fiala and Dugoff models. In this thesis, we are considering the linear bicycle model since our operational design domain is normal highway driving where the cornering manauvers are normal and the tire slip angle is small. In the next section, we are going to describe the bycicle vehicle model in details.

2.1 Model of Vehicle Lateral Motion

The dynamical bicycle model in terms of yaw rate and body side slip angle [20] is considered for the development of the lateral control. In the bicycle model, the left and right front wheels are represented by one single front wheel and similarly the left and right rear wheels are represented by one central rear wheel. The model is illustrated in Figure 2.1. The vehicle body side slip angle β is defined as the angle between the longitudinal axis of the vehicle and the orientation of the vehicle longitudinal velocity vector v at the Center of Gravity (CG). It is important to distinguish between the vehicle body side slip angle and the tire slip angle, which is defined as the angle between the direction of the velocity vector of the wheel and the wheel plane. The yaw rate $\dot{\psi}$ is the rate of change of the vehicle yaw angle. The vehicle yaw angle ψ is measured with respect to the global X axis. The lateral dynamics of the vehicle are controlled by the front wheel steering angle δ. The longitudinal velocity of the vehicle v is assumed to be constant.

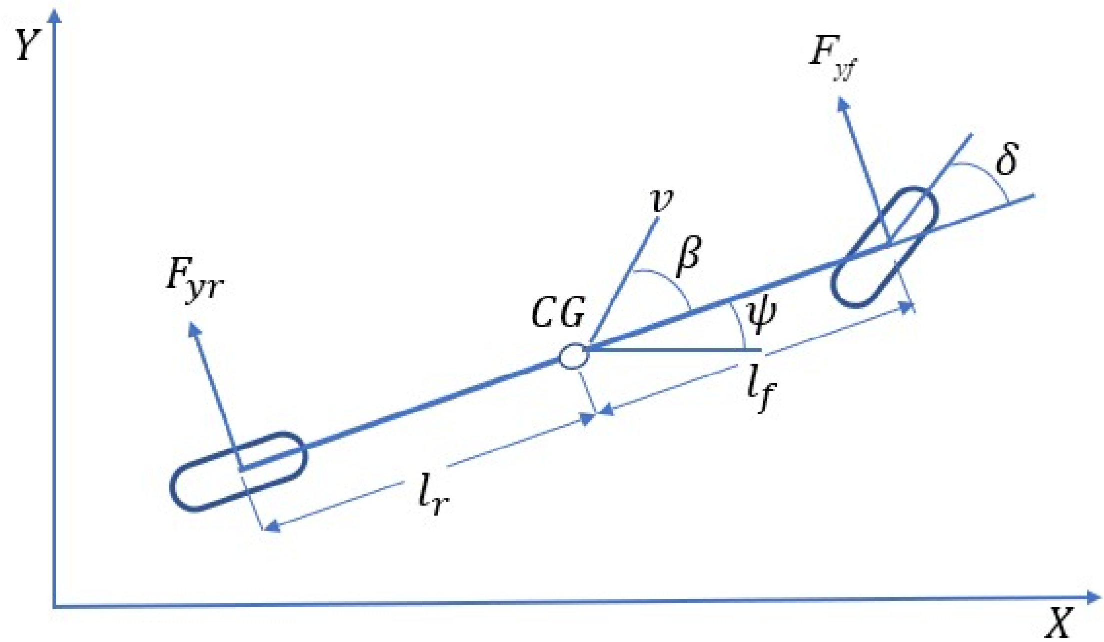

Figure 0.1 Bicycle model for vehicle lateral dynamics.

Applying Newton second law of motion along the Y axis yields the differential equation,

$$ma_y = F_{yf} + F_{yr} \tag{2.1}$$

where F_{yf}, F_{yr} are the lateral forces acting on the front and rear wheels respectively, m is the mass of the vehicle, and a_y is the lateral acceleration of the vehicle.

$$a_y = v(\dot{\beta} + \dot{\psi}) \tag{2.2}$$

Substituting (2.2) in (2.1) yields,

$$mv(\dot{\beta} + \dot{\psi}) = F_{yf} + F_{yr} \tag{2.3}$$

Taking the moment balance about the Z axis yields the differential equation for the yaw dynamics,

$$I_z\ddot{\psi} = l_f F_{yf} - l_r F_{yr} \tag{2.4}$$

where l_f, l_r are the distances from the center of gravity of the vehicle (CG) to the front and rear tires, respectively and I_z is the moment of inertia about the Z axis.

For small tire slip angles, the lateral tire forces can be approximated as a linear function of tire slip angle as,

$$F_{yf} = C_f \alpha_f \tag{2.5}$$

$$F_{yr} = C_r \alpha_r \tag{2.6}$$

where C_f, C_r are the cornering stiffness at the front and rear tires, respectively, and α_f, α_r are the slip angles of the front and rear tires, respectively.

The front and rear tire slip angles are related to the bicycle model states (β and $\dot{\psi}$) as,

$$\alpha_f = \delta - \beta - \frac{l_f\dot{\psi}}{v} \tag{2.7}$$

$$\alpha_r = -\beta + \frac{l_r\dot{\psi}}{v} \tag{2.8}$$

Substituting (2.7) in (2.5) and then (2.5) in (2.3) and (2.4), and substituting (2.8) in (2.6) and then (2.6) in (2.3) and (2.4) yields,

$$\dot{\beta} = \frac{a_{11}}{v}\beta + \left(\frac{a_{12}}{v^2} - 1\right)\dot{\psi} + \frac{b_1}{v}\delta \tag{2.9}$$

$$\ddot{\psi} = a_{21}\beta + \frac{a_{22}}{v}\dot{\psi} + b_2\delta \tag{2.10}$$

where,

$$a_{11} = -\frac{\left(C_r + C_f\right)}{m} \qquad a_{12} = \frac{C_r l_r - C_f l_f}{m} \qquad b_1 = \frac{C_f}{m}$$

$$a_{21} = \frac{C_r l_r - C_f l_f}{I_z} \qquad a_{22} = -\frac{C_r l_r^{\,2} + C_f l_f^{\,2}}{I_z} \qquad b_2 = \frac{C_f l_f}{I_z}$$

The state space representation of the model is given by

$$\begin{bmatrix} \dot{\beta} \\ \ddot{\psi} \end{bmatrix} = \begin{bmatrix} \frac{a_{11}}{v} & \frac{a_{12}}{v^2} - 1 \\ a_{21} & \frac{a_{22}}{v} \end{bmatrix} \begin{bmatrix} \beta \\ \dot{\psi} \end{bmatrix} + \begin{bmatrix} \frac{b_1}{v} \\ b_2 \end{bmatrix} \delta \tag{2.11}$$

where $\left[\beta \quad \dot{\psi}\right]'$ is the state vector and δ is the control input.

2.2 Vehicle Lateral State and Road Bank Angle Estimation

Yaw rate and body side slip angle together completely describe a vehicle's motion in the road plane. While yaw rate feedback alone is enough for most active steering systems in normal driving conditions, it is not enough for vehicle stability control systems such as, rollover prevention and yaw stability control, especially on low-friction road surfaces. In this case, Side slip angle feedback is very important to control it from becoming too large. Side slip angle is used in this research in a model-based estimation of the self-aligning moment estimation, as explained in details in section 3.2.

Road bank angle can significantly deteriorate the behavior of automatic steering control systems, as well as vehicle stability control systems. Providing real-time information about road bank angle helps such control systems to maintain a consistent and stable behavior. Both road bank angle and side slip angle are too expensive to measure in current vehicle systems. In this section, a state and disturbance observer is designed to estimate the road bank angle disturbance along with the vehicle lateral state (side slip angle and yaw rate) using Extended Kalman filter. The observer combines the dynamical vehicle single track model in terms of side slip angle and yaw rate with two sensor measurements, lateral acceleration and yaw rate, taking into account the influence of road bank angle on lateral acceleration measurement.

Global Positioning System (GPS) combined with inertial measurement unit methods for estimating road bank angle and side slip angle are widely used, as in [21]-[25]. The limitation of GPS-based methods in general is that they are unreliable in urban driving environments where tall buildings and urban canyons can prevent access to GPS satellite signals and that leads to faulty estimates that could cause instability in control systems that are using these estimates. Another disadvantage of the GPS-inertial measurement unit-based methods is that the inertial sensors often have to be of very high quality in order to obtain a reasonable drift-free estimates. High quality inertial measurement units are extremely expensive to be used in current road vehicles. In [26], lateral disturbance estimator for side wind force and road bank angle is developed using the linear Kalman Filter (KF). The two degrees of freedom linear bicycle vehicle model is used. This model is linear assuming the longitudinal speed of the vehicle is constant, but in reality, it is constantly changing in highway driving, which requires tuning KF separately for each speed in the speed range (usually 0-130kph) and then construct look up tables for Kalman gains based on speed, which is a time-consuming process. In our method, we are also using the same model, but we assum that the longitudinal speed is varying and we treat it as a third state, which makes the model no longer linear. We linearize the model using the first order Taylor series expansion and then we use (EKF) instead of KF. This avoids the time-consuming tuning process of the Kalman gains for different speeds, and eliminates the need for look up tables. Also, in [26], the measurement model consists of the self-aligning torque estimate and the yaw rate measurement. An accurate estimate of self-aligning torque requires estimating lateral forces, normal forces, tire slip angle, mechanical trail, and pneumatic trail first. Also, self-aligning torque estimation is tire parameters dependent, which means that if we change the tire type in the vehicle, we must change the parameters in the estimator, which is impractical. In our approach, we are fusing the lateral acceleration measurement with the yaw rate measurement. Both measurements can be easily obtained from onboard vehicle inexpensive sensors. In [27] and [28], the recursive least squares (RLS) method is used to estimate the road bank angle with other variables. The disadvantage of RLS is its reliance on a persistent excitation input signal, if the input signals to the estimator are not dynamically persistent enough, the estimate will diverge. In [29], a plant-inverse based technique to estimate and compensate for the lateral disturbances is developed. This method treats the lateral disturbance as indeterministic, which means that the disturbance can be coming from any source, it does not distinguish what the disturbance is, which means there is no explicit estimate of road bank, which makes this method less versatile than methods that treat the disturbance as deterministic. In [30], A constrained dual Kalman filter for estimation of vehicle parameters and road bank angle is developed. In [31], yaw rate and roll rate are fused to estimate the bank angle and road grade. In [32], a proportional–integral H_∞ filter based on the game theory approach is developed for bank angle estimation. In [34], a multiple Model filter with two modes is introduced for estimating the vehicle yaw-rate, lateral velocity, road bank angle and crosswind force.

This section presents the development of an approach to estimate the vehicle side slip angle and road-bank angle in real time by combining lateral acceleration and yaw rate measurements from IMU with the dynamical single-track model. The single-track model is considered linear based on the assumption that the longitudinal speed is constant. In our method, we assume that the longitudinal speed is varying, not constant, which makes the model no longer linear because its equations are divided by longitudinal speed. The speed is considered as a third state that is updated at every time step. We linearize the model using Taylor series expansion and we use EKF for the estimation. This way, we avoid the time-consuming tuning process to come up with look up tables based on speed that has to be done if we assume the longitudinal speed is constant and use the linear Kalman filter. The developed estimation algorithm was validated by experimental results on a test vehicle. It was verified that the algorithm provides reliable road bank angle and slip angle estimation that can be potentially used in vehicle stability controllers.

2.2.1 Vehicle Lateral State and Road Bank Angle Observer Design

The vehicle model explained in section 2.1 is considered in the observer design as summarized in the differential equations (2.9) and (2.10) after modifying it by adding the road bank force dynamics.

Road bank angle affects the side slip angle dynamics, so (2.9) becomes

$$\dot{\beta} = \frac{a_{11}}{v}\beta + \left(\frac{a_{12}}{v^2} - 1\right)\dot{\psi} + \frac{1}{mv}F_b + \frac{b_1}{v}\delta \tag{2.12}$$

where, $F_b = mg\sin(\theta)$ is the road bank force and θ is the road bank angle.

The vehicle yaw dynamics are not influenced by the road bank force, hence (2.10) stays the same even in the presence of road bank force.

The resulting state space representation of the model with road bank angle consideration is given by,

$$\begin{bmatrix} \dot{\beta} \\ \ddot{\psi} \\ \dot{F}_b \end{bmatrix} = \begin{bmatrix} \frac{a_{11}}{v} & \frac{a_{12}}{v^2} - 1 & \frac{1}{mv} \\ a_{21} & \frac{a_{22}}{v} & 0 \\ 0 & 0 & 0 \end{bmatrix} \begin{bmatrix} \beta \\ \dot{\psi} \\ F_b \end{bmatrix} + \begin{bmatrix} \frac{b_1}{v} \\ b_2 \\ 0 \end{bmatrix} \delta \tag{2.13}$$

Since we are not assuming that the longitudinal speed v is constant, this makes the model no longer linear and has to be linearized.

The model is discretized for the EKF implementation and linearized using the first order Taylor series expansion as given below,

$$\begin{bmatrix} \beta_{k+1} \\ \dot{\psi}_{k+1} \\ v_{k+1} \\ F_{b_{k+1}} \end{bmatrix} = \begin{bmatrix} 1 & 0 & 0 & 0 \\ 0 & 1 & 0 & 0 \\ 0 & 0 & 1 & 0 \\ 0 & 0 & 0 & 1 \end{bmatrix} \begin{bmatrix} \beta_k \\ \dot{\psi}_k \\ v_k \\ F_{bk} \end{bmatrix} + T_s \begin{bmatrix} \frac{a_{11}}{v_k} & \frac{a_{12}}{v_k^2} - 1 & a_{13} & \frac{1}{mv_k} \\ a_{21} & \frac{a_{22}}{v_k} & -\frac{a_{22}}{v_k^2}\dot{\psi}_k & 0 \\ 0 & 0 & 0 & 0 \\ 0 & 0 & 0 & 0 \end{bmatrix} \begin{bmatrix} \beta_k \\ \dot{\psi}_k \\ v_k \\ F_{bk} \end{bmatrix} + \begin{bmatrix} \frac{b_1}{v_k} \\ b_2 \\ 0 \\ 0 \end{bmatrix} \delta_k \tag{2.14}$$

where,

$a_{13} = -\frac{a_{11}}{v_k^2}\beta_k - \frac{a_{12}}{v_k^3}\dot{\psi}_k - \frac{1}{mv_k^2}F_b$, and $\begin{bmatrix} \beta_k & \dot{\psi}_k & v_k & F_{bk} \end{bmatrix}'$ is the new state vector after linearization.

Two sensor measurements are used in the observer design, lateral acceleration, and yaw rate.

The measured lateral acceleration with influence from road bank force is given by,

$$a_y meas = a_y + \frac{F_b}{m} \tag{2.15}$$

The lateral acceleration is related to the single-track model states as,

$$a_{yk} = v_k(\dot{\beta}_k + \dot{\psi}_k) \tag{2.16}$$

Substituting (2.12) in (2.16), and then (2.16) in (2.15) yields,

$$a_y meas = a_{11}\beta_k + \frac{a_{12}}{v_k}\dot{\psi}_k + \frac{1}{mv_k}F_{bk} + b_1\delta_k \tag{2.17}$$

The resulting linearized measurement model is given below,

$$y = \begin{bmatrix} \dot{\psi} \\ a_y meas \end{bmatrix} = \begin{bmatrix} 0 & 1 & 0 & 0 \\ a_{11} & \frac{a_{12}}{v_k} & \frac{a_{12}\dot{\psi}_k}{v_k{}^2} & \frac{1}{m} \end{bmatrix} \begin{bmatrix} \beta_k \\ \dot{\psi}_k \\ v_k \\ F_{bk} \end{bmatrix} + \begin{bmatrix} 0 \\ b_1 \end{bmatrix} \delta_k \tag{2.18}$$

After discretizing and linearizing the model, it is now possible to implement EKF algorithm to estimate the side slip angle and yaw rate using the standard EKF equations.

Prediction:

$$A_k = \frac{\partial f}{\partial x}\Big|_{k-1}$$

$$\hat{X}_k = f\left(\hat{X}_{k-1}\right)$$

Update:

$$P_k = A_{k-1}P_{k-1}A^T{}_{k-1} + Q$$

$$K = P_k C^T{}_{k-1}(C_{k-1}P_k C^T{}_{k-1} + R)^{-1}$$

$$\hat{X}_{k|k} = X_{k|k-1} + K\left(Y_k - h\left(\hat{X}_k\right)\right)$$

where,

Q is the covariance of the state vector, and R is the measurement covariance chosen as,

$$Q = \begin{bmatrix} 0.01 & 0 & 0 & 0 \\ 0 & 0.001 & 0 & 0 \\ 0 & 0 & 0.001 & 0 \\ 0 & 0 & 0 & 100000 \end{bmatrix}, \quad R = \begin{bmatrix} 1 & 0 \\ 0 & 100 \end{bmatrix}$$

P_k is the error covariance matrix initialized as the identity 4x4 matrix, A_k is the model Jacobian matrix as given in (2.14), and C_k is the measurement Jacobian matrix as given in (2.18).

The road bank force is estimated from the observer and then we obtain the road bank angle as $\theta = \sin^{-1}\left(\frac{F_b}{mg}\right)$.

2.2.2 Observer Experimental Results

The algorithm was validated on a test vehicle equipped with dSPACE AutoBox, and other sensors such as IMU and steering angle sensor. A high precision combination of Global Positioning System (GPS) and inertial navigation system (INS) sensors unit (GPS/INS) is installed in the vehicle to be used as ground truth for validating the side slip angle estimation from the EKF algorithm, but was not used in the estimation algorithm itself. The road bank angle is validated by driving on roads with previously known bank angles, and on both curved and straight roads. For example, in Figures 2.2-2.5, there are two sections of curved roads with bank angles, the first one is 13 degrees and the second one is 19degrees, and there is a straight section in between with very little bank angle. In this scenario, we started recording right before we entered the first bank, until we exited the second bank. As can be seen in Figure 2.2, the estimator worked reasonably well in estimating the two large banks, and the little bank in the straight section, with smooth transitioning between the three different sections. Figure 2.3 shows the vehicle speed during the maneuver. The side slip angle and the yaw rate were validated with measurements from a high precision GPS/INS system, as can be seen in Figure 2.4 and Figure 2.5, which is reasonably close. The process and measurement covariance matrices $\mathbf{Q}$ and $\mathbf{R}$ were tuned on the road until the estimated road bank angle reasonably matched the previously known road bank angles, and the estimated side slip angle matched the measured side slip angle from the high precision GPS/INS unit.

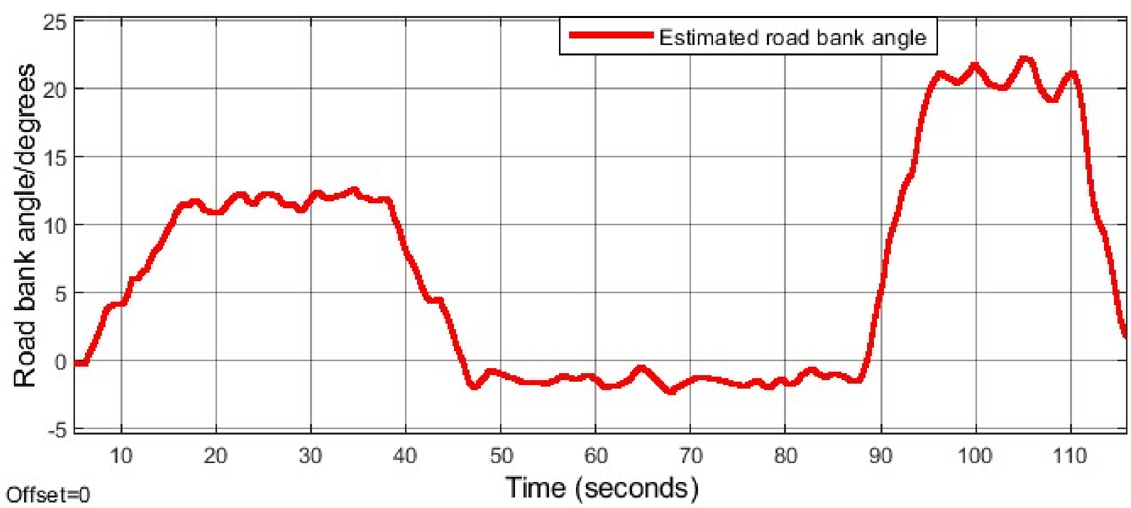

Figure 0.2 Estimated Road Bank Angle

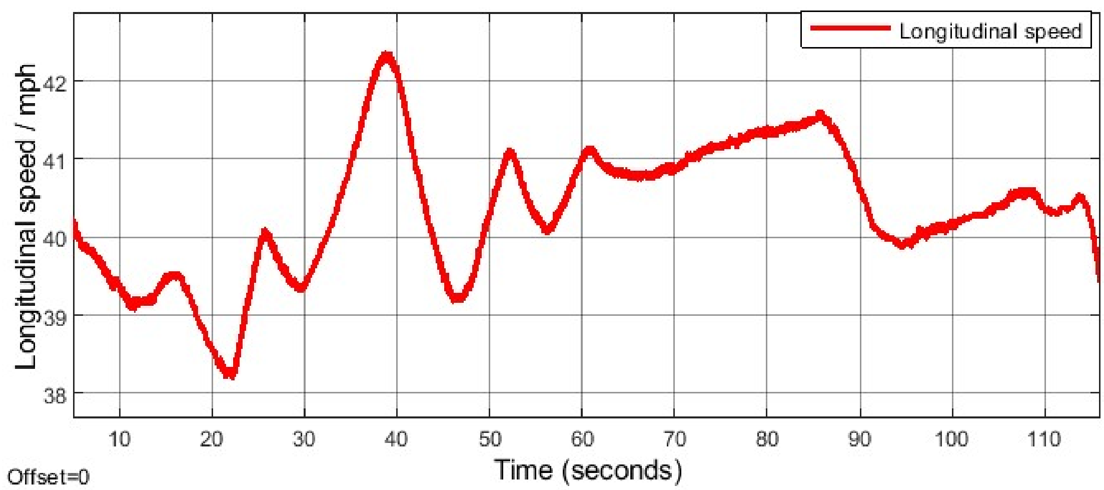

Figure 0.3 Vehicle speed during the maneuver.

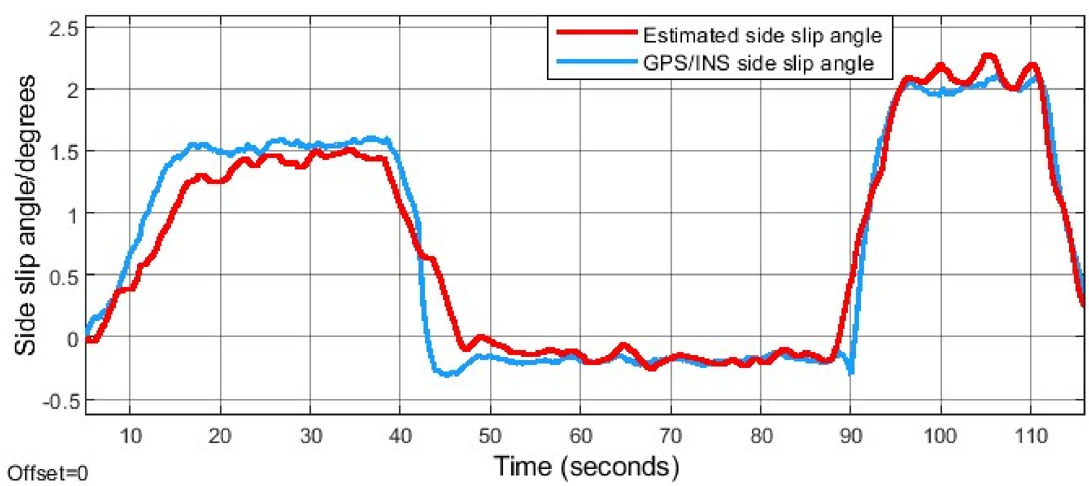

Figure 0.4 Estimated side slip angle

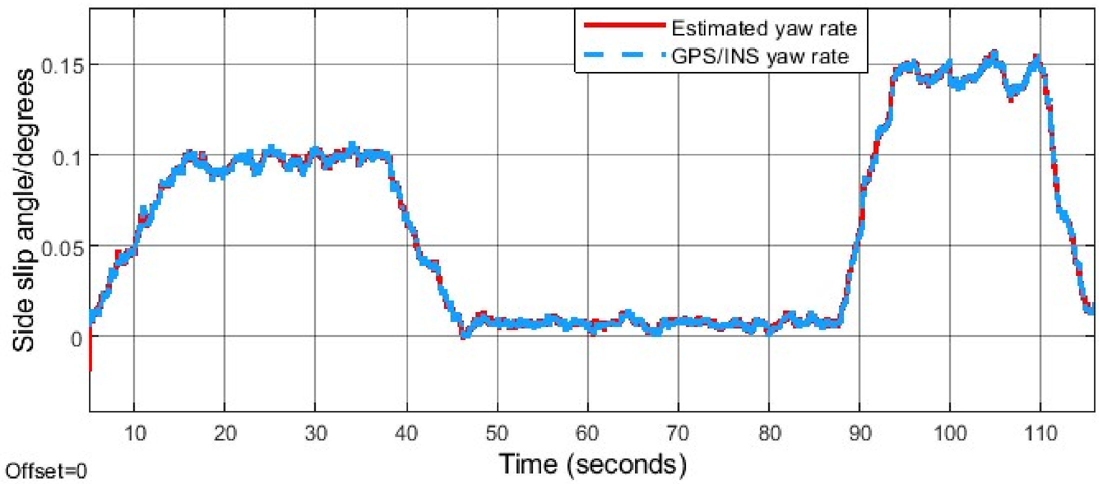

Figure 0.5 Estimated Road Bank Angle.

Figures 2.6-2.11 demonstrate driving on a test track with 6 lanes road with different known banks. The bank starts in lane 6 with 38 degrees and then decreases gradually as we transition from lane 6 to lane 1. It is worth mentioning that the speeds were chosen to reflect the speed limit for each lane. We drove on all 6 lanes and took separate recording on each lane. Figure 2.6 demonstrates the road bank estimate on lane 6. Figure 2.7 demonstrates the road bank estimate on lane 5. Figure 2.8 demonstrates the road bank estimate on lane 4. Figure 2.9 demonstrates the road bank estimate on lane 3. Figure 2.10 demonstrates the road bank estimate on lane 2. Figure 2.11 demonstrates the road bank estimate on lane. As can be seen, our road bank angle estimate started with about 38 degrees on lane 6 and decreased as expected as we transitioned to the lanes with less bank.

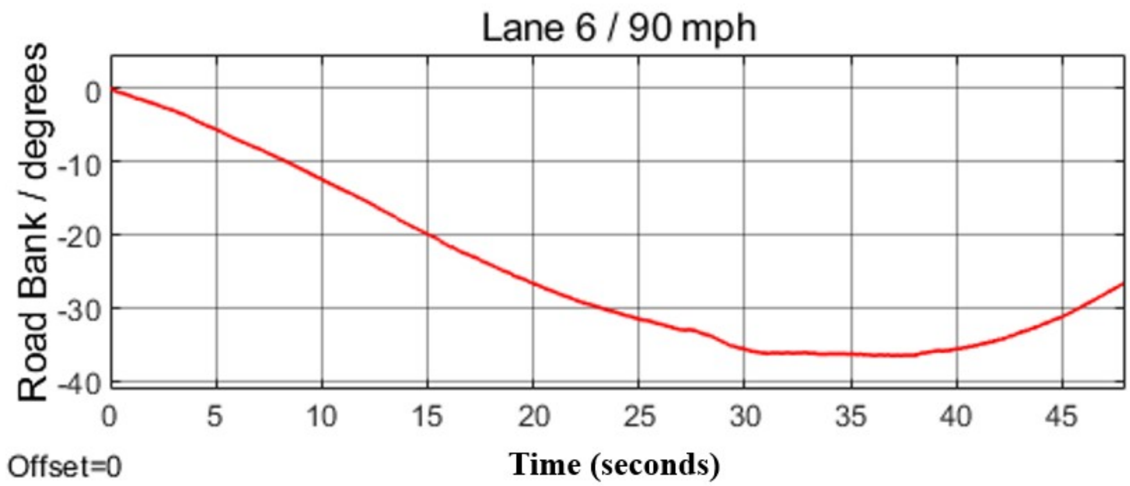

Figure 0.6 Driving on lane 6 at 90mph.

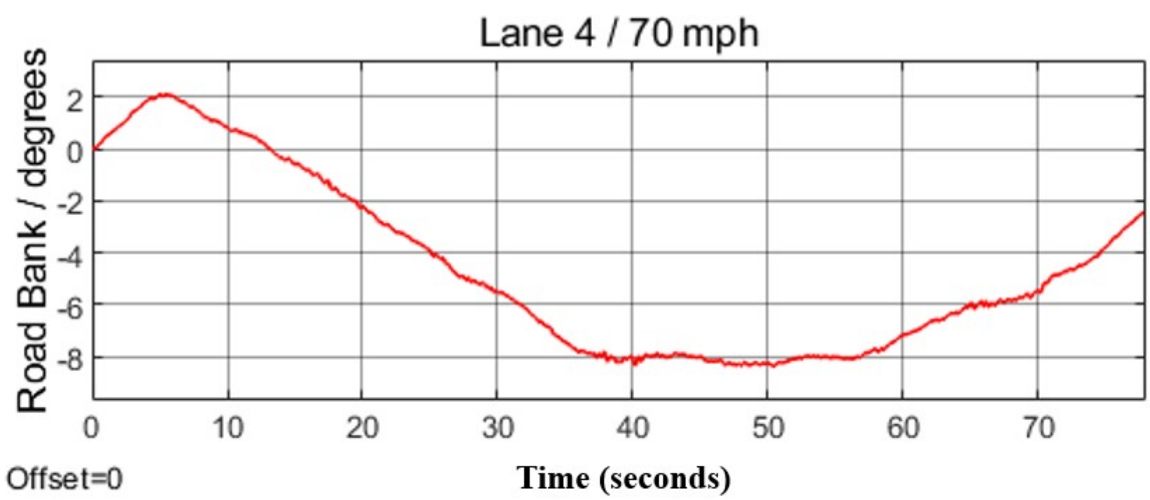

Figure 0.7 Driving on lane 4 at 70mph.

Figure 0.8 Driving on lane 3 at 60mph.

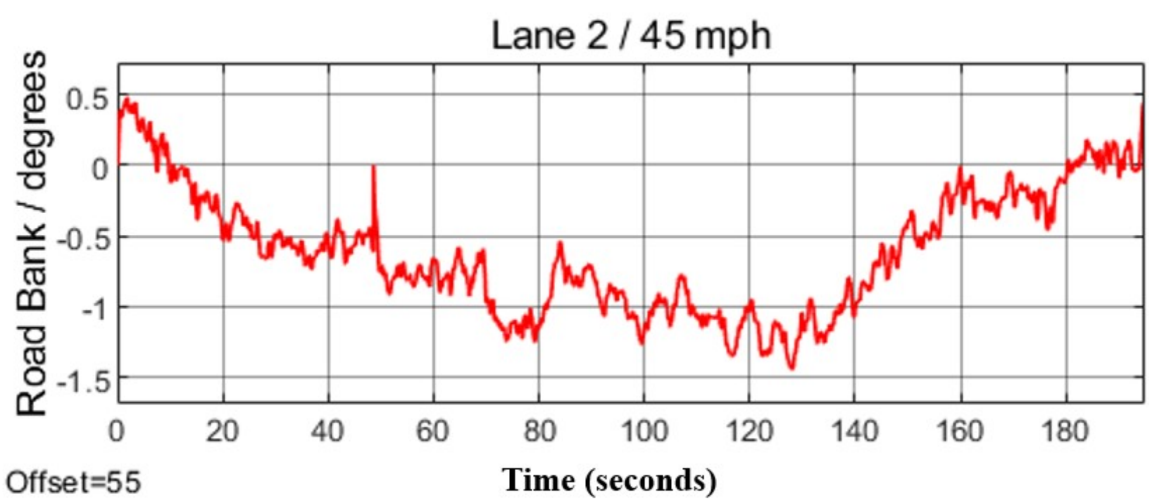

Figure 0.9 Driving on lane 2 at 45mph.

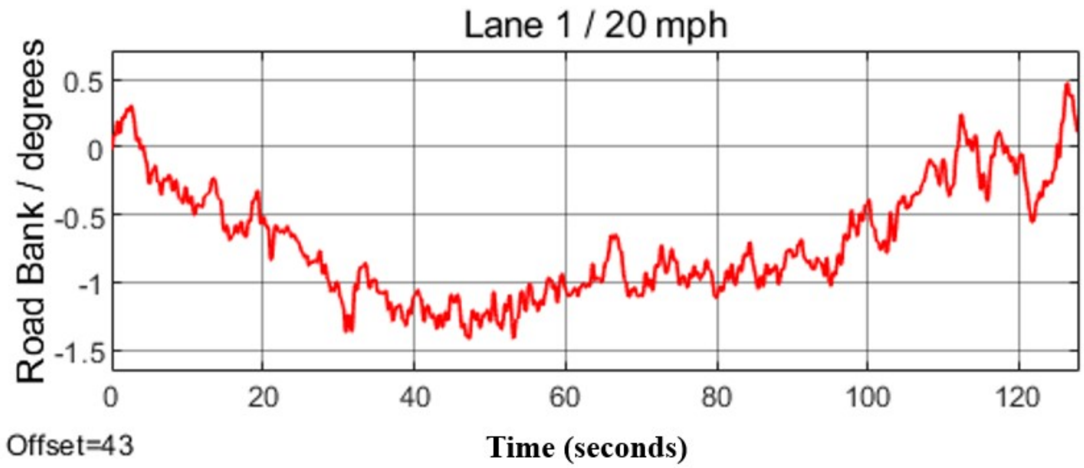

Figure 0.10 Driving on lane 1 at 20mph.

CHAPTER THREE

STEERING SYSTEM MODEL

¶
¶
¶

Recently, electric power steering (EPS) systems have been used to replace traditional hydraulic power steering (HPS) systems in vehicles for the several advantages they have over HPS systems. EPS systems are more efficient because they don't use power from the engine as HPS systems do. Vehicles with EPS systems come with electric motor to replace the hydraulic pumps or pistons which reduces the vehicle's weight. In addition, EPS systems are superior in improving the vehicle's steering performance, steering feel and safety as well as reducing environmental pollution.

EPS is a key technology for automated driving lateral functions. The built-in steering control module with an electric motor enables the EPS to support all lateral driver assistance functions in autonomous vehicles such as, trajectory following control, evasive steering assist, lane keeping assist, lateral collision avoidance, road departure protection, traffic jam assist, correction of driver maneuvers, and automated parking. All those lateral functions plan a trajectory for the vehicle to follow based on the vision sensors (camera, lidar, radar) and the trajectory is controlled by the steering angle. The role of the EPS in the autonomous mode (driverless mode) is different than its role in the nonautonomous mode (manual driving mode). In the autonomous mode, its role is to follow the steering angle requested by the lateral driver assistance function and the driver torque is considered as disturbance to be rejected. In the non-autonomous mode, the role of the EPS is to control the motor torque to generate assistant motor torque for the driver and then both the assistant motor torque and the driver torque are added to generate the required torque to turn the wheel.

Figure 3.1 shows the functional configuration of the steering system. In the autonomous mode, the LLC outputs the desired steering torque to follow the desired steering angle requested by the HLC. The ECU in the steering system provides servo control to track the desired steering torque. To control the desired torque, the ECU contains two servo controllers: a steering torque controller to compute the required current for torque tracking, and a current controller to compute the required voltage for current tracking.

The EPS system consists of many sub-components as illustrated in Figure 3.1, and each component has its own parameters. Obtaining a high-fidelity model is not easy and not necessary for the steering angle controller design in the autonomous driving mode. In addition, the dynamics of the individual components are negligible compared to the overall steering system dynamics in the normal range of steering. The EPS can be represented by two lumped inertias, the inertia of steering wheel and the inertia of the electric motor and rack and pinion, the two inertias are separated by a very stiff torsion bar spring that makes the system moves as a whole and the resulting measured inertia will reflect both inertias. With this assumption we can estimate the lumped parameters of the EPS and well represent it as a second order system with one degree of freedom (pinion angle) [35]. This model is valid in the autonomous mode (driverless mode) but in the manual driving mode it is necessary to take into consideration the driver steering wheel angle and represent the system as two degrees of freedom (pinion angle and steering wheel angle). It is important to mention that the above assumptions may not hold true for all steering operating conditions. In this case more detailed mathematical models are needed as developed in.

Figure 0.1 Electric Power Steering (EPS) system

The model is given by:

$$J\ddot{\theta}_p + b\dot{\theta}_p + F\,\mathrm{sgn}\left(\dot{\theta}_p\right) = \tau_p - \tau_a \tag{3.1}$$

where $\left[\theta_p \quad \dot{\theta}_p\right]'$ is the state vector, θ_p is the pinion angle, $\dot{\theta}_p$ is the pinion angular velocity, $\ddot{\theta}_p$ is the pinion angular acceleration, τ_p is the pinion torque, τ_a is the aligning moment, J is the equivalent moment of inertia, b is the equivalent viscous damping, F is Coulomb friction constant.

A state space representation is given by:

$$\begin{bmatrix} \dot{\theta}_p \\ \ddot{\theta}_p \end{bmatrix} = \begin{bmatrix} 0 & 1 \\ 0 & -\frac{b}{J} \end{bmatrix} \begin{bmatrix} \theta_p \\ \dot{\theta}_p \end{bmatrix} - \begin{bmatrix} 0 \\ \frac{F}{J}\operatorname{sgn}\left(\dot{\theta}_p\right) \end{bmatrix} + \begin{bmatrix} 0 \\ \frac{1}{J} \end{bmatrix} \tau_p - \begin{bmatrix} 0 \\ \frac{1}{J} \end{bmatrix} \tau_a \tag{3.2}$$

In this model, the EPS lumped parameters, equivalent moment of inertia J, equivalent viscous damping b, and coulomb friction constant F are identified by recursive least squares. τ_a is the self-aligning moment disturbance caused by tire forces resisting the steering motion.

3.2 Steering Model Parameter Identification

In this section, we describe the procedure and the estimation algorithm used for estimating the EPS lumped mechanical parameters described in the previous section, followed by experimental estimation results. These parameters will be used in the steering angle SMC developed in chapter 4, as SMC requires a priori estimate or bound on the model parameters.

3.2.1 EPS Parameter Identification Algorthm

The EPS lumped parameters are identified using the recursive least squares algorithm (RLS) [35] using data collected in the test vehicle. The vehicle was placed on hoist to temporarily eliminate the aligning moment caused by lateral forces and then sine sweep torque commands were sent to the EPS and data was recorded. The main signals of interest to the estimation algorithm are: motor angle, motor angular velocity and angular acceleration, and measured motor torque. The standard RLSE algorithm was then used for the parameter estimation as shown below:

$$y(k) = \alpha^T \phi(k) + e(k) \tag{3.3}$$

$$e(k) = y(k) - \hat{\alpha}^T(k)\phi(k-1) \tag{3.4}$$

$$K(k) = \frac{P(k-1)\phi(k)}{1 + \phi^T(k)P(k-1)\phi(k)} \tag{3.5}$$

$$P(k) = \frac{1}{\lambda}\left[P(k-1) - \frac{P(k-1)\phi(k)\phi^T(k)P(k-1)}{\lambda + \phi^T(k)P(k-1)\phi(k)}\right] \tag{3.6}$$

$$\hat{\alpha}(k) = \hat{\alpha}(k-1) + K(k)e(k) \tag{3.7}$$

where,

$$\phi(k) = \left[\ddot{\theta}_p \quad \dot{\theta}_p \quad \text{sgn}\left(\dot{\theta}_p\right)\right]$$
$$\alpha^T = \left[J \quad b \quad F\right]$$
$$y(k) = \tau_p$$

$\tau_a = 0$ because the vehicle is placed on hoist.

$e(k)$ is the identification error and k denotes sampling time, $P(k)$ is the covariance matrix, and $K(k)$ is the gain vector.

3.2.2 Experimental Results of EPS Parameter Identification

Figures 3.2-3.6 show the experimental results of the EPS parameters identification using RLS. Figure 3.2 shows the input torque signal used to excite the EPS. Figure 3.3 shows the estimated viscous damping, which took one second to converge. Figure 3.4 shows the estimated damping, which took about 5 seconds to converge. Figure 3.5 shows the estimated coulomb friction constant, which took about 5 seconds to settle down. For validation of the estimated parameters, Figure 3.6 shows the identified vs. the measured torque.

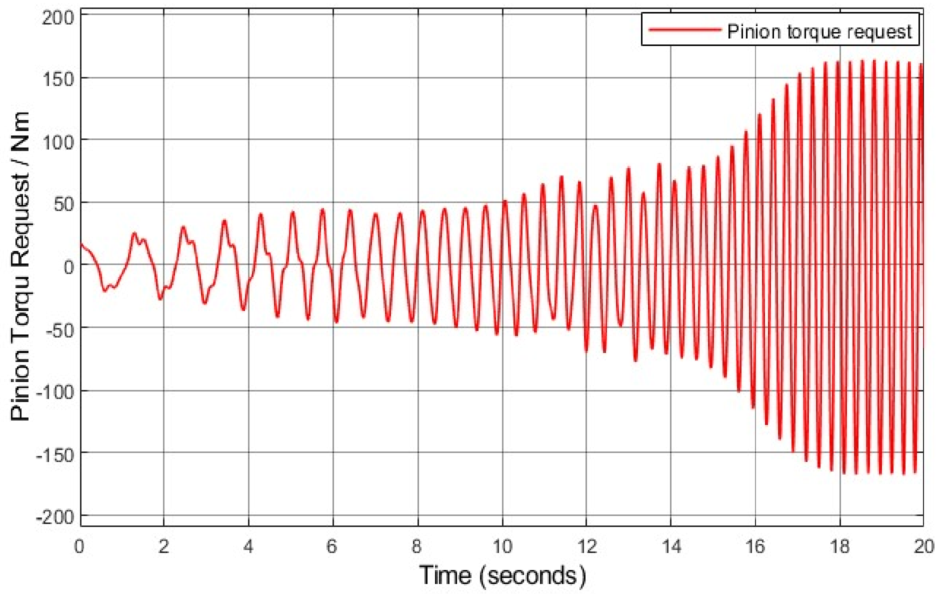

Figure 0.2 Excitation signal for parameters estimation.

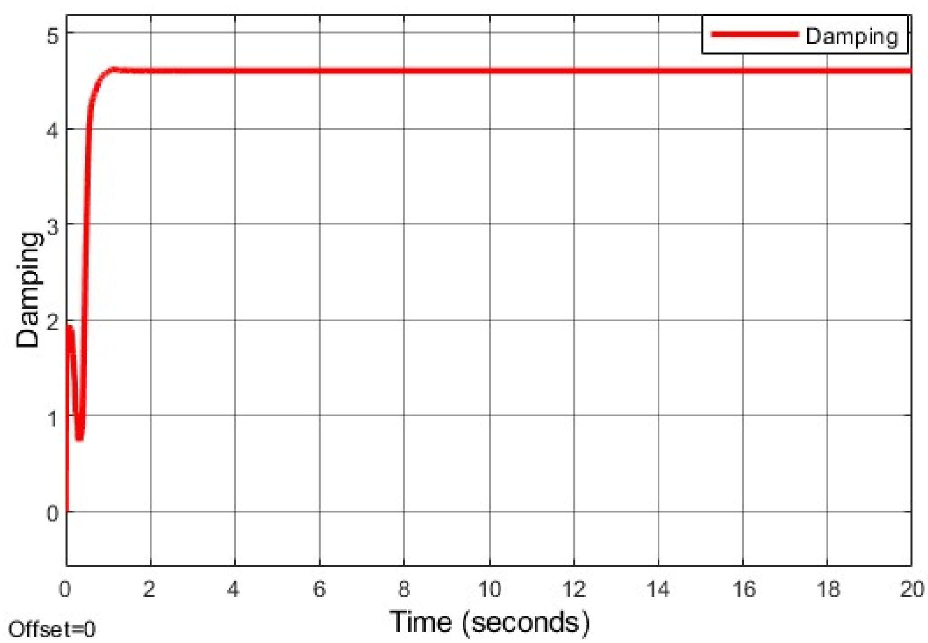

Figure 0.3 Viscous damping

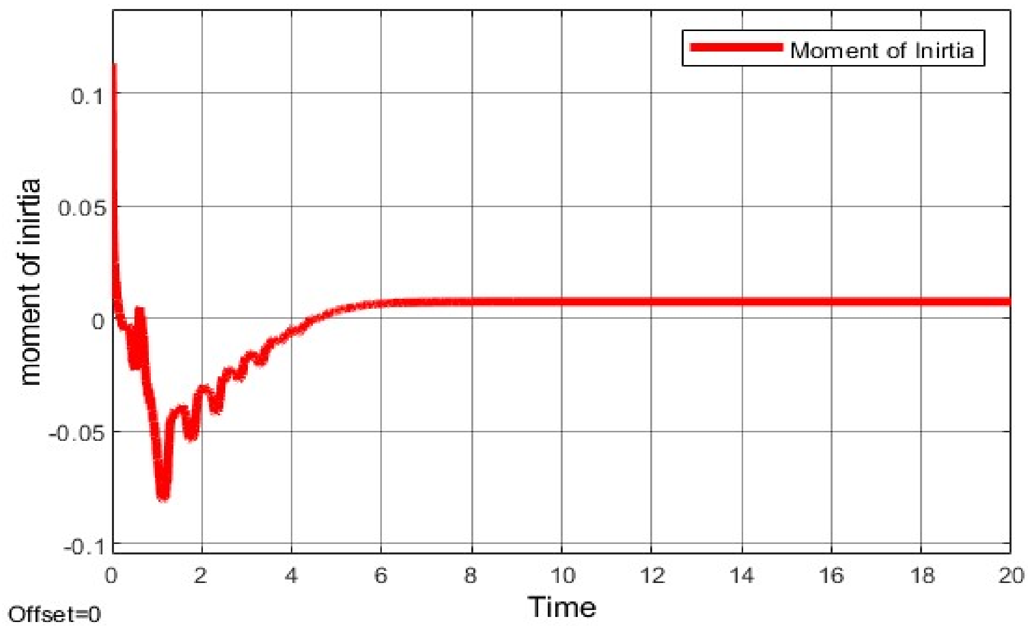

Figure 0.4 Moment of inertia.

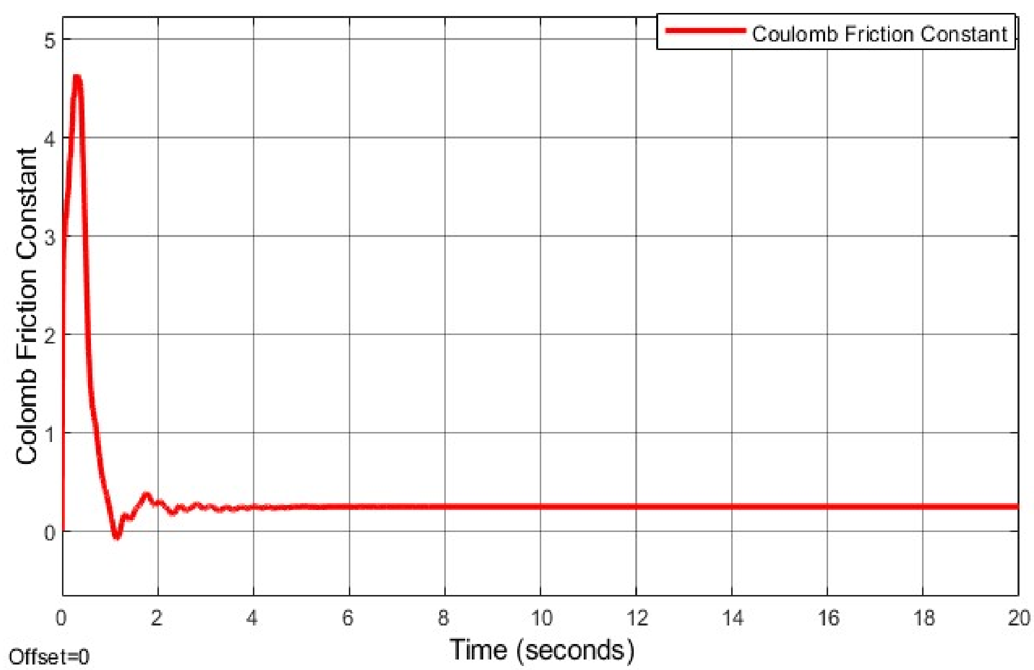

Figure 0.5 Coulomb friction constant.

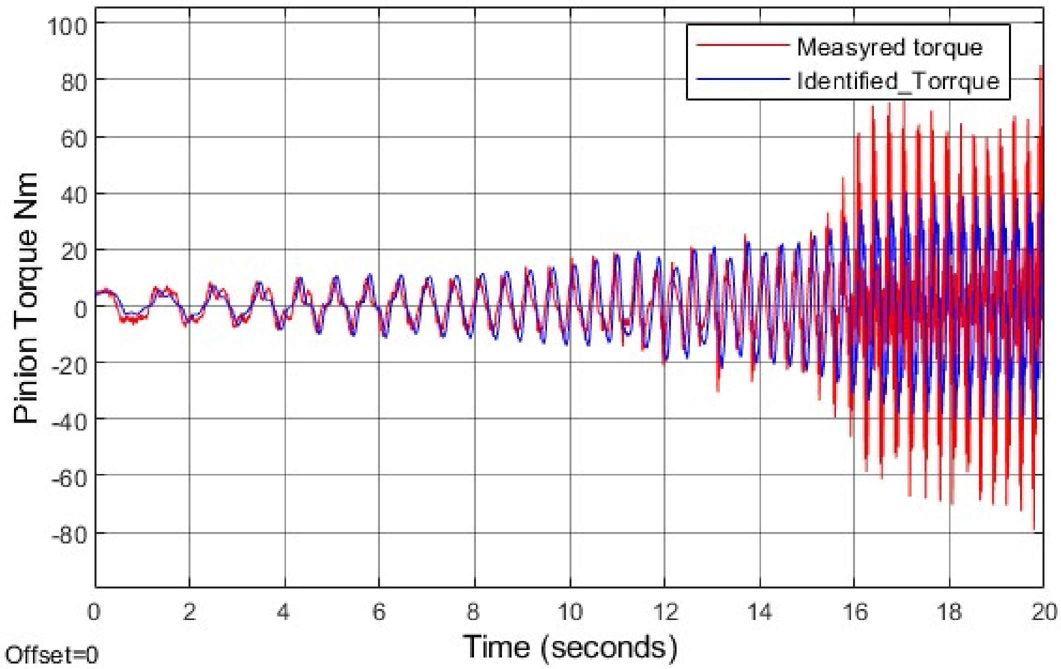

Figure 0.6 Measured torque vs. identified torque.

3.3 Model Based Self Aligning Moment Estimation with Experomental Results

In this section we develop a model-based strategy to estimate the self-aligning moment. Self-aligning moment, denoted by τ_a in the steering model, results from lateral forces acting on the steering system when the vehicle undergoes a turn. One portion of the aligning moment is due to pneumatic trail t_p which is the distance between the center of the tire and the point on the tire where the lateral forces are applied. The other portion of the aligning moment is due to the mechanical trail t_m that results from the wheel caster angle. Because a big portion of the steering control effort goes toward overcoming the tire self-aligning moment, it has to be accurately estimated.

Assuming a front wheel drive vehicle, the overall aligning moment is given by:

$$\tau_a = \left(t_p + t_m\right) F_{yf} \tag{3.8}$$

where F_{yf} is the lateral force acting on the front wheel and it is a function of front tire slip angle α_f in the linear region where the slip angle is small, i.e. $F_{yf} = C_f \alpha_f$, C_f being the cornering stiffness of the front tire. The tire slip angle can be computed as:

$$\alpha_f = \delta - \beta - \frac{l_f \dot{\psi}}{v} \tag{3.9}$$

where δ is the front road wheel angle, β is the vehicle body side slip angle, $\dot{\psi}$ is yaw rate, and l_f is the distance from the center of gravity of the vehicle to the front axle. The steering wheel angle can be measured from the angle sensor. The side slip angle and yaw rate are estimated in section 2.2.1.

The mechanical trail t_m is assumed constant and determined experimentally in the test vehicle. The pneumatic trail t_p is computed from Pacejka tire magic formula as:

$$t_p = DT \cos(CT \arctan(BT\alpha_f - ET(BT\alpha_f - \arctan(BT\alpha_f)))) \tag{3.10}$$

where the parameters DT, CT, BT, ET are functions of tire normal force, lateral forces, and other tire coefficients whose values depend on tire type and characteristics. These coefficients are usually obtained from the tire manufacturer.

The drawback of this method of estimating the self-aligning moment is its dependency on tire parameters, which can vary from one type of tire to another. In other words, changing the type of vehicle tires would require changing the tire parameters in the controller code, which is something that a customer cannot do. In chapter 4, two other methods for estimating the self-aligning that do not require any information about the tire parameters are developed.

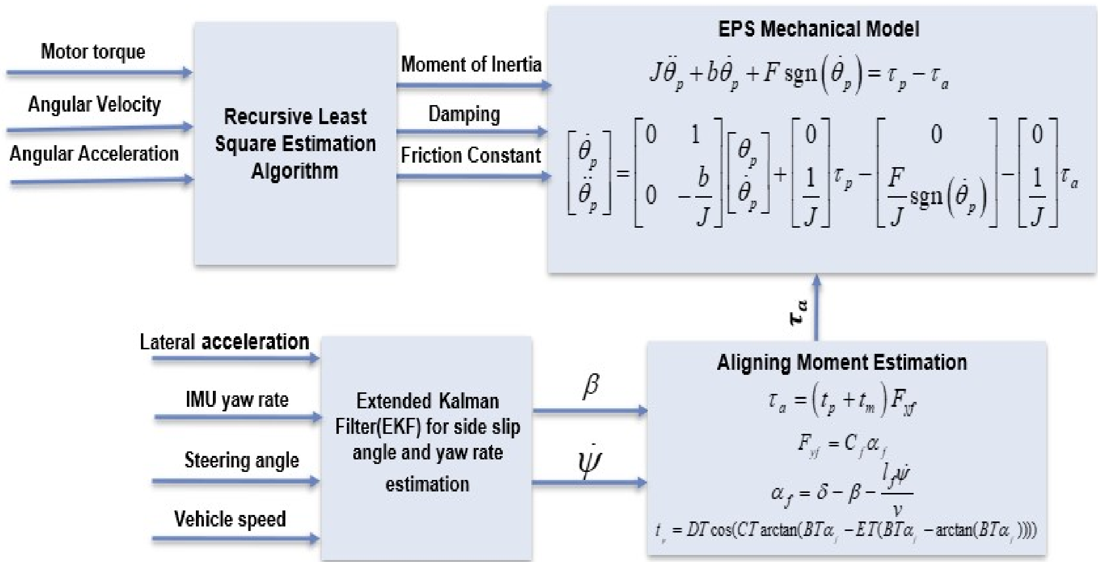

Figure 0.7 Steering System Model

Figures 3.8-3.12 demonstrate the results of the aligning moment estimation using the side slip angle estimated from the state observer that was implemented in chapter 2. Figures 3.8 and 3.9 show the side slip angle and the yaw rate, respectively, that were used in the aligning moment estimation validated with a high precision GPS/INS. As can be seen from Figures 3.10 and 3.11, since we are in the linear region of the tire, lateral forces and self-aligning moment increase as the tire slip angle increases as expected. It can be seen from Figure 3.12 that the pneumatic trail is maximum when the tire slip angle is zero and it decreases as the tire slip angle increases as expected.

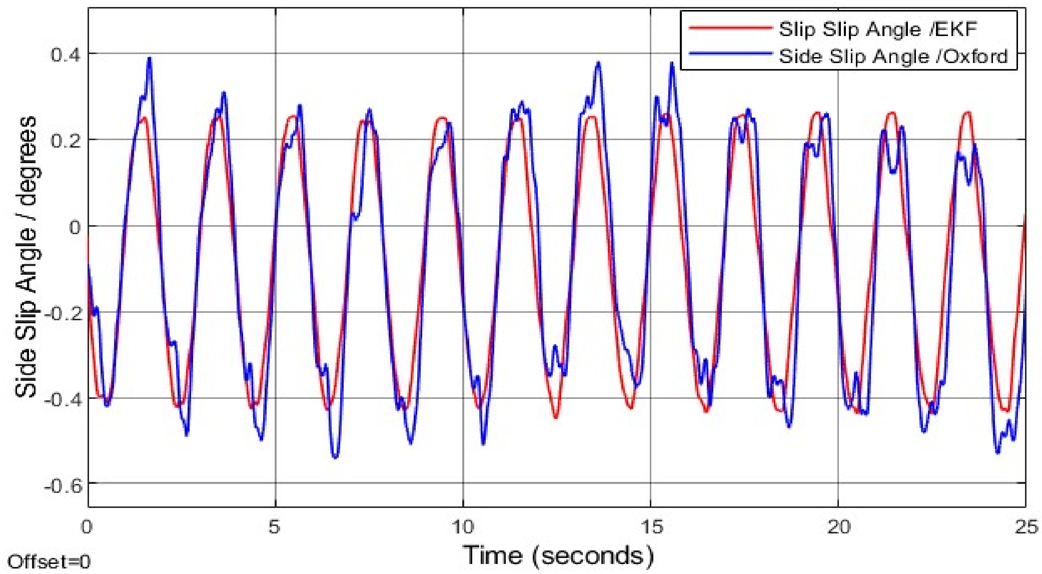

Figure 0.8 Validation of estimated side slip angle with a high precision GPS/INS.

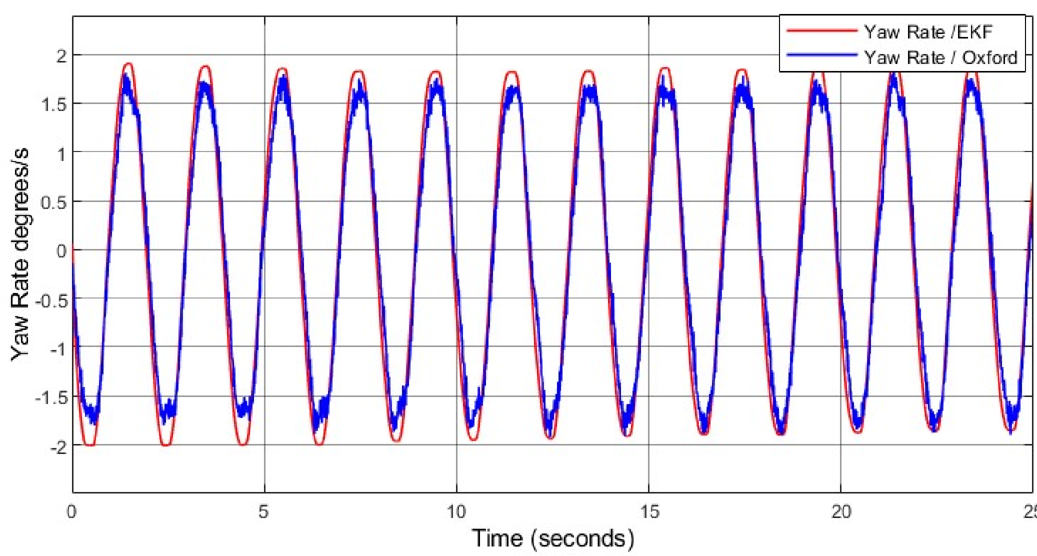

Figure 0.9 Validation of estimated yaw rate with a high precision GPS/INS.

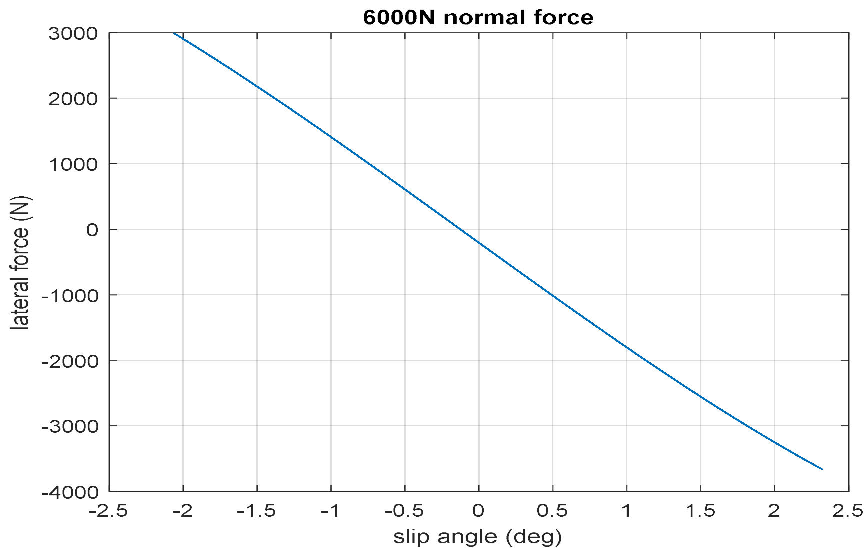

Figure 0.10 Lateral forces vs. tire slip angle.

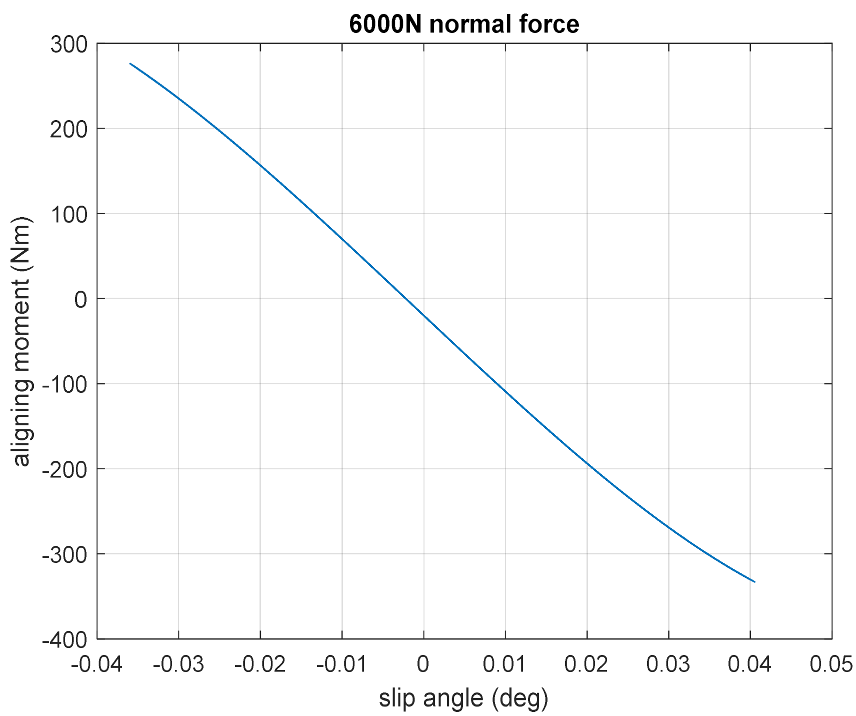

Figure 0.11 Aligning moment vs. slip angle.

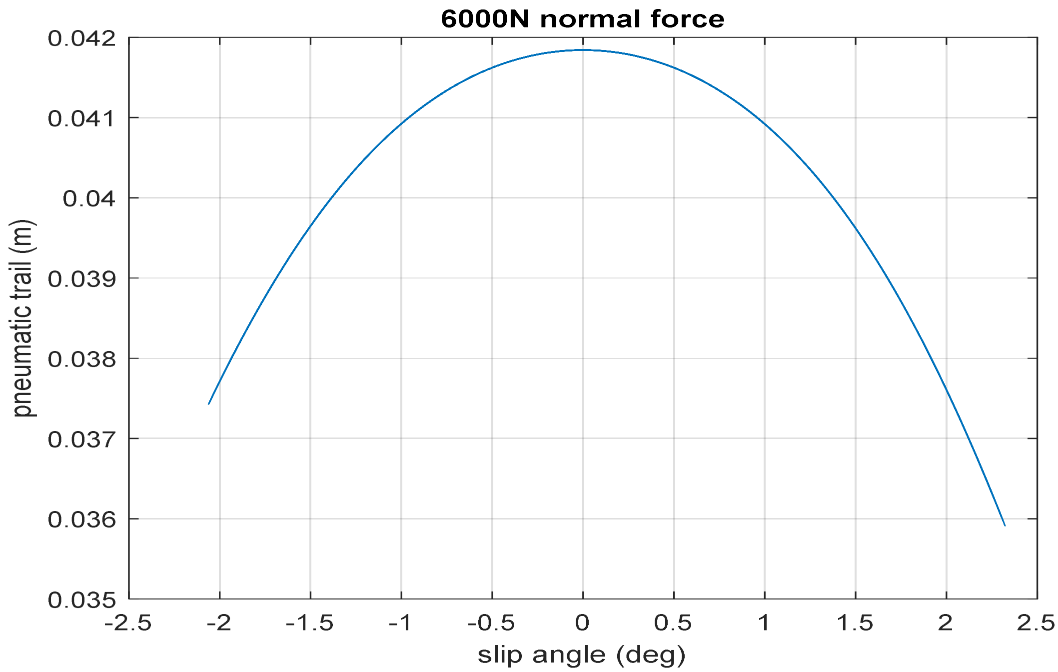

Figure 0.12 Pneumatic trail vs. tire slip angle.

CHAPTER FOUR

STEERING ANGLE CONTROL

4.1 Introduction

The SAC is responsible for delivering the steering angle requested by the trajectory tracking controller. The performance of the SAC has a significant impact on the performance of the trajectory tracking controller. The role of the SAC is to compute the steering torque that is required to achieve the desired angle and send it to the steering actuator, which is the electric power steering (EPS). The EPS has a torque controller that controls the torque to move the wheels. In this chapter, we discuss the challenges faced in developing steering angle control, followed by proposed methods to treat them.

One of the greatest challenges faced in steering control is overcoming the backlash in gears and the stiction (static friction), which both usually appear at the zero angular velocity crossing when we change the steering direction and they cause asymmetrical hysteresis behavior in the steering angle response. Both backlash and stiction are considered as inherent nonlinearities because they naturally come with the system's hardware and motion. Because of their discontinuous nature, these nonlinearities cannot be locally approximated by linear functions, and for this reason they are also called hard nonlinearities [1]. Such nonlinearities have undesirable effect on the behavior of a control system, such as delays, instabilities and limit cycles. Because such nonlinearities cannot be handled by linear control methods, strong nonlinear control techniques must be developed to predict the system's behavior in their presence and compensate for them properly.

Another challenge is the uncertainty in the EPS mechanical parameters. Usually, the EPS is provided by the manufacturer as a black box, with no medel or model parameters. Experimental identification of these parameters is a time-consuming process that requires a special procedure and a special vehicle setting as explained in chapter 3. This procedure has to be repeated for every different vehicle or if we change the EPS in the same vehicle, which is time consuming and impractical. In addition, experimental identification of these parameters might not always result in accurate results.

A significant part of the steering angle control effort goes toward overcoming the tire self-aligning moment disturbance, which is caused by tire forces acting on the steering system and resisting the steering motion when the vehicle undergoes a turn. Accurate estimate of self-aligning moment is required for precise steering control. The model-based method that we developed in chapter 3 requires knowledge of the tire parameters, which are usually obtained from the tire manufacturer. The limitation of this method is that if we change the tires of the vehicle to a different type, those parameters are not valid anymore, and that will affect the accuracy of the self-aligning moment estimate, and as a result, the controller performance will be affected. To overcome the limitation of this method, two other methods are developed that treats the self- aligning moment as disturbance and estimate it without any required information about the tire parameters.

Researchers investigated the control of Electric Power Steering (EPS) for autonomous vehicles. Sliding mode control (SMC) was investigated in [35]-[40], which is one of the major approaches to dealing with parametric uncertainties and disturbances. The only drawback of SMC is the chattering caused by the discontinuous nature of the control law. Chattering is undesirable in applications where the control input signal is acceleration or torque, but is acceptable in electrical systems where the control input signal is voltage. The chattering problem can be mitigated by replacing the sign function in the SMC law by a saturation function as in [36], but this limits the bandwidth of the controller and reduces its tracking capability. In [41], model predictive control (MPC) was designed for evasive steering maneuvers to take into account the voltage constraints. MPC is not as robust as SMC and adaptive control and requires high computational power, since a solution is computed at every time step. Also, in [41], the self-aligning moment disturbance was estimated using the linear relationship between the lateral forces and the side slip angle and that only works in the small slip angle range (-4 to 4 degrees). This method is tire parameter dependent, which means if the tires of the vehicle are changed to a different type, these parameters will not be valid anymore. A nonlinear damping steering wheel angle controller is developed in [42]. The limitation of nonlinear damping control is that it restricts the system's relative degree not to be higher than one. Backstepping is an approach to deal with this relative degree restriction. In [43], the well-known PID control method is used to control the steering angle of a steer by wire steering system. The PID method is not robust to parameter uncertainty and disturbances. Lyapunov based methods were investigated in [44] and [45] without taking into account parametric uncertainties. Even though backstepping control is mentioned in the title in [44], but reading the controller derivation carefully, it does not have the recursive design feature of backstepping control. In [45], a disturbance observer based on extended state observer and active disturbance rejection controller is designed to overcome the weaknesses and limitations of PID control. In [46], a radial basis function neural network

PID controller is implemented to generate electric current control signals to the steering motor to track the target steering angle. In [47], the recursive least squares (RLS) method is used to estimate the unknown parameters of the driver interaction unit of the steer-by-wire system on-line. The RLS method requires a persistently exciting signal in order for the estimated parameters to converge, otherwise the parameters estimates will diverge and that will affect the controller behavior and might also cause instability because the controller that is using them is based on the "certainty equivalence" principle, which means that the controller is capable of stabilizing the plant only when the estimated parameters converge to their true values. In this dissertation, an adaptive backstepping controller is developed to overcome the limitations of the "certainty equivalence" methods and eliminate the need for persistent excitation. In [48], a steering angle controller is developed for distributed drive electric autonomous vehicles. The adaptation in most of the previous methods is only in the disturbance estimation, not the unknown parameters, and most of them specifically deal with the self-aligning moment disturbance and ignore the static friction.

Two nonlinear control approaches are developed in the next two sections to overcome the challenges discussed above, robust control/ SMC and adaptive backstepping control, which are the two major approaches to dealing with model parameter uncertainty and disturbances.

4.2 Sliding Mode Control (SMC) of EPS Angle

As discussed in chapter 1, SMC is one of the major approaches to dealing with modeling inaccuracies and disturbances. As outlined in [1], the design of sliding mode control allows an nth order problem to be replaced by an equivalent first order problem, since it is much easier to control a first order system. It becomes then easy to prove that for the transformed problem, perfect performance can be achieved in the presence of model imprecesion. The SMC method changes the dynamics of a dynamical system by applying a discontinuous control signal that forces the system to "slide" along a sliding manifold or a sliding surface of the system's normal behavior. The design of SMC involves first constructing the sliding surface, usually denoted by "s" such that the system trajectory has a desirable behavior when it reaches this surface, and then designing the feedback control gains such that the system trajectory stays on the sliding surface ever after. The typical structure of a SMC consists of a nominal part, just like an inverse law, plus an added discontinuous term to deal with model imprecision and disturbances. This discontinuous term in the control law leads to the chattering phenomena explained in chapter 3. Our approach to eliminate this chattering problem is a VG SMC. Both VG and FG SMCs are derived and compared in section 4.2.2 of this chapter.

As discussed earlier, a significant part of the steering angle control effort goes toward overcoming the tire self-aligning moment disturbance. Also, the controller has to overcome the static friction when the steering direction is changed. A sliding mode observer is designed in section 4.2.1 of this chapter to estimate the disturbance caused by the self-aligning moment and the static friction plus any other disturbance, such as the driver torque. The observer also estimates the state vector in addition to the disturbance.

4.2.1 Sliding Mode Observer Design

Given the steering model in chapter 3, the general state space representation is,

$$\dot{\mathbf{x}} = \mathbf{A}\mathbf{x} + \mathbf{B}\mathbf{u} + \mathbf{D}\mathbf{w} \tag{4.1}$$

$$\mathbf{y} = \mathbf{C}\mathbf{x} \tag{4.2}$$

where,

$\mathbf{A} = \begin{bmatrix} 0 & 1 \\ 0 & -\dfrac{b}{J} \end{bmatrix}, \mathbf{B} = \begin{bmatrix} 0 \\ \dfrac{1}{J} \end{bmatrix}, \mathbf{C} = \begin{bmatrix} 1 & 0 \end{bmatrix}$, $\mathrm{u} = \tau_p$, the term $\mathbf{Dw}$ represent the unknown input term.

We assume $\mathbf{A}, \mathbf{B}$ and $\mathbf{C}$ are known but $\mathbf{D} \in \mathbb{R}^{n \times w}$ and $\mathbf{w} \in \mathbb{R}^{w \times 1}$ are unknown.

We would like to estimate the state vector $\mathbf{x} = \begin{bmatrix} \theta_p & \dot{\theta}_p \end{bmatrix}'$ and the disturbance w plus any added disturbance from measuring only the output $y = \theta_p$ and input $u = \tau_p$ and assuming that the unknown input term $\mathbf{Dw}$ is bounded. A sliding mode observer is formulated as,

$$\dot{\hat{\mathbf{x}}} = \mathbf{A}\hat{\mathbf{x}} + \mathbf{B}\mathbf{u} + \mathbf{L}\left(\mathbf{y} - \mathbf{C}\hat{\mathbf{x}}\right) + \mathbf{s} \tag{4.3}$$

Equation (4.3) is expaned below,

$$\begin{bmatrix} \dot{\hat{x}}_1 \\ \dot{\hat{x}}_2 \end{bmatrix} = \begin{bmatrix} 0 & 1 \\ 0 & -b/J \end{bmatrix} \begin{bmatrix} \hat{x}_1 \\ \hat{x}_2 \end{bmatrix} - \begin{bmatrix} 0 \\ \dfrac{1}{J} F \operatorname{sgn}\left(\hat{x}_2\right) \end{bmatrix} + \begin{bmatrix} 0 \\ 1/J \end{bmatrix} \tau_p + \begin{bmatrix} l_1 \\ l_2 \end{bmatrix} \left(y - \begin{bmatrix} 1 & 0 \end{bmatrix} \begin{bmatrix} \hat{x}_1 \\ \hat{x}_2 \end{bmatrix} \right) + \begin{bmatrix} s_1 \\ s_2 \end{bmatrix}$$

$$\hat{\mathbf{y}} = \mathbf{C}\hat{\mathbf{x}} \tag{4.4}$$

Also, $\hat{x}_1 = \theta_1$, $\hat{x}_2 = \dot{\theta}_1$, and $\left[\mathbf{A}, \mathbf{C}\right]$ is assumed to be an observable pair.

The unknown term $\mathbf{Dw}$ is not included in (4.3), instead a correction term $\mathbf{s} \in \mathbb{R}^{n \times 1}$ is added, which is a sliding mode function to be determined.

The error dynamics are given by,

$$\mathbf{e}_x = \mathbf{x} - \hat{\mathbf{x}} \tag{4.5}$$

$$\begin{aligned}\dot{\mathbf{e}}_x &= \dot{\mathbf{x}} - \dot{\hat{\mathbf{x}}} \\ &= \mathbf{Ax} + \mathbf{Bu} + \mathbf{Dw} - \left(\left(\mathbf{A} - \mathbf{LC}\right)\hat{\mathbf{x}} + \mathbf{Bu} + \mathbf{Ly} + \mathbf{s}\right) \\ &= \left(\mathbf{A} - \mathbf{LC}\right)\mathbf{e}_x + \mathbf{Dw} - \mathbf{s} \\ &= \mathbf{A}_o\mathbf{e}_x + \mathbf{Dw} - \mathbf{s}\end{aligned} \tag{4.6}$$

where $\mathbf{A}_o = \mathbf{A} - \mathbf{LC}$ is the Hurwitz observer matrix.

We need to find an $\mathbf{s}$ to drive the error $\mathbf{e}_x \to \mathbf{0}$, then either $\left\|\mathbf{Dw} - \mathbf{s}\right\| \to 0$ or $E\left[\mathbf{Dw} - \mathbf{s}\right] \to 0$ and we claim that $\mathbf{s}$ represents the unknown input term $\mathbf{Dw}$.

Step1: The first step in designing the observer is to choose the observer gains $\left[l_1 \quad l_2\right]'$ such that the observer matrix, given by:

$$\mathbf{A}_o = \mathbf{A} - \mathbf{LC} = \begin{bmatrix} 0 & 1 \\ 0 & -\frac{b}{J} \end{bmatrix} - \begin{bmatrix} l_1 \\ l_2 \end{bmatrix}\begin{bmatrix} 1 & 0 \end{bmatrix} = \begin{bmatrix} -l_1 & 1 \\ -l_2 & -\frac{b}{J} \end{bmatrix} \tag{4.7}$$

is a stable matrix. This can be achieved if the characteristic equation of (4.7), given by $\gamma^2 + \left(l_1 + \frac{b}{J}\right)\gamma + \left(l_1\frac{b}{J} + l_2\right)$, has stable roots. The observer poles were chosen to be $\left[-5 + j5 \quad -5 - j5\right]$ and we solved for the observer gains using the pole placement method.

The corresponding observer gains are $\left[l_1 \quad l_2\right]' = \left[10 \quad 50\right]'$ computed by matching the poles of the characteristic equation with the desired stable poles. The eigenvalues of the resulting observer matrix are, -10.773 and -74.641. Substituting the observer gains and the system parameters in the observer matrix yields $\mathbf{A_o} = \begin{bmatrix} -10 & 1 \\ -50 & -75.415 \end{bmatrix}$.

Step2: The second step is to choose a positive definite matrix $\mathbf{Q} \in \mathbb{R}^{n\times n}$ such that $\mathbf{Q} = \mathbf{Q}^T > \mathbf{0}$, and then solve for $\mathbf{P} = \mathbf{P}^T \succ \mathbf{P} \in \mathbb{R}^{n\times n}$ from the algebraic Lyapunov equation given by,

$$\mathbf{A}_o^T\mathbf{P} + \mathbf{P}\mathbf{A}_o = -\mathbf{Q} \tag{4.8}$$

Expanding (4.8) yeilds,

$$\begin{bmatrix} -l_1 & 1 \\ -l_2 & -b/J \end{bmatrix}^T \begin{bmatrix} p_{11} & p_{12} \\ p_{12} & p_{22} \end{bmatrix} + \begin{bmatrix} p_{11} & p_{12} \\ p_{12} & p_{22} \end{bmatrix} \begin{bmatrix} -l_1 & 1 \\ -l_2 & -b/J \end{bmatrix} = -\begin{bmatrix} q_{11} & q_{12} \\ q_{12} & q_{22} \end{bmatrix}$$

$\mathbf{Q}$ is chosen to be $\mathbf{Q} = \begin{bmatrix} 1 & 0 \\ 0 & 1000 \end{bmatrix}$

Solving for $\mathbf{P}$ from (4.8) results in $\mathbf{P} = \begin{bmatrix} 18.246 & -3.6392 \\ -3.6392 & 6.5817 \end{bmatrix}$

Step3: The third step is to find the correction factor $\mathbf{s}$. The correction factor is found using Lyapunov stability criterion. A Lyapunov function candidate is defined as a function of the observer error as,

$$v = \mathbf{e}_x^T\mathbf{P}\mathbf{e}_x \tag{4.9}$$

Taking the derivative of (4.9) yields,

$$\begin{aligned} \dot{v} &= \mathbf{e}_x^T\mathbf{P}\dot{\mathbf{e}}_x + \dot{\mathbf{e}}_x^T\mathbf{P}\mathbf{e}_x \\ &= \mathbf{e}_x^T\mathbf{P}\left(\mathbf{A}_o\mathbf{e}_x + \mathbf{D}\mathbf{w} - \mathbf{s}\right) + \left(\mathbf{A}_o\mathbf{e}_x + \mathbf{D}\mathbf{w} - \mathbf{s}\right)^T\mathbf{P}\mathbf{e}_x \\ &= -\mathbf{e}_x^T\mathbf{Q}\mathbf{e}_x + 2\mathbf{e}_x^T\mathbf{P}\left(\mathbf{D}\mathbf{w} - \mathbf{s}\right) \end{aligned} \tag{4.10}$$

Based on Lyapunov stability criterion, if $\dot{v}$ is less than zero then the error will converge to zero. This goal can be achieved if the term $2\mathbf{e}_x^T\mathbf{P}\left(\mathbf{D}\mathbf{w} - \mathbf{s}\right)$ always contributes a negative value.

We can find the solution by the supposition that the unknown term $\mathbf{Dw}$ can be represented by matrices **P** and **C** and a vector function $\mathbf{h}(\mathbf{w})$ as,

$$\mathbf{Dw} = \mathbf{P}^{-1}\mathbf{C}^{T}\mathbf{h}(\mathbf{w}), \ \left\|\mathbf{h}(\mathbf{w})\right\| < \bar{h} \tag{4.11}$$

where $\mathbf{h}(\mathbf{w})$ is bounded by some positive constant $\bar{h}$.

Suppose also that the sliding mode variable $\mathbf{s}$ can be chosen as:

$$\mathbf{s} = \rho\frac{\mathbf{P}^{-1}\mathbf{C}^{T}\mathbf{C}\mathbf{e}_{x}}{\left\|\mathbf{C}\mathbf{e}_{x}\right\|} = \rho\mathbf{P}^{-1}\mathbf{C}^{T}sign(\mathbf{e}_{y}) \tag{4.12}$$

where $\mathbf{e}_{y} = \mathbf{C}\mathbf{e}_{x}$

Substituting (4.11) and (4.12) in (4.10) yields:

$$\begin{aligned} \dot{v} &= -\mathbf{e}_{x}^{T}\mathbf{Q}\mathbf{e}_{x} + 2\mathbf{e}_{x}^{T}\mathbf{P}\left(\mathbf{P}^{-1}\mathbf{C}^{T}\mathbf{h}(\mathbf{w}) - \rho\frac{\mathbf{P}^{-1}\mathbf{C}^{T}\mathbf{C}\mathbf{e}_{x}}{\left\|\mathbf{C}\mathbf{e}_{x}\right\|}\right) \\ &= -\mathbf{e}_{x}^{T}\mathbf{Q}\mathbf{e}_{x} + 2\mathbf{e}_{x}^{T}\mathbf{C}^{T}\mathbf{h}(\mathbf{w}) - 2\rho\frac{\mathbf{e}_{x}^{T}\mathbf{C}^{T}\mathbf{C}\mathbf{e}_{x}}{\left\|\mathbf{C}\mathbf{e}_{x}\right\|} \\ &< -\mathbf{e}_{x}^{T}\mathbf{Q}\mathbf{e}_{x} + 2\left\|\mathbf{e}_{x}^{T}\mathbf{C}^{T}\right\|\left\|\mathbf{h}(\mathbf{w})\right\| - 2\rho\left\|\mathbf{C}\mathbf{e}_{x}\right\| \\ &< -\mathbf{e}_{x}^{T}\mathbf{Q}\mathbf{e}_{x} + 2\left\|\mathbf{C}\mathbf{e}_{x}\right\|\left(\bar{h} - \rho\right) \end{aligned} \tag{4.13}$$

By inspection, $\dot{v} < 0$ *if* $\rho > \bar{h}$. In order to guarantee the negative definiteness of $\dot{v}$, We choose ρ sufficiently large to make sure $\rho > \bar{h}$ and compute the sliding mode correction term as $\mathbf{s} = \rho\mathbf{P}^{-1}\mathbf{C}^{T}sign(\mathbf{e}_{y})$.

Knowing $\mathbf{P}^{-1}$ and $\mathbf{C}^{T}$, we start by guessing a values for $\mathbf{Dw}$ and then solve for $\mathbf{h}(\mathbf{w})$ to satisfy $\mathbf{Dw} = \mathbf{P}^{-1}\mathbf{C}^{T}\mathbf{h}(\mathbf{w})$ and its bound $\left\|\mathbf{h}(\mathbf{w})\right\| < \bar{h}$, and then we choose ρ greater than $\bar{h}$.

It follows from (4.6), since $\mathbf{e}_x \to \mathbf{0}$, that the expected value of the term $\mathbf{Dw}-\mathbf{s}$ is zero and $E[\mathbf{Dw}-\mathbf{s}]=(E[\mathbf{Dw}]-E[\mathbf{s}])=0$, and the unknown input $\mathbf{Dw}$ can be estimated as $\mathbf{Dw} \approx E[\mathbf{s}]$. In applications, low pass filtering is used to average the correction term $\mathbf{s}$, i.e., $\mathbf{Dw}=\dfrac{\mathbf{I}}{s\tau+1}\mathbf{s}$.

<u>4.2.2 Fixed Gain and Variable Gain SMCs Derivations</u>

In this section, we derive both fixed and VG SMCs to stabilize the system given in (3.1) repeated below,

$$J\ddot{\theta}_p + b\dot{\theta}_p + F\,\mathrm{sgn}\left(\dot{\theta}_p\right) = \tau_p - \tau_a$$

The control objective is to track the steering angle command with minimum error while compensating for the disturbances. We define the tracking error as the difference between desired and measured steering angle,

$$e = \theta_p - \theta_{p_{des}} \tag{4.14}$$

$$\dot{e} = \dot{\theta}_p - \dot{\theta}_{p_{des}} \tag{4.15}$$

A sliding function is defined as:

$$S = \dot{e} + \lambda e,\ \lambda \succ 0 \tag{4.16}$$

If $\lambda \succ 0$ and $S = 0$ then the error will decay to zero exponentially. Our goal is to find a control $u = \tau_p$ that makes $S \to 0$ as $t \to \infty$

A Lyapunov function candidate is chosen as:

$$V = \frac{1}{2}S^2 \tag{4.17}$$

Taking the derivative of (4.17) yields:

$$\dot{V} = S\dot{S} \tag{4.18}$$

Taking the derivative of (4.16) yields:

$$\dot{S} = \ddot{e} + \lambda\dot{e} = \left(\ddot{\theta}_p - \ddot{\theta}_{p_{des}}\right) + \lambda\left(\dot{\theta}_p - \dot{\theta}_{p_{des}}\right) \tag{4.19}$$

We have from (3.1),

$$\dot{S} = \frac{1}{J}\left(-b\dot{\theta}_p - F\,\mathrm{sgn}\left(\dot{\theta}_p\right) + \tau_p - \tau_a\right) - \ddot{\theta}_{pdes} + \lambda\left(\dot{\theta}_p - \dot{\theta}_{p_{des}}\right) \tag{4.20}$$

Substituting (4.20) in (4.18) yields,

$$\dot{V} = S\left(-\frac{b}{J}\dot{\theta}_p - \frac{F}{J}\mathrm{sgn}\left(\dot{\theta}_p\right) + \frac{1}{J}\tau_p - \frac{1}{J}\tau_a - \ddot{\theta}_{p_{des}} + \lambda\left(\dot{\theta}_p - \dot{\theta}_{p_{des}}\right)\right) \tag{4.21}$$

$\dot{V}$ is negative definite if

$$\begin{gathered} -\frac{b}{J}\dot{\theta}_p - \frac{F}{J}\mathrm{sgn}\left(\dot{\theta}_p\right) + \frac{1}{J}\tau_p - \frac{1}{J}\tau_a - \ddot{\theta}_{p_{des}} + \lambda\left(\dot{\theta}_p - \dot{\theta}_{p_{des}}\right) = \\ \begin{cases} < 0\,for S > 0 \\ = 0\,for S = 0 \\ > 0\,for S < 0 \end{cases} \end{gathered} \tag{4.22}$$

A control law that can achieve this requirement is:

$$\begin{aligned} \tau_p = {} & b\dot{\theta}_p + F\,\mathrm{sgn}\left(\dot{\theta}_p\right) + \tau_a + J\ddot{\theta}_{p_{des}} - J\lambda\left(\dot{\theta}_p - \dot{\theta}_{p_{des}}\right) \\ & -\eta\,\mathrm{sgn}\left(S\right),\ \eta \succ 0 \end{aligned} \tag{4.23}$$

For VG SMC, we choose η to be equal to $k_1 + k_2 S^2$ and the control law becomes:

$$\tau_p = b\dot{\theta}_p + F\,\mathrm{sgn}\left(\dot{\theta}_p\right) + \tau_a + J\ddot{\theta}_p - J\lambda\left(\dot{\theta}_p - \dot{\theta}_{p_{des}}\right) - \left(k_1 + k_2 S^2\right)\mathrm{sgn}\left(S\right) \tag{4.24}$$

The overall gain $\eta = k_1 + k_2 S^2$, depends on the magnitude of S as:

$\eta \to k_1$ as $S \to 0$ and $\eta \to$ large value as $S \to$ large value.

When we are too far from the sliding surface, the gain is large which enables fast convergence to the sliding surface (this represents transitioning driving and evasive maneuvers angle requests).

Once we reach the sliding surface, the gain is very small and just enough to keep us from deviating from the sliding surface (this represents driving on straight road and constant radius curves), which eliminates chattering and the need for gain look up tables.

For FG SMC, we choose η to be equal to K and the control law becomes,

$$\tau_p = b\dot{\theta}_p + F\,\mathrm{sgn}\left(\dot{\theta}_p\right) + \tau_a + J\ddot{\theta}_{p_{des}} - J\lambda\left(\dot{\theta}_p - \dot{\theta}_{p_{des}}\right) - K\,\mathrm{sgn}\left(S\right),\quad K > 0 \qquad (4.25)$$

As can be seen, the gain $\eta = K$ is constant and does not depend on the magnitude of S, which means we will always have a constant gain regardless of the magnitude of the error, unlike the VG SMC that adjusts its gain automatically based on the magnitude of the error.

In general, and regardless if it is fixed or variable gain sliding mode control, η is called the reaching phase gain and it is tuned to control the speed of convergence to the sliding surface. λ is the sliding phase gain and it is tuned to control steady state error once we are on the sliding surface.

4.2.3 Simulation Results of Observer Based Sliding Mode Control

This section shows the observer results and the variable gain observer-based SMC performance. To validate the aligning moment estimation, it was compared to the model-based estimation developed in chapter three.

In the observer design, we approximated and guessed $\mathbf{Dw}$ to be $\begin{bmatrix}0\\5\end{bmatrix}[1]$, we know $\mathbf{C}^T = [1 \quad 0]'$, and computed $\mathbf{P}^{-1} = \begin{bmatrix}0.0609 & 0.0337\\0.0337 & 0.1706\end{bmatrix}$, then we substituted those terms in $\mathbf{Dw} = \mathbf{P}^{-1}\mathbf{C}^T\mathbf{h}(\mathbf{w})$ to solve for $\mathbf{h}(\mathbf{w})$ as,

$$\begin{bmatrix}0\\5\end{bmatrix}[1] = \begin{bmatrix}0\\5\end{bmatrix} = \begin{bmatrix}0.0609 & 0.0337\\0.0337 & 0.1706\end{bmatrix}\begin{bmatrix}1\\0\end{bmatrix}h(w) \le \begin{bmatrix}0.0609\\0.0337\end{bmatrix}\bar{h}$$

$\rightarrow \begin{bmatrix}0\\5\end{bmatrix} \le \begin{bmatrix}0.0609\\0.0337\end{bmatrix}\bar{h} \rightarrow \bar{h} \ge 148.37$, ρ then was chosen to be $350 \succ \bar{h} \succ 148.37$.

Figures 4.1- 4.6 demonstrate the simulation results of the sliding mode observer and the observer-based SMC to a sine wave steering angle request. Figure 4.1 compares the correction term s_2 with the estimated disturbance resulting from low pass filtering it. The correction term is a vector $\mathbf{s} = [s_1 \quad s_2]'$, but we are only interested in s_2 because s_1 is just an estimate of zero. The estimated disturbance is obtained by averaging the correction term s_2 as explained in section 4.1.1. Figure 4.2 compares the estimated disturbance and the actual disturbance. As can be seen from Figure 4.2, from 0 to about 20s, it was only pure aligning moment from the model, and then from 20s to about 50s an additional random disturbance was added to the aligning moment to emulate disturbance torque from the driver, and then at 50s the additional disturbance was removed, it can be seen that the observer estimated both the aligning moment and the random disturbance very well. The noticed spikes in the estimate at the zero angular velocity crossing when we reversed the steering direction is due to the static friction or the breakaway friction.

Figure 4.3 shows the VG SMC response and its capability to reject the disturbance, excellent tracking was achieved and robustness to disturbances was demonstrated. Figure 4.4 shows the controller output which is the pinion torque. The noticed glitches in the torque correspond exactly to the glitches in the disturbance estimate in Figure 4.2 at the zero-velocity crossing when we reverse direction, due to the compensation of the controller to the static friction. Figures 4.5 and 4.6 show the results of the state vector estimation, the pinion angle and pinion angular velocity, respectively, which matches very well with the actual measured states from the model. The estimated states are fed back and used in the controller instead of the actual states from the model.

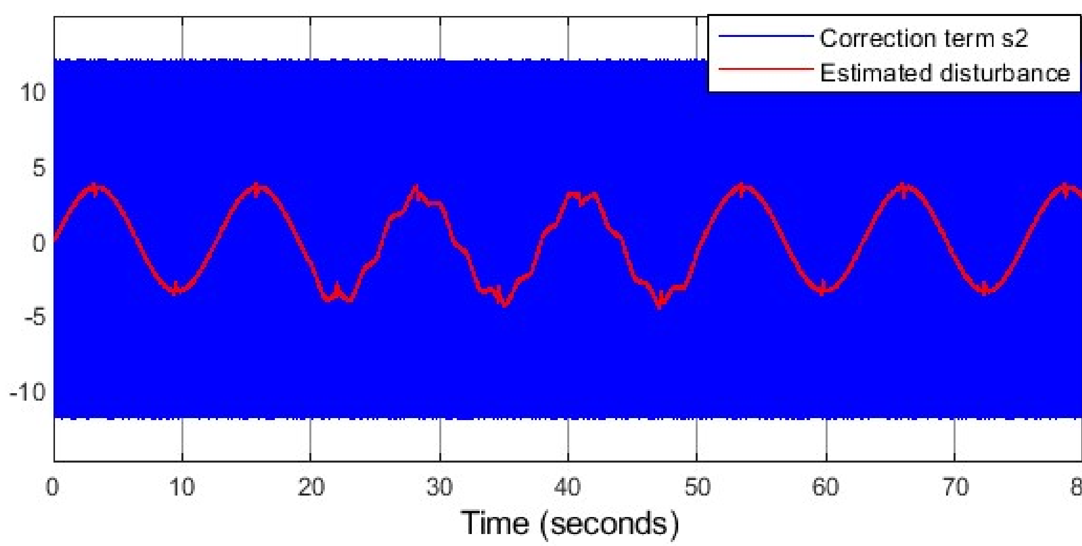

Figure 0.1 Estimated disturbance resulting from low pass filtering s_2.

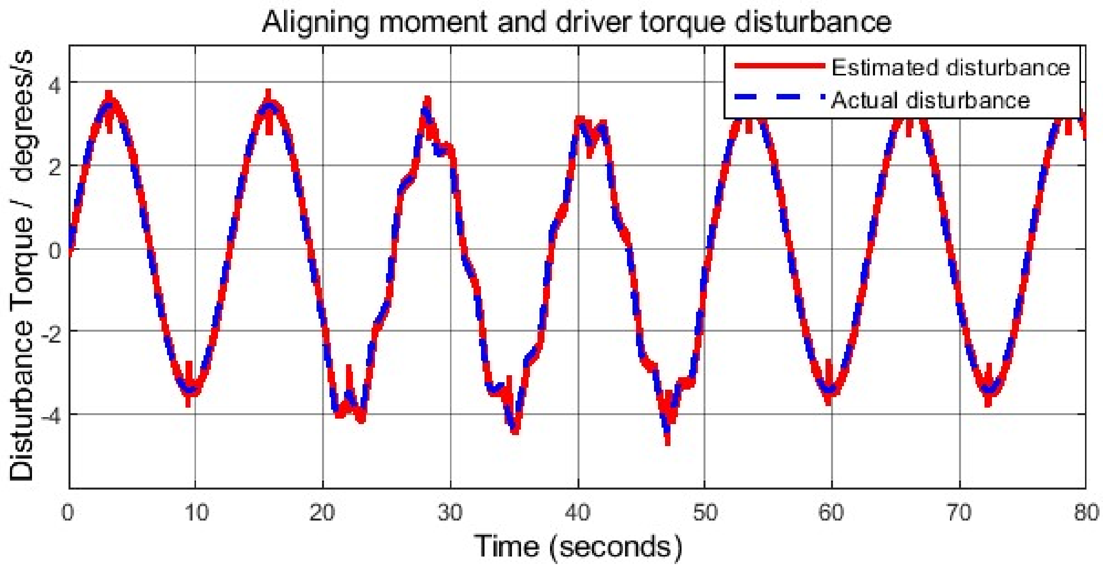

Figure 0.2 Estimated disturbance vs. actual disturbance.

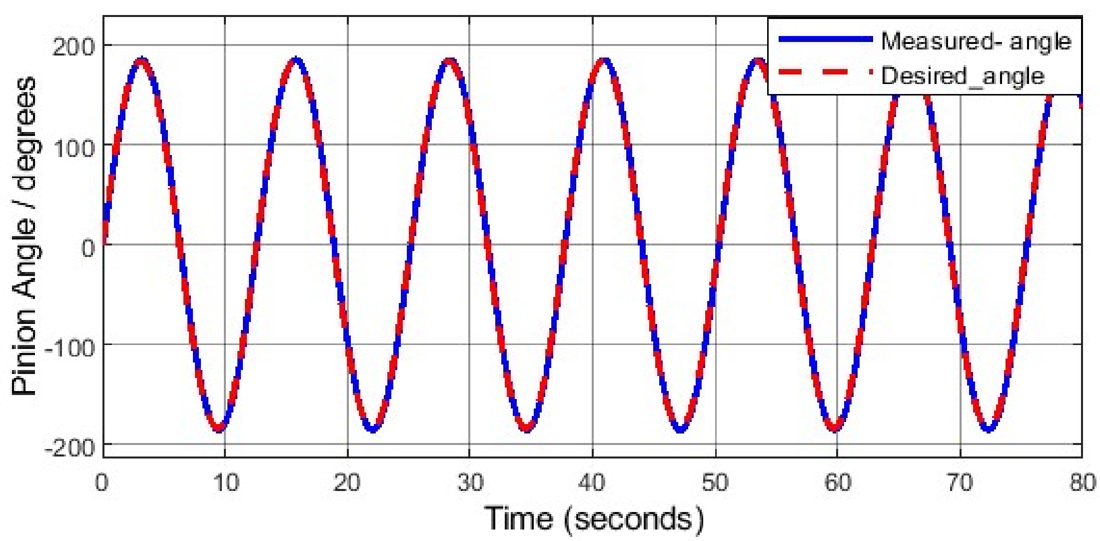

Figure 0.3 Desired angle vs. actual angle.

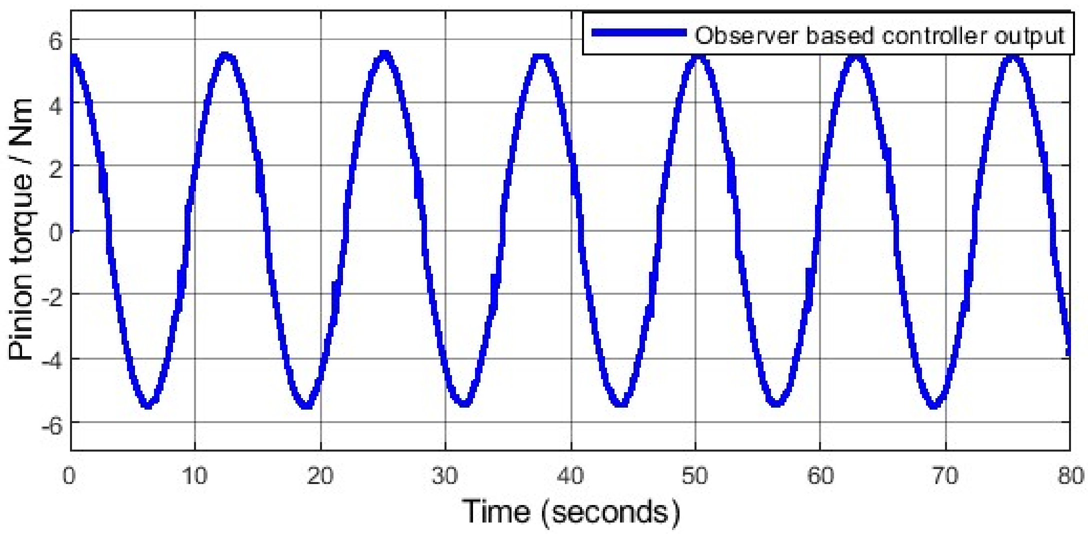

Figure 0.4 Observer based VG SMC controller output.

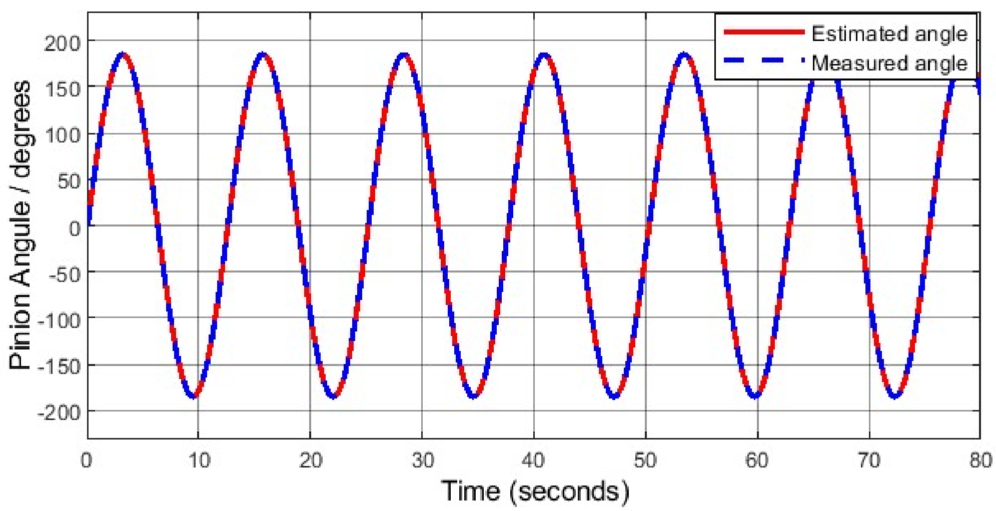

Figure 0.5 Estimated angle vs. measured angle.

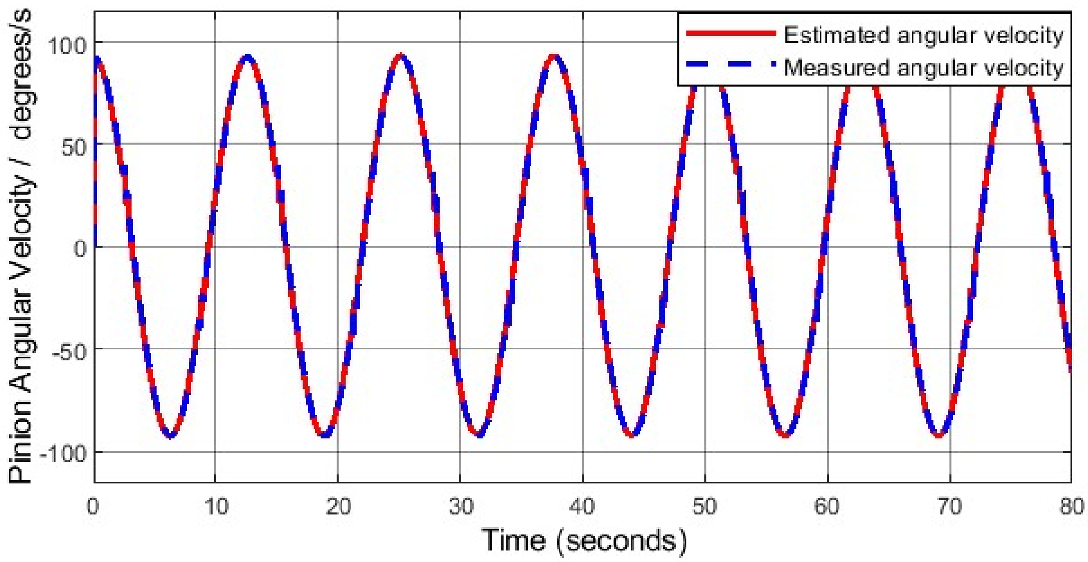

Figure 0.6 Estimated angular velocity vs. measured angular velocity.

4.2.4 Simulation Results of Comparison of FG and VG SMCs

To compare the performance of the VG SMC with the FG SMC, both were tested at multiple scenarios with the same steering angle requests (a big angle and a small angle), and their performance is compared. Both the angle response and the control output (torque request) were plotted. Although the FG SMC showed satisfactory results, there was obvious chattering in the control output which affected the controller response. The VG SMC showed much better and smoother performance due to the significant reduction in the chattering. Figures 4.7- 4.10 show the responses of both the fixed and VG SMC to a square wave or step of small steering angle (30 degrees) and Figures 4.11- 4.14 show the responses of both controllers to a square wave or step of large steering angle (200 degrees). In the FG SMC, two different sets of tuning parameters were needed for the small and big angles. The reaching phase gain that worked for the small SA request, $\eta = K = 15$, was not sufficient for the large SA request and we had to increase it manually to $\eta = K = 100$. In the VG SMC, initially the parameters k_1, k_2 were tuned once and then the controller adjusted the reaching phase gain $\eta = k_1 + k_2 S^2$ automatically for both the small and large angle requests to achieve the desired performance without having to change any gains manually, or tune the controller gains differently for large and small angles, which eliminated the need for gain scheduling. Similarly, Figures 4.15-4.18 compare the response of both fixed and VG SMC to a triangular wave. The idea in the VG SMC is that we want the reaching phase gain to be large only when the error is big and we are too far from the surface. We try to make it decrease gradually as we approach the sliding surface until it teaches a very small value once we are on the surface, just to keep us from deviating from the surface, and that eliminates chattering

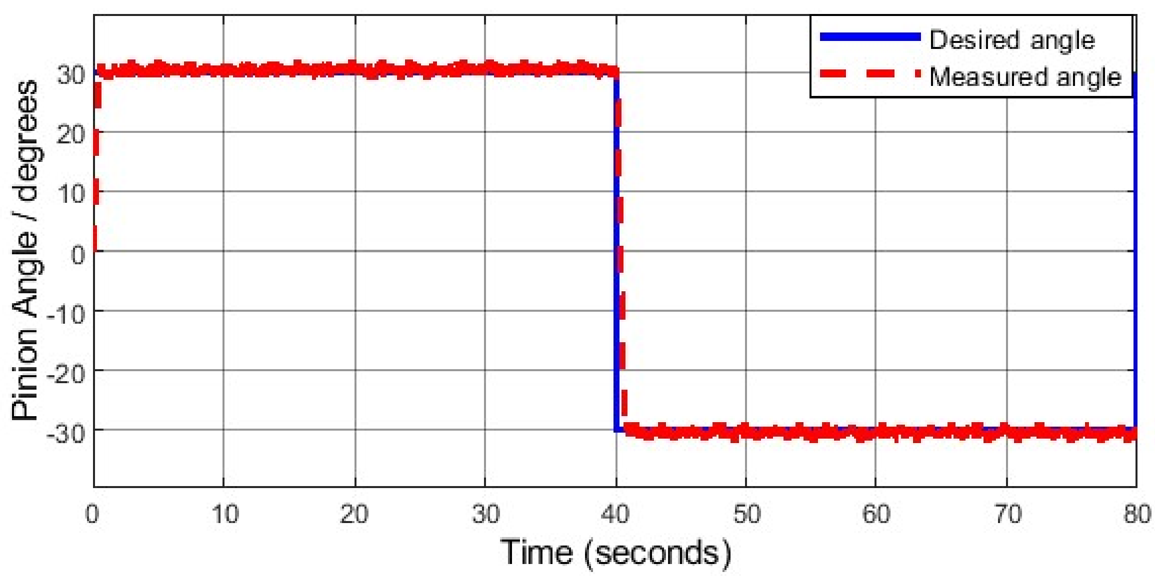

Figure 0.7 FG SMC response to a small steering angle request.

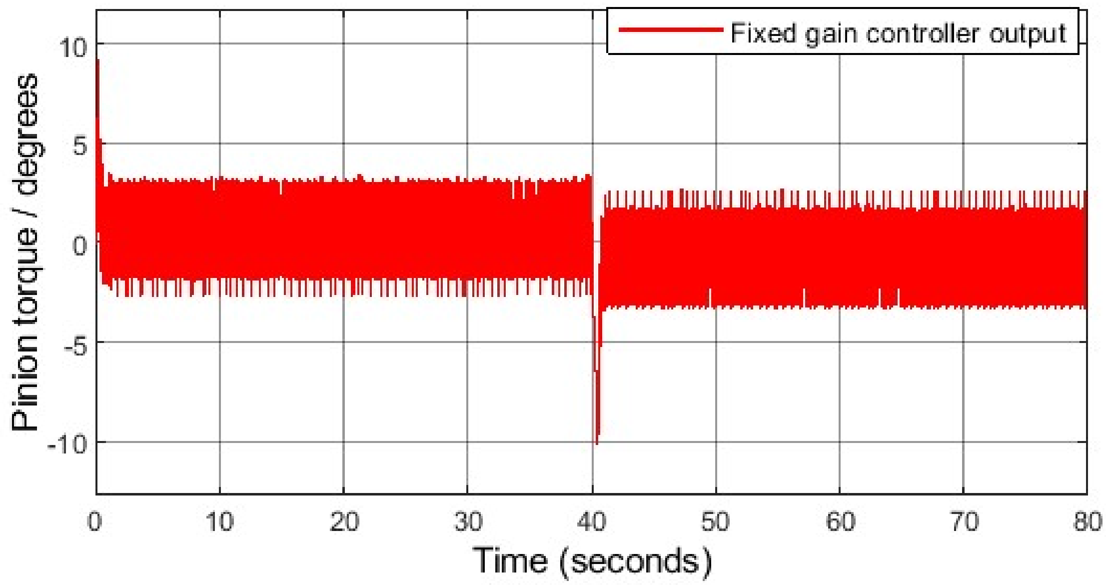

Figure 0.8 FG SMC output corresponding to the senario in Figure 4.7.

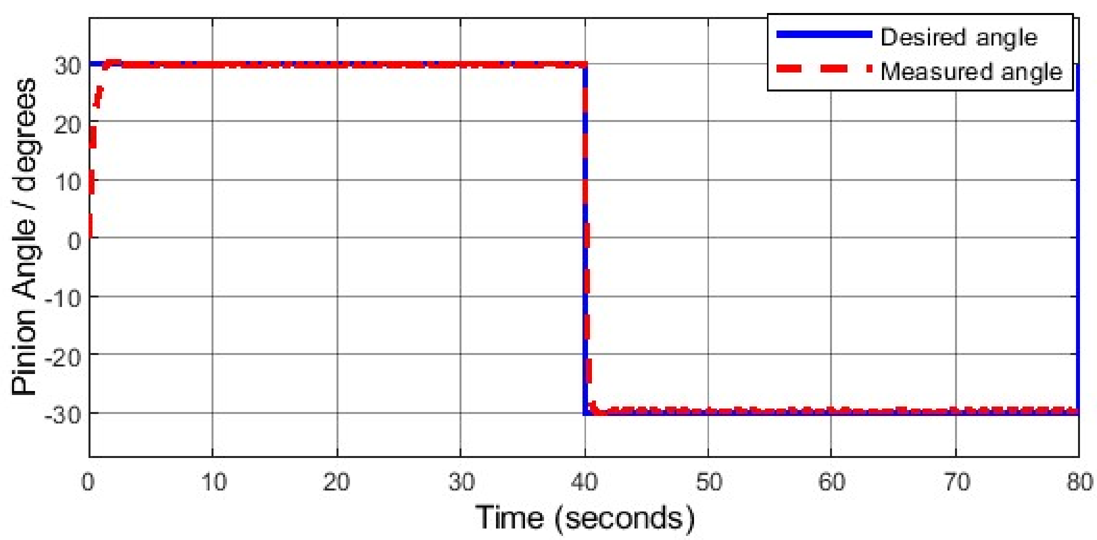

Figure 0.9 VG SMC response to a small steering angle request.

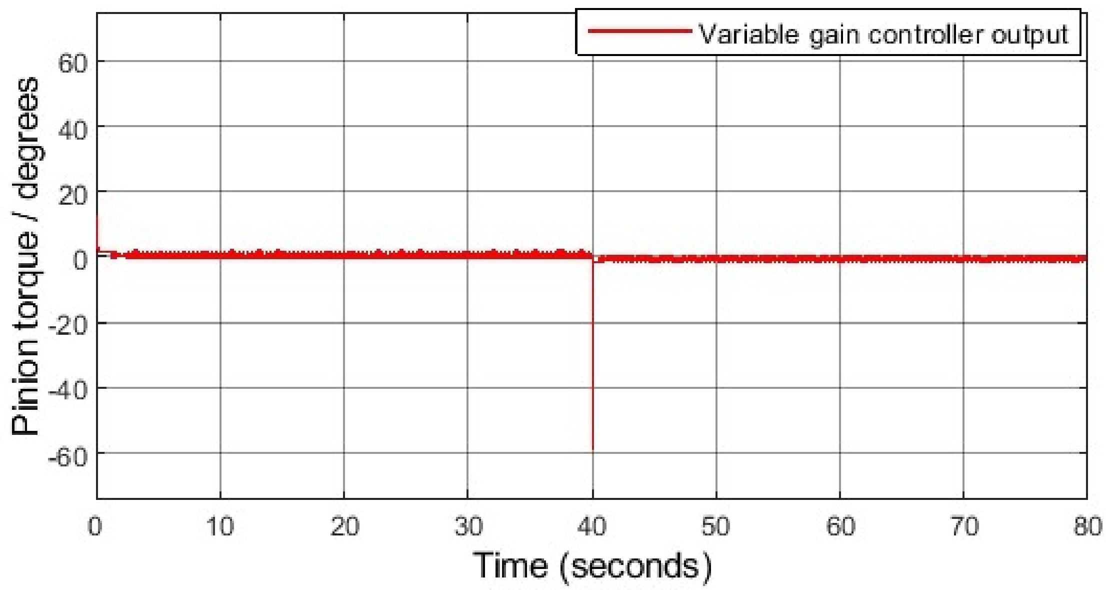

Figure 0.10 VG SMC output corresponding to the senario in Figure 4.9.

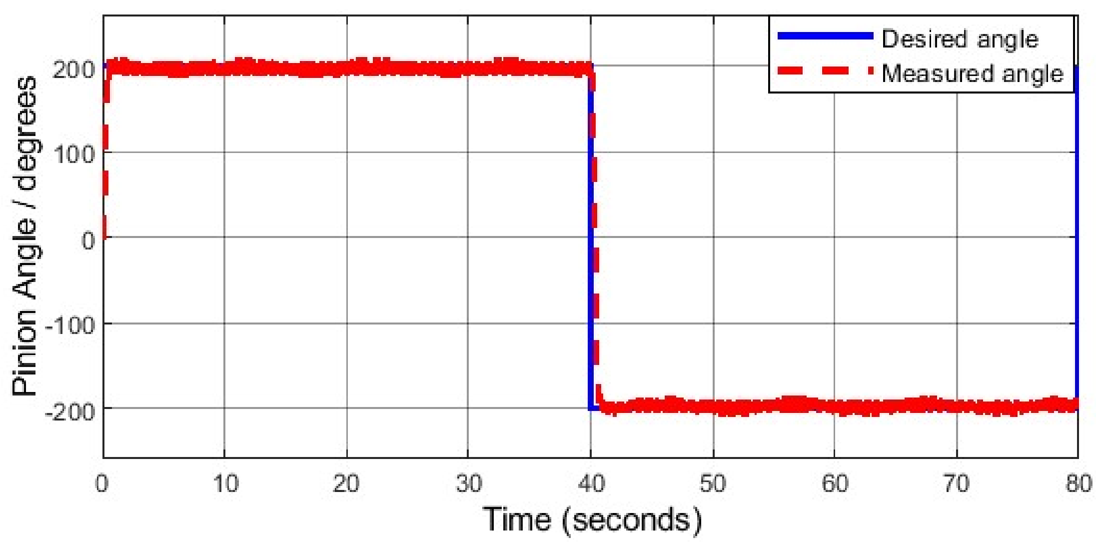

Figure 0.11 FG SMC response to a large steering angle request.

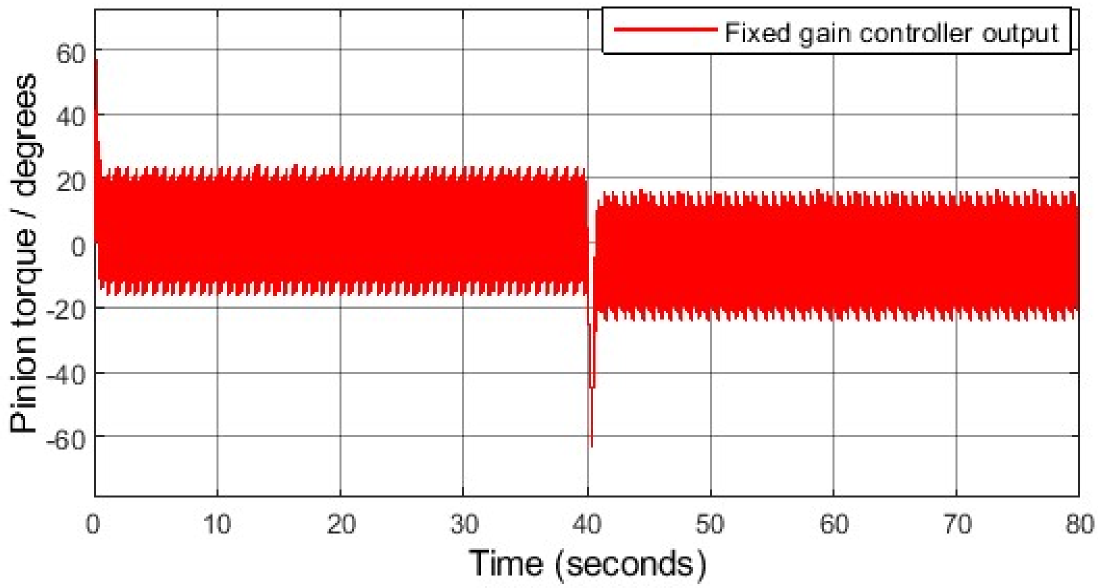

.

Figure 0.12 FG SMC output corresponding to the scenario in Figure 4.11.

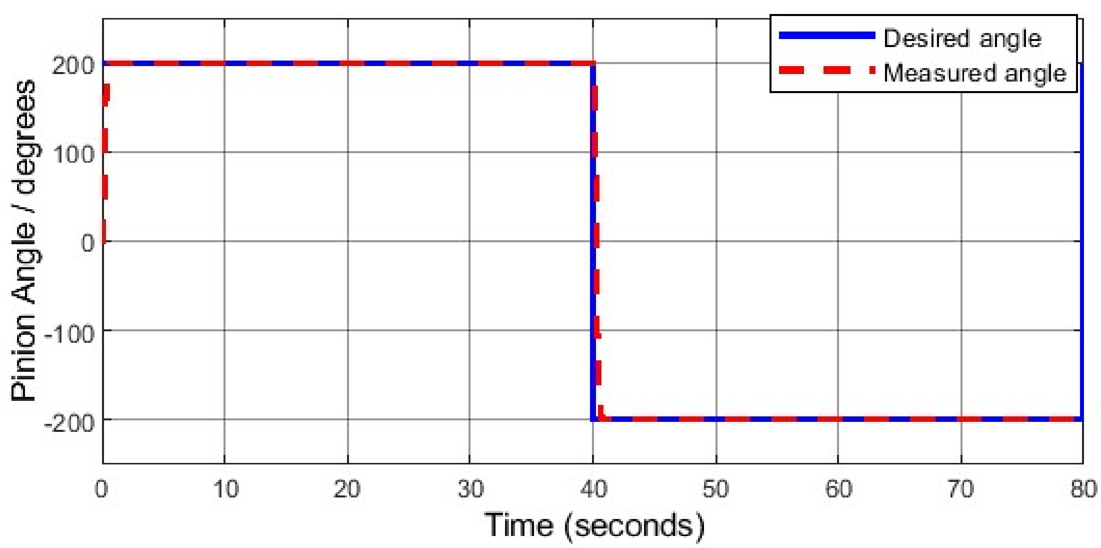

Figure 0.13 VG SMC response to a large steering angle request.

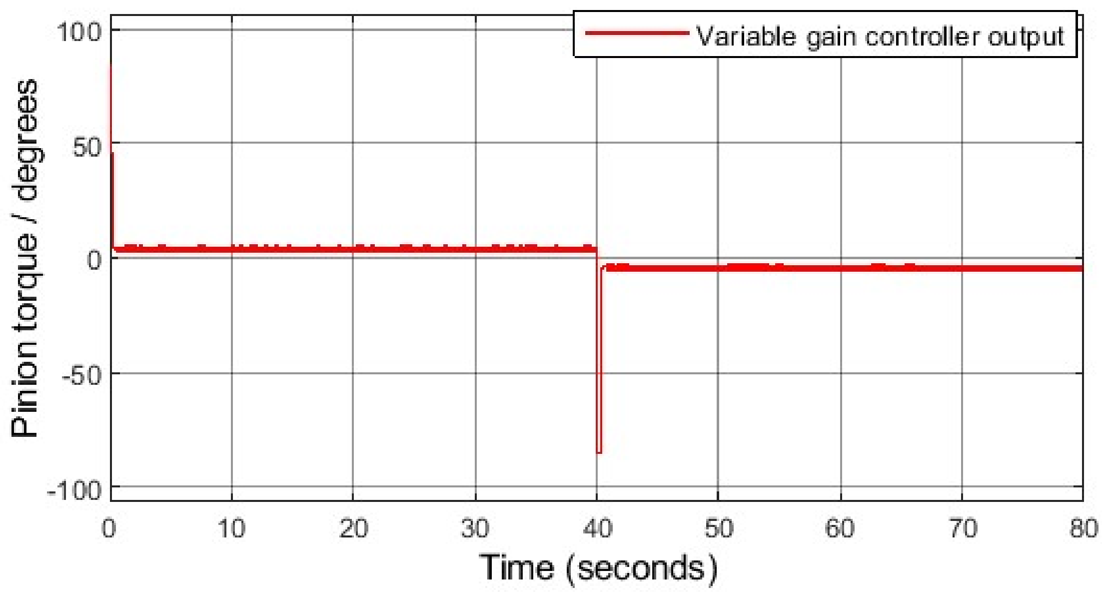

Figure 0.14 VG SMC output corresponding to the scenario in Figure 4.13.

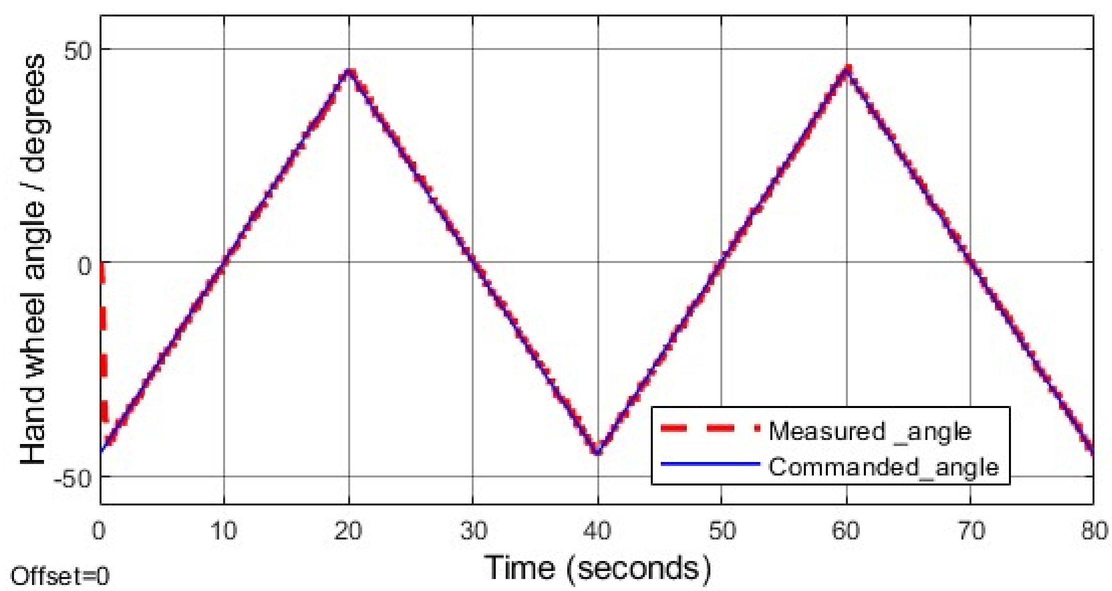

Figure 0.15 FG SMC response to a triangle wave steering angle request

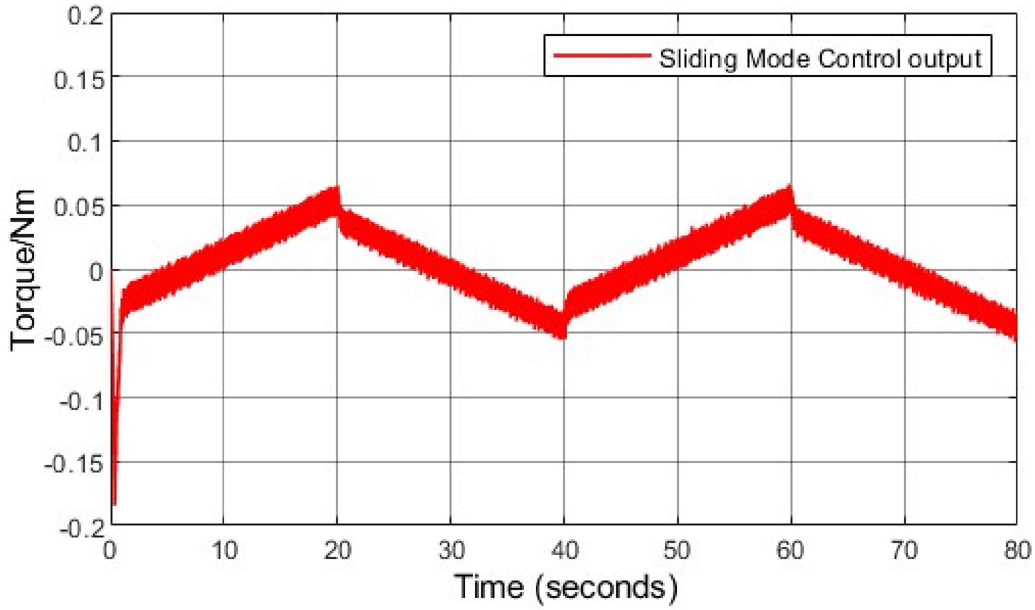

Figure 0.16 FG SMC output corresponding to the scenario in Figure 4.15.

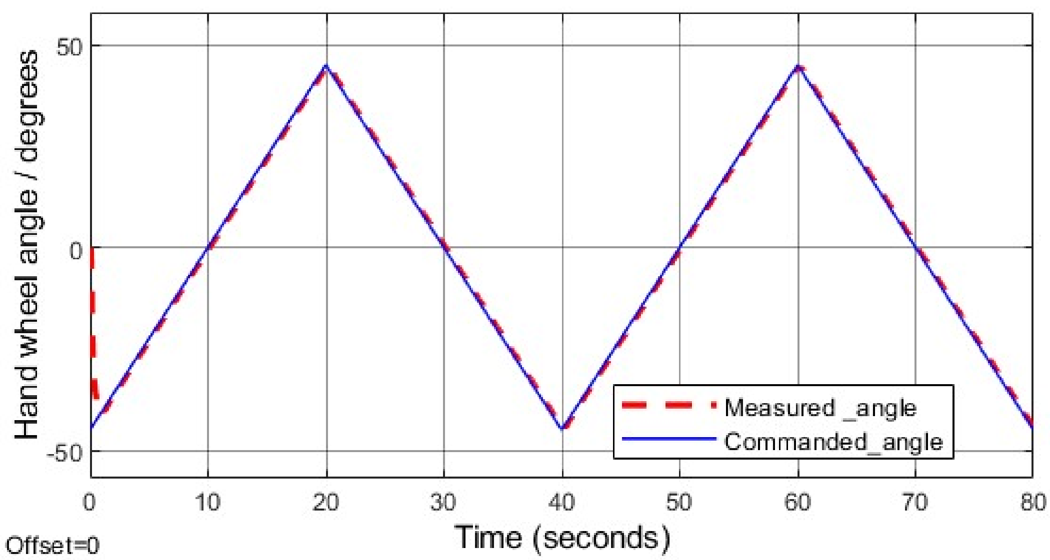

Figure 0.17 FG SMC response to a triangular wave steering angle request

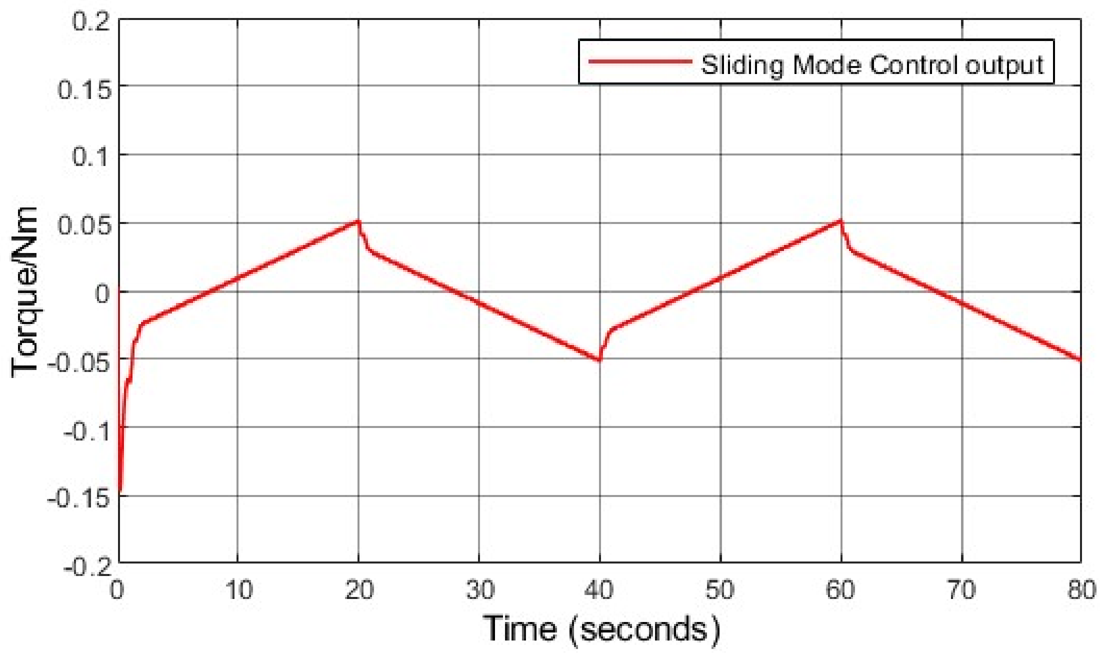

Figure 0.18 FG SMC output corresponding to the scenario in Figure 4.17.

4.2.5 Experimental Results of Variable Gain SMC

Experiments were performed on the test vehicle to validate the VG SMC. The vehicle is equipped with dSPACE AutoBox and EPS to actuate steering. The EPS in the vehicle is designed for autonomous highway driving, for this reason it has limitations on torque and torque gradient, it also has active damping on top of the viscous damping inherent in the system to add more stability. These limitations are hardcoded in the EPS software and can't be changed by the end user. The experimental results show both the angle and the torque controllers' response. The torque controller closes the loop of the SA controller torque request, but we have no control over its performance since it is a black box from the EPS manufacturer, but we can measure the actual torque and compare it with the SMC torque request to help us analyze the results. A signal generator was used to send steering angle commands to the SMC which computes the torque command required to achieve the desired angle and sends it to the torque controller.

Initially the VG SMC controller parameters were tuned to be $k_1 = 10$, $k_2 = 0.001$, $\lambda = 50$, then the controller automatically adjusted the reaching phase gain, $\eta = k_1 + k_2 S^2$, based on the magnitude of S, which is a function of error and error derivative, which means that the controller automatically adjusts the gain based on the size of the error and the error derivative.

Figure 4.19 is a response of a steering angle controller using other linear methods just to demonstrate the effect of the asymmetrical hysteresis behavior of the steering system, caused by stiction and backlash, on the steering angle response and compare it with the proposed method. As can be seen, the behavior in left and right directions is not the same, which is caused by asymmetry and bias caused by the steering angle sensor offset.

Figures 4.20 and 4.21 show the steering angle and the steering torque responses respectively, due to a square wave steering angle command of 18 degrees amplitude at about 17.9 mps/40 mph. Because of actuator limitations and delay, there will always be some delay in the angle response in the real vehicle, unlike simulations which assumes perfect actuator. As can be seen from figure 4.20, rise time is less than 200 ms which is very reasonable for a step response, steady state angle error is very close to zero, and there is about 20 percent first overshoot. A first overshoot in the step response is system inherent, it is due to the phase lag in the dynamics of the steering counter force. As can be seen from Figure 4.21, the torque request was saturated at about 1.5 Nm in motor torque unit (42 Nm in pinion torque unit), which can also contribute to a delay in the angle response. The small glitch in the middle of the steering angle transient response in figure 4.20 is due to the active damping in the torque controller, as can be seen in the oscillatory behavior of the torque response in figure 4.21. Figures 4.22-4.23 show the response of the same scenario as the previous one at a higher speed, 31.3 mps/70 mph. Because of the limitations of the test track, we could not get a longer recording at this speed.

Figures 4.24-4.25 show the response to a sine wave steering angle request of 40 degrees amplitude at 17.9 mps/40 mph. The delay is only 60 ms which is due to the torque gradient limits that can be noticed in the torque response in Figure 4.25. Figures 4.26-4.27 show the response to a sine wave steering angle request of 9 degrees amplitude at 31.3 mps/70 mph. Usually it is more challenging to achieve the small angle request because at small angles, there is less torque to overcome friction, and movment is not going to occur until there is enough torque at the motor shaft to overcome friction. It can be noticed that there is some chattering in Figures 4.26-4.27, especially at the zero angular velocity crossing because of the controller trying to overcome friction, but it is very minor and can hardly be felt in the steering wheel. The tracking error is very close to zero and the controller was able to overcome the force of friction very well when we reversed direction. Figures 4.28-4.29 show the controller response to a steering angle request of a ramp down to -150 degrees and then ramp back to zero at 9 mps/20 mph.

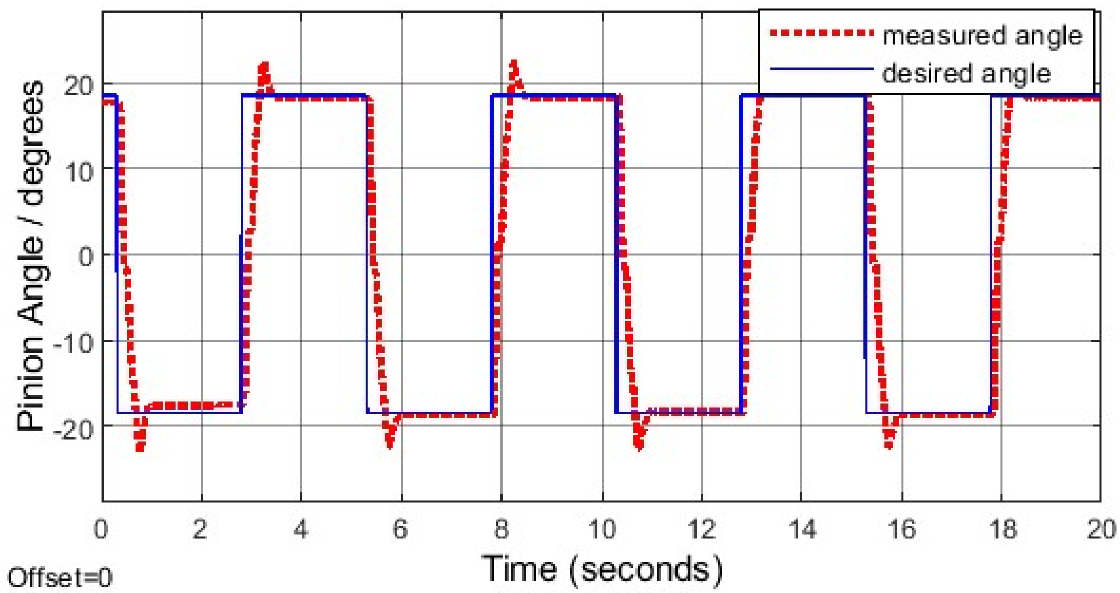

Figure 0.19 VG SMC response for a steering angle square wave request at 17.9 mps/40 mph.

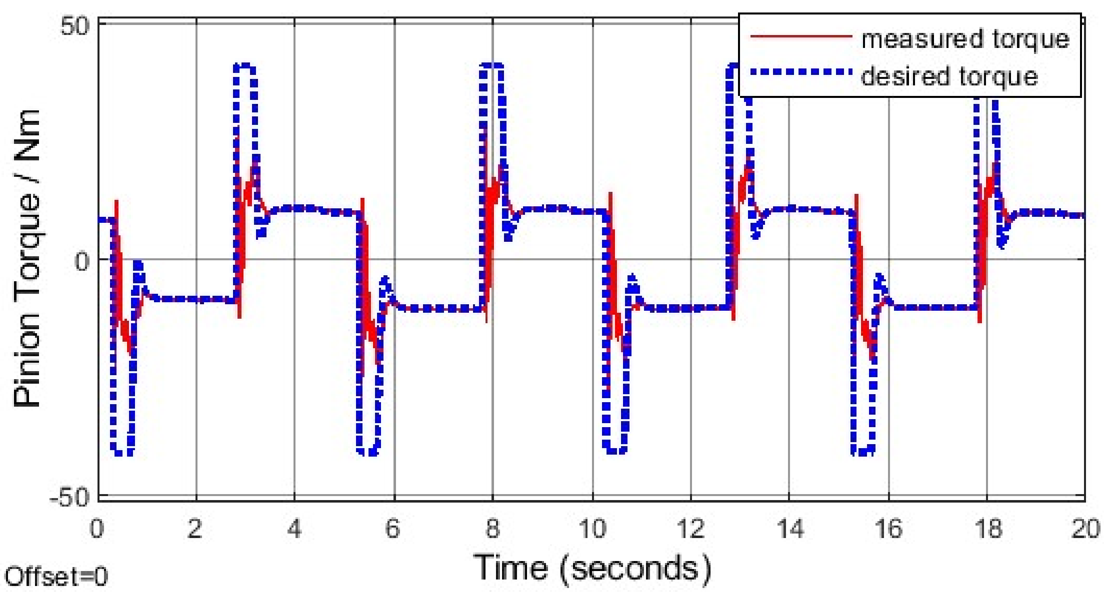

Figure 0.20 STC response corresponding to the scenario in Figure 4.20.

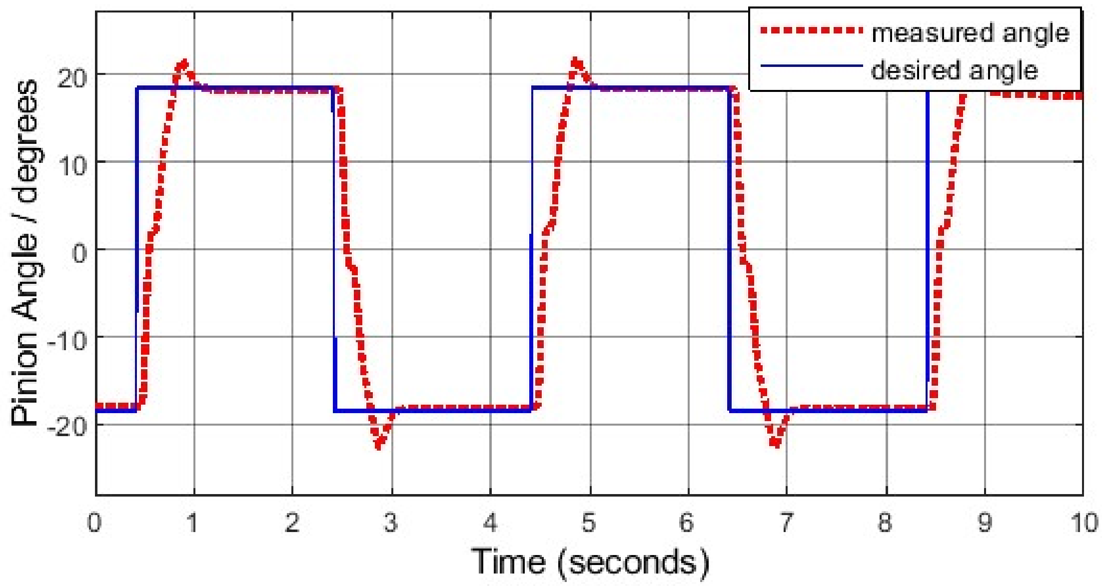

Figure 0.21 VG SMC response for a steering angle square wave request at 31.3 mps/70 mph.

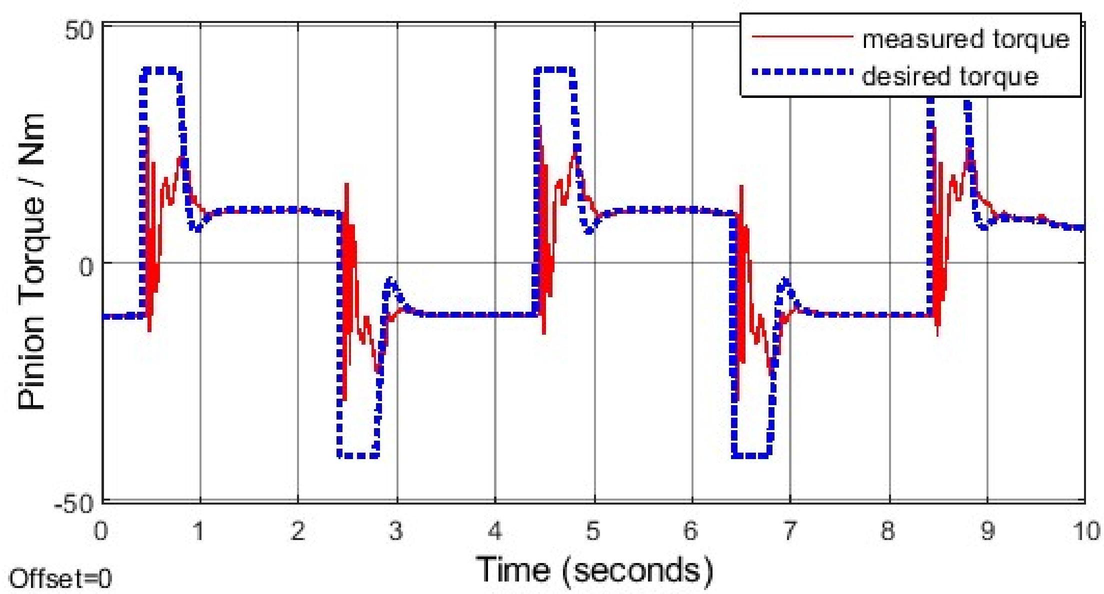

Figure 0.22 STC response corresponding to the scenario in Figure 4.22.

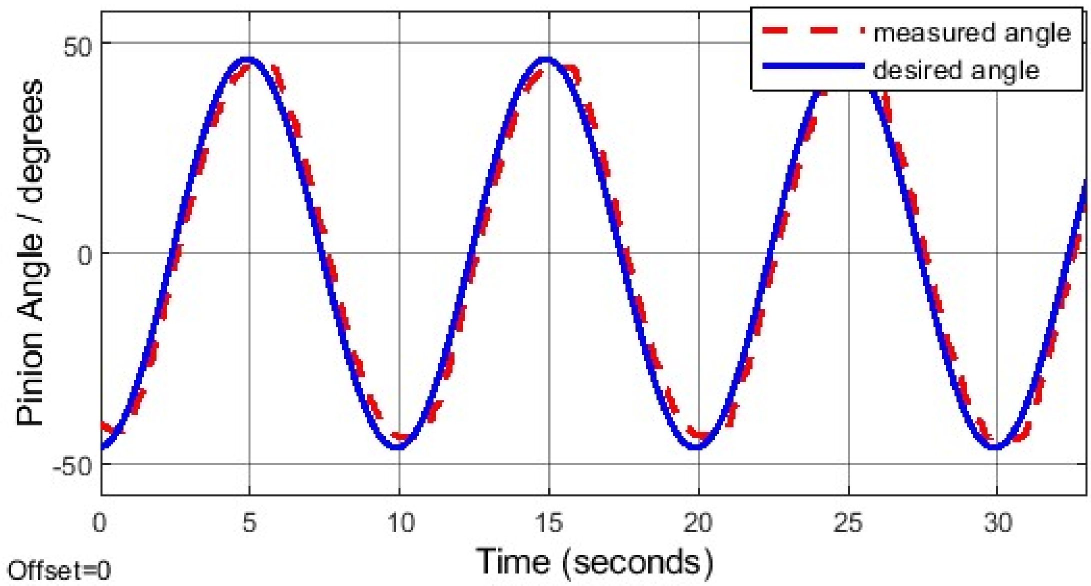

Figure 0.23 VG SMC response for a sinusoidal steering angle request at 17.9 mps/ 40 mph.

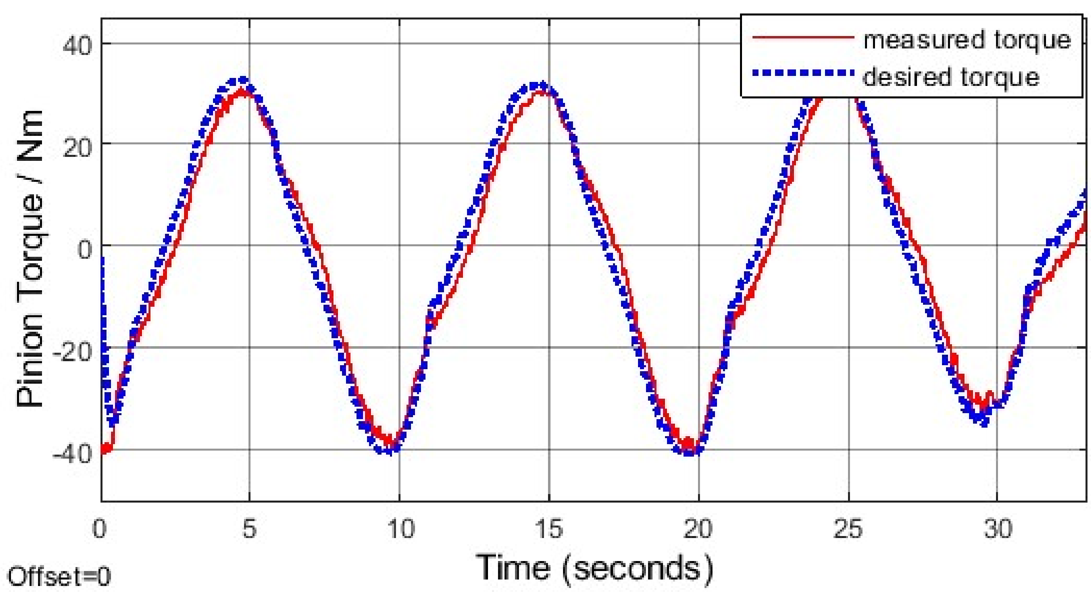

Figure 0.24 STC response corresponding to the scenario in Figure 2.24.

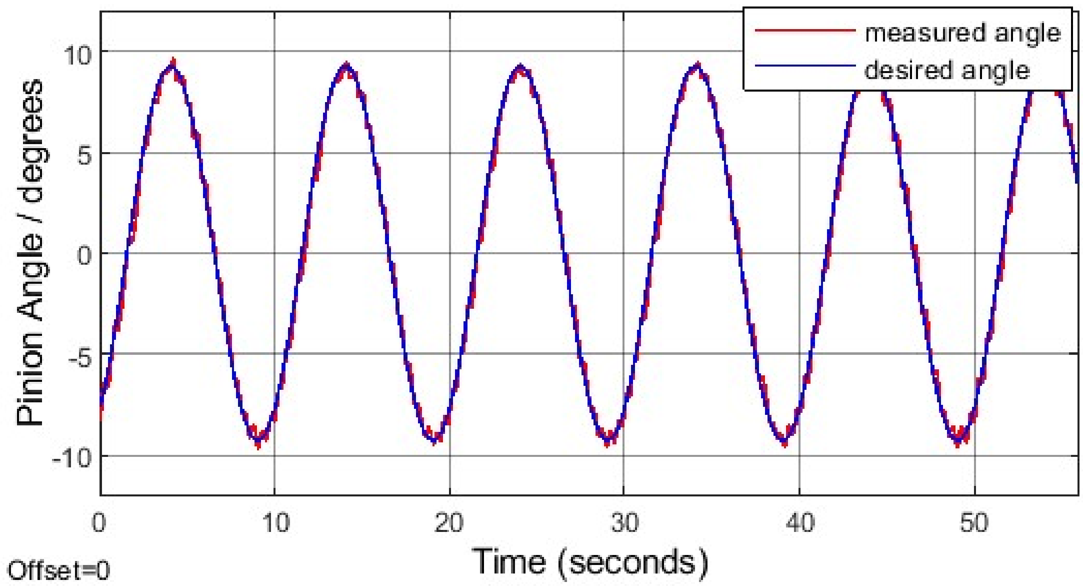

Figure 0.25 VG SMC response for sinusoidal steering angle request at 31 mps/70 mph.

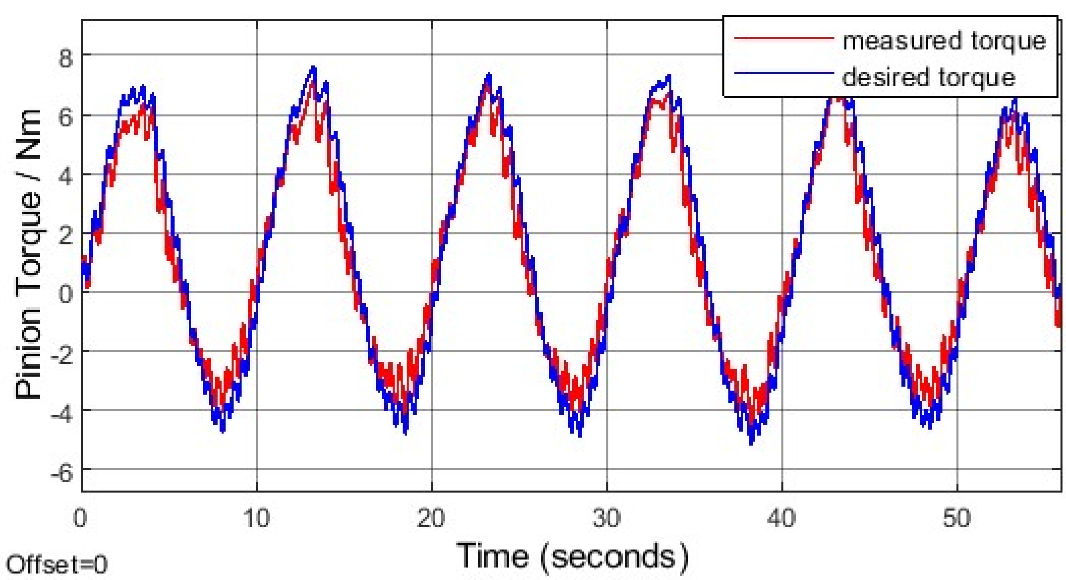

Figure 0.26 STC response corresponding to the scenario in Figure 4.26.

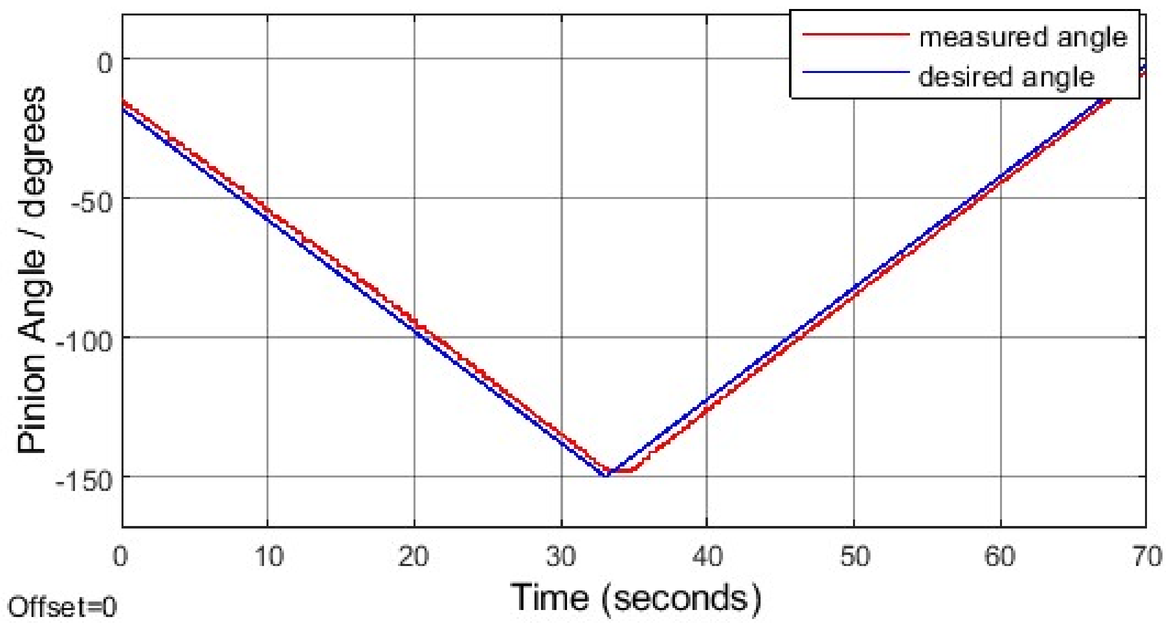

Figure 0.27 VG SMC response for a steering angle triangular wave at 9mps/20mph.

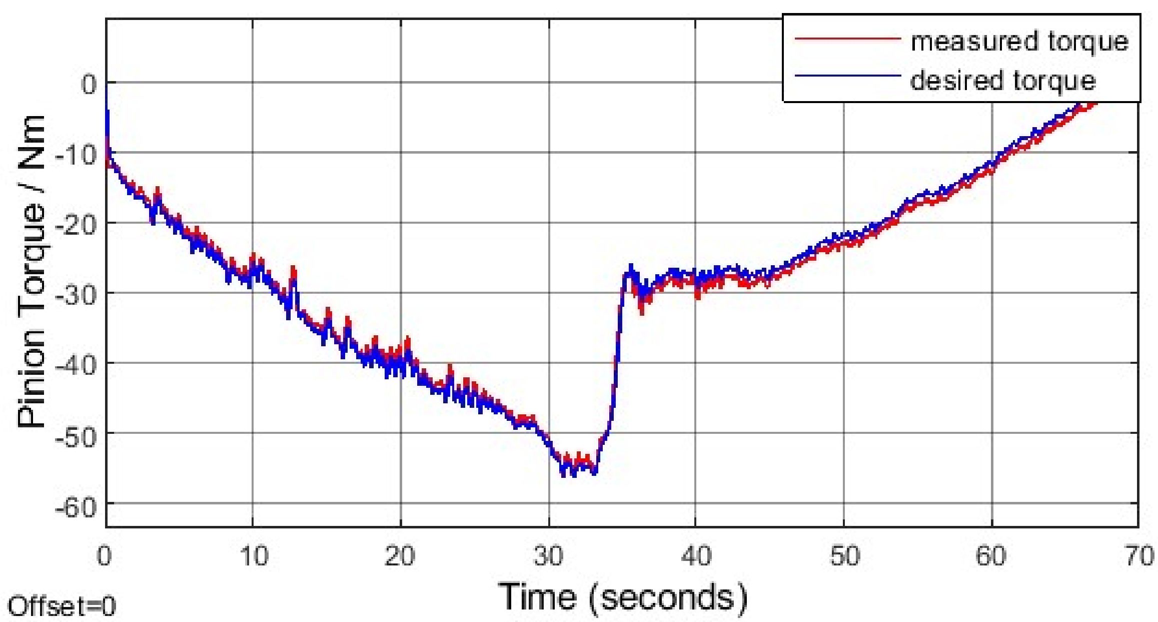

Figure 0.28 STC response corresponding to the scenario in Figure 4.28

4.3 Adaptive Backstepping (ABS) Control of EPS Angle

As discussed earlier, robust, and adaptive control are the two major and complementary approaches to dealing with model inaccuracies. To design a robust controller, a priori reasonable estimates of the parameter bounds is required, while in adaptive control, no a priori information about the unknown parameters is required because of the learning behavior of adaptive control systems. An adaptation mechanism is developed in adaptive control to adjust the parameters in the control law online. The objective of the adaptation is to make the controller tracking error converge to zero. A powerful and unique approach to adaptive control is adaptive backstepping control (ABS).

Backstepping control (BS) is a recursive Lyapunov based design that breaks the control design problem of the whole system into a sequence of lower order design problems. This allows solving stabilization, regulation, and tracking problems under less restrictive conditions because of the flexibility that exists with lower orders systems. This property does not exist in other methods. The method was proposed by Krstic, Kanellakopoulos and Kokotovic in the beginning of 1990s in [12]. This book provides a comprehensive explanation of the backstepping control design procedure, with its applications to adaptive control of nonlinear systems. The key idea of backstepping is to design a series of control laws recursively by treating some of the state variables of a system as “virtual controls” or “pseudo controls” and designing for them intermediate control laws. The method is applicable to classes of linear and nonlinear systems in the strict feedback or pure feedback forms.

BS can be considered as feedback linearization on a Lyapunov function, where the nonlinearities in the derivative of the Lyapunov function are cancelled, however, the useful nonlinear terms need not be cancelled because they can be utilized to improve the closed loop system behavior. The fact that useful nonlinear terms can be retained in the Lyapunov function derivative is the most important advantage of backstepping over other nonlinear control methods such as input-state and input-output feedback linearization.

The theory of backstepping consists of two parts, non-adaptive backstepping, or simply backstepping, and adaptive backstepping (ABS). In non-adaptive backstepping, the controlled plant parameters are assumed to be known; whereas in adaptive backstepping, the parameters are assumed to be unknown and parameters update laws have to be developed to estimate them, whereby creating a powerful adaptive control technique. ABS is a nonmodular adaptive control design, which means that the parameter estimator is part of the controller module and there is a built-in interaction between the estimator and the control law. Unlike the traditional estimation-based adaptive control methods, backstepping is not a "certainty equivalence" approach, which means that the plant parameters don't have to converge to their true values in order for the controller to have perfect tracking. In the ABS approach, stronger control laws are designed that achieve the desired control objective by adjusting the parameters update laws or by attenuating the effect of parameter estimation errors. In the next section, we are going to develop a steering controller using the ABS approach. As outlined in [1], parameter convergence in adaptive control is "on a need-to-know basis". If the system is highly dynamic and we can't stabilze the closed loop system and reach our tracking and regulation objectives unless the plant parameters converge, then they will converge

4.3.1 ABS Steering Angle Controller design

The control objective is to design an adaptive backstepping tracking control law $u(t)$ for (3.2), repeated below,

$$\begin{bmatrix} \dot{\theta}_p \\ \ddot{\theta}_p \end{bmatrix} = \begin{bmatrix} 0 & 1 \\ 0 & -\frac{b}{J} \end{bmatrix} \begin{bmatrix} \theta_p \\ \dot{\theta}_p \end{bmatrix} - \begin{bmatrix} 0 \\ \frac{F}{J}\operatorname{sgn}\left(\dot{\theta}_p\right) \end{bmatrix} + \begin{bmatrix} 0 \\ \frac{1}{J} \end{bmatrix} \tau_p - \begin{bmatrix} 0 \\ \frac{1}{J} \end{bmatrix} \tau_a$$

such that the output $y(t) = x_1(t) = \theta_p(t)$ tracks a reference signal $y_r(t) = \theta_{p_{desired}}(t)$ where $y_r(t), \dot{y}_r(t)$, and $\ddot{y}_r(t)$ are piecewise continuous and bounded. The adaptive controller can ensure the boundedness of the closed-loop states and asymptotic tracking. It is designed by combining a parameter estimator, which provides estimates of unknown parameters and disturbances with a control law.

Define the state variables as $x_1 = \theta_p, x_2 = \dot{\theta}_p$, with control input $u = \tau_p$, and let $\phi_1 = \frac{b}{J}$, $\phi_2 = \frac{1}{J}\left(F\operatorname{sgn}(\dot{\theta}_p) + \tau_a\right)$, $b_2 = \frac{1}{J}$

The resulting system is given by,

$$\begin{aligned} \dot{x}_1 &= x_2 \\ \dot{x}_2 &= -\phi_1 x_2 - \phi_2 + b_2 u \end{aligned} \tag{4.26}$$

It can be seen from (4.26) that the system satisfies the matching condition, because the uncertainty (unknown parameters) and the control input u appear in the same equation, which means that the uncertainty and the control are "matched" and the level of uncertainty is zero. In this case, the terms containing unknown parameters can be directly cancelled by u when they are known and the adaptive design is straightforward. In other cases (not applicable to our system) when the parametric uncertainty enters the system one or more integrator before the control input u does, the adaptive design gets more complicated to avoid over-parameterization.

In the backstepping design procedure, we divide the system into subsystems, we stabilize each subsystem separately and then we stabilize the whole system.

Step 1: To proceed, we stabilize the first subsystem $\dot{x}_1 = x_2$ using the stabilizing function α_1.

We treat x_2 (pinion angular velocity) as the intermediate or virtual control of the subsystem $\dot{x}_1 = x_2$, then we find a stabilizing function α_1 which is the desired value of x_2 that makes x_1 track a reference signal y_r as time goes to infinity, $x_1(t) \rightarrow y_r$ as $t \rightarrow \infty$. Since there will be an error between the virtual control x_2 and the stabilizing function α_1, we construct a new state space equation by change of variables, and we call it the “error system” or the z-domain system. The states of this error system are the differences between the real states and the stabilizing functions, and the control objective is to stabilize all the error states asymptotically.

We define the first tracking error in the new state space equation as:

$$z_1 = x_1 - y_r \tag{4.27}$$

The second error variable in the new state space is the difference between the state x_2 and its stabilizing function α_1,

$$z_2 = x_2 - \alpha_1 - \dot{y}_r \tag{4.28}$$

Taking the derivative of z_1 yields,

$$\begin{aligned}\dot{z}_1 &= \dot{x}_1 - \dot{y}_r \\ &= z_2 + \alpha_1\end{aligned} \tag{4.29}$$

Then we stabilize the first error system (4.27) by the Lyapunov function,

$$V_1(z_1) = \frac{1}{2} z_1^{\ 2} \tag{4.30}$$

which yields the derivative,

$$\dot{V}_1 = z_1 \dot{z}_1 = z_1 (z_2 + \alpha_1) = z_1 z_2 + z_1 \underbrace{\alpha_1}_{-c_1 z_1}. \tag{4.31}$$

Clearly, if $z_2 = 0$ (we will prove it in step 2), then choosing $\alpha_1 = -c_1 z_1$ makes $\dot{V}_1$ negative definite, $\dot{V}_1 = z_1 z_2 + c_1 z^2{}_1 \prec 0,\ \forall z_1 \neq 0, c_1 \succ 0$, and z_1 is guaranteed to converge to zero, whereby achieving global asymptotic tracking: $x_1 \to y_r$ as $t \to \infty$.

Substituting $\alpha_1 = -c_1 z_1$ in (4.28) and (4.30) yields, respectively,

$$\begin{aligned}\dot{z}_1 &= z_2 + \alpha_1 \\ &= z_2 - c_1 z_1\end{aligned} \tag{4.32}$$

$$\dot{V}_1 = z_1 z_2 - c_1 z_1^{\ 2},\ c_1 \succ 0 \tag{4.33}$$

Step 2: The next step is to develop a backstepping control law for $u(t)$. To proceed, we need to find the derivative of z_2 in (4.28), which satisfies,

$$\begin{aligned}\dot{z}_2 &= \dot{x}_2 - \dot{\alpha}_1 - \ddot{y}_r \\ &= -\phi_1 x_2 + b_2 u - \phi_2 - \dot{\alpha}_1 - \ddot{y}_r\end{aligned} \tag{4.34}$$

$$\dot{\alpha}_1 = c_1 (c_1 z_1 - z_2) \tag{4.35}$$

Since ϕ_1, ϕ_2, and b_2 are unknown, the task is to develop an adaptive controller consisting of a control law and adaptive laws to obtain estimates of ϕ_1, ϕ_2, and b_2. Denote $\hat{\phi}_1$ to be the estimate of ϕ_1 and $\hat{\phi}_2$ to be the estimate of ϕ_2. The estimation errors are $\tilde{\phi}_1 = \phi_1 - \hat{\phi}_1$, and $\tilde{\phi}_2 = \phi_2 - \hat{\phi}_2$. Denote b_2^{-1} by p_2, $\hat{p}_2$ is an estimate of p_2, and $\tilde{p}_2 = p_2 - \hat{p}_2$ is the estimation error.

To stabilize the (z_1, z_2) error system given by (4.32) and (4.34), we choose a composite Lyapunov function candidate. This time it is chosen to also include stabilizing terms for the estimates of ϕ_1, ϕ_2, and p_2.

$$V_2\left(z_1, z_2, \tilde{\phi}_1, \tilde{\phi}_2, \tilde{p}_2\right) = V_1 + \frac{1}{2}z_2^{\,2} + \frac{1}{2}\gamma_1\tilde{\phi}_1^{\,2} + \frac{1}{2}\gamma_2\tilde{\phi}_2^{\,2} + \frac{|b|}{2}\gamma_3\tilde{p}_2^{\,2} \tag{4.36}$$

$$\begin{aligned} \dot{V}_2 &= \dot{V}_1 + z_2\dot{z}_2 - \gamma_1\tilde{\phi}_1\dot{\hat{\phi}}_1 - \gamma_2\tilde{\phi}_2\dot{\hat{\phi}}_2 - |b|\gamma_3\tilde{p}_2\dot{\hat{p}}_2 \\ &= -c_1z_1^{\,2} + z_2\left(z_1 - \phi_1x_2 + b_2u - \phi_2 - \dot{\alpha}_1 - \ddot{y}_r\right) - \gamma_1\tilde{\phi}_1\dot{\hat{\phi}}_1 - \gamma_2\tilde{\phi}_2\dot{\hat{\phi}}_2 - |b|\gamma_3\tilde{p}_2\dot{\hat{p}}_2 \end{aligned} \tag{4.37}$$

We need to find the backstepping control law u and the adaptive laws $\dot{\hat{\phi}}_1, \dot{\hat{\phi}}_2$, and $\dot{\hat{p}}_2$ that makes (4.37) negative definite.

By inspection, choosing the term ($z_1 - \phi_1x_2 + b_2u - \phi_2 - \dot{\alpha}_1 - \ddot{y}_r$) in (4.37) to be equal to $-c_2z_2$ yields,

$$u = \underbrace{b_2^{-1}}_{p_2}\left(-z_1 - c_2z_2 + \phi_1x_2 + \phi_2 + \dot{\alpha}_1 + \ddot{y}_r\right) \tag{4.38}$$

Since ϕ_1, ϕ_2, and p_2 are unknown, we cannot substitute the control law (4.38) in (4.37), instead we replace ϕ_1, ϕ_2, and p_2 by their estimates $\hat{\phi}_1$, $\hat{\phi}_2$, $\hat{p}_2$, respectively, then (4.38) becomes,

$$u = \hat{p}_2\left(-z_1 - c_2z_2 + \hat{\phi}_1x_2 + \hat{\phi}_2 + \dot{\alpha}_1 + \ddot{y}_r\right) \tag{4.39}$$

Let $\bar{u} = -z_1 - c_2z_2 + \hat{\phi}_1x_2 + \hat{\phi}_2 + \dot{\alpha}_1 + \ddot{y}_r$

$u = \hat{p}_2\bar{u} \Rightarrow b_2 u = b_2\hat{p}_2\bar{u}$

We have with $\hat{p}_2 = p_2 - \tilde{p}_2$,

$$b_2 u = \bar{u} - b_2\tilde{p}_2\bar{u} \tag{4.40}$$

and then substitute (4.40) in (4.37) which yields,

$$\begin{aligned}
\dot{V}_2 &= -c_1 {z_1}^2 + z_2\left(z_1 - \phi_1 x_2 + b_2 u - \phi_2 - \dot{\alpha}_1 - \ddot{y}_r\right) - \gamma_1\tilde{\phi}_1\dot{\hat{\phi}}_1 - \gamma_2\tilde{\phi}_2\dot{\hat{\phi}}_2 - |b_2|\gamma_3\tilde{p}_2\dot{\hat{p}}_2 \\
&= -c_1 {z_1}^2 + z_2\left(z_1 - \phi_1 x_2 + \bar{u} - b_2\tilde{p}_2\bar{u} - \phi_2 - \dot{\alpha}_1 - \ddot{y}_r\right) - \gamma_1\tilde{\phi}_1\dot{\hat{\phi}}_1 - \gamma_2\tilde{\phi}_2\dot{\hat{\phi}}_2 - |b_2|\gamma_3\tilde{p}_2\dot{\hat{p}}_2 \\
&= -c_1 {z_1}^2 + z_2\left(z_1 - \phi_1 x_2 + -z_1 - c_2 z_2 + \hat{\phi}_1 x_2 + \hat{\phi}_2 + \dot{\alpha}_1 + \ddot{y}_r - \phi_2 - \dot{\alpha}_1 - \ddot{y}_r\right) \\
&\quad - \gamma_1\tilde{\phi}_1\dot{\hat{\phi}}_1 - \gamma_2\tilde{\phi}_2\dot{\hat{\phi}}_2 - b_2\tilde{p}_2\bar{u}z_2 - |b_2|\gamma_3\tilde{p}_2\dot{\hat{p}}_2 \\
&= -c_1 {z_1}^2 - c_2 {z_2}^2 - \phi_1 x_2 z_2 + \hat{\phi}_1 x_2 z_2 + \hat{\phi}_2 z_2 - \phi_2 z_2 - \gamma_1\tilde{\phi}_1\dot{\hat{\phi}}_1 - \gamma_2\tilde{\phi}_2\dot{\hat{\phi}}_2 - b_2\tilde{p}_2\bar{u}z_2 - |b_2|\gamma_3\tilde{p}_2\dot{\hat{p}}_2 \\
&= -c_1 {z_1}^2 - c_2 {z_2}^2 - \tilde{\phi}_1 x_2 z_2 - \tilde{\phi} z_2 - \gamma_1\tilde{\phi}_1\dot{\hat{\phi}}_1 - \gamma_2\tilde{\phi}_2\dot{\hat{\phi}}_2 - b_2\tilde{p}_2\bar{u}z_2 - |b_2|\gamma_3\tilde{p}_2\dot{\hat{p}}_2 \\
&= -c_1 {z_1}^2 - c_2 {z_2}^2 - \tilde{\phi}_1\left(x_2 z_2 + \gamma_1\dot{\hat{\phi}}_1\right) - \tilde{\phi}_2\left(z_2 + \gamma_2\dot{\hat{\phi}}_2\right) - |b_2|\gamma_3\tilde{p}_2\left(\dot{\hat{p}}_2 + \frac{1}{\gamma_3} sign(b_2)\bar{u}z_2\right)
\end{aligned} \tag{4.41}$$

Next, we need to choose update laws for $\hat{\phi}_1$, $\hat{\phi}_2$, and $\hat{p}_2$ such that (4.41) is negative definite.

Choosing the update laws for $\hat{\phi}_1$, $\hat{\phi}_2$, and $\hat{p}_2$ to be $\dot{\hat{\phi}}_1 = -\frac{1}{\gamma_1} x_2 z_2$, $\dot{\hat{\phi}}_2 = -\frac{1}{\gamma_2} z_2$,

$\dot{\hat{p}}_2 = -\frac{1}{\gamma_3} sign(b_2)\bar{u}z_2$, respectively, yields,

$$\dot{V}_2 = -c_1 {z_1}^2 - c_2 {z_2}^2, \forall z_1 \neq 0, \forall z_2 \neq 0, c_1 \succ 0, c_2 \succ 0 \tag{4.42}$$

With (4.36) and (4.42), the LaSalle-Yoshizawa theorem [12], stated below, guarantees the global uniform boundness of $z_1(t)$, $z_2(t)$, $\hat{\phi}_1(t)$, $\hat{\phi}_2(t)$, $\hat{p}_2$, and the convergence of $z_1(t) \to 0$ and $z_2(t) \to 0$ as $t \to \infty$. This results in asymptotic tracking such that $\lim_{t\to\infty}\left(x_1(t) - y_r(t)\right)$. The boundness of x_1 follows from the boundness of z_1 and

y_r since $x_1 = z_1 + y_r$. The boundness of x_2 follows from the boundness of $z_2, \dot{y}_r$, and α_1 since $x_2 = z_1 + \alpha_1 + \dot{y}_r$. It follows from those facts that $u(t)$ is also bounded since

$$u(t) = \hat{p}_2\left(-z_1 - c_2 z_2 + \hat{\phi}_1 x_2 + \hat{\phi}_2 + \dot{\alpha}_1 + \ddot{y}_r\right)$$

Lasalle-Yoshizawa Theorem [1]

Let $x = 0$ be an equilibrium point of $\dot{x} = f(x,t)$ and suppose f is locally Lipschitz in x uniformly in t. Let $V : R^n \to R_+$ be a continuously differentiable function such that

$$\dot{V} = \frac{\partial V}{\partial x}(x) f(x,t) \leq -W(x) \leq 0, \quad \forall t \geq 0, \forall x \in \mathbb{R}^n,$$

where W is a continuous function. Then all solutions of $\dot{x} = f(x,t)$ are globally uniformly bounded and satisfy $\lim_{t\to\infty} W(\|x(t)\|) = 0$. In addition, if $W(x)$ is positive definite, then the equilibrium $x = 0$ is globally uniformly asymptotically stable (GUAS).

Converting the backstepping control law u and the adaptive laws from the z-domain to the x-domain yields,

$$u = \hat{p}_2\left(\hat{\phi}_1 x_2 + \hat{\phi}_2 - (1 + c_1 c_2) x_1 - (c_1 + c_2) x_2 + (1 + c_1 c_2) y_r + (c_1 + c_2)\dot{y}_r + \ddot{y}_r\right) \quad (4.43)$$

Converting the update laws to the x-domain yields,

$$\dot{\hat{\phi}}_1 = \frac{1}{\gamma_1} x_2 (x_2 + c_1 x_1 - c_1 y_r - \dot{y}_r) \quad (4.44)$$

$$\dot{\hat{\phi}}_2 = \frac{1}{\gamma_1} (x_2 + c_1 x_1 - c_1 y_r - \dot{y}_r) \quad (4.45)$$

$$\dot{\hat{p}}_2 = -\frac{1}{\gamma_3} sign(b_2)\bar{u}\left(c_1(x_1 - y_r) + x_2 - \dot{y}_r\right) \tag{4.46}$$

where $\bar{u} = \hat{\phi}_1 x_2 + \hat{\phi}_2 - (1 + c_1c_2)x_1 - (c_1 + c_2)x_2 + (1 + c_1c_2)y_r + (c_1 + c_2)\dot{y}_r + \ddot{y}_r$

The parameters c_1 and c_2 are called the Lyapunov coefficients, which are design parameters that are tuned to improve the controller response in terms of steady state error, overshoot, oscillations, and speed of convergence. The parameters γ_1, γ_2, and γ_3 are the adaptation gain parameters for ϕ_1, ϕ_2, and b_2, respectively. The closed loop system is illustrated in Figure 4.30.

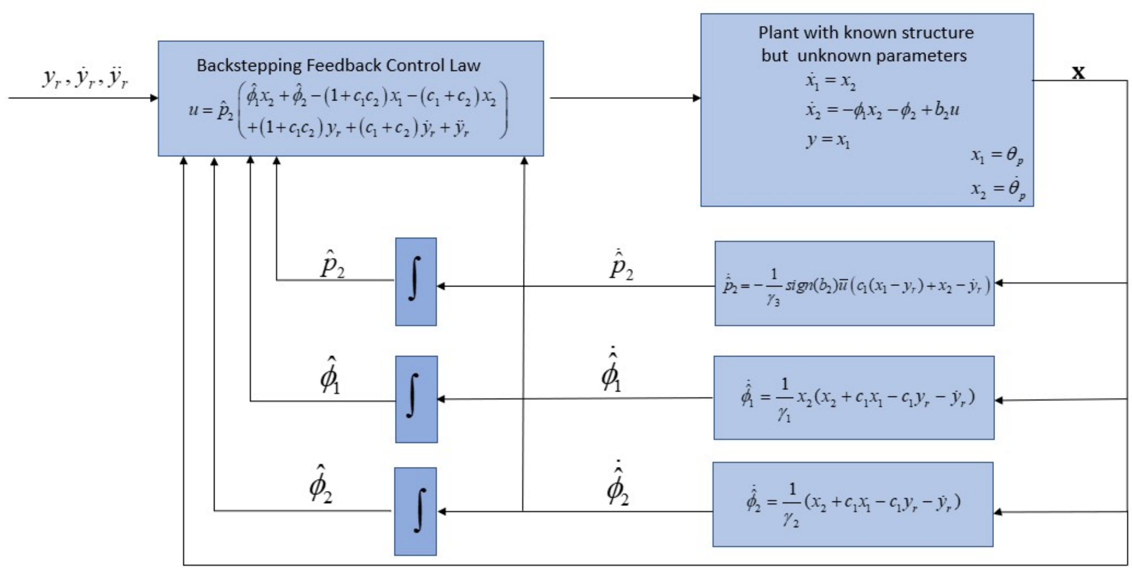

Figure 0.29 ABS steering angle controller closed loop system.

4.3.2 Simulation Results

Simulations were conducted in Matlab using the steering model developed in chapter 3. A signal generator was used to generate steering angle commands. In Figures 3.31-3.35, we started with a zero angle and ramped up to about 90 degrees steering angle request. From Figure 4.31, it can be seen that the actual steering angle is tracking the desired angle very well. The angle error went to zero asymptotically at steady state as can be seen from Figure 4.32. Figure 4.33 shows the steering torque command computed by the controller to actuate the EPS. Figure 4.34 compares the estimated disturbance from the adaptive BS law and the actual disturbance from the model. The jump over steady state at 6 seconds when we transitioned from zero angle is due to the static friction that was estimated by the adaptive BS law and compensated very well by the controller as can be seen from Figures 4.31 and 4.33. Figure 4.35 shows the errors in the new coordinate system, the z-domain, which are given by $z_1 = x_1 - y_r$, $z_2 = x_2 - \alpha_1 - \dot{y}_r$. Figures 4.36-4.42 demonstrate the controller response to a sinusoidal steering angle request of about 46 degrees. Excellent steering angle tracking is achieved as can be seen from Figure 4.36 and Figure 4.37. Figure 4.38 and Figure 4.39 compare the actual and estimated disturbance with two different values of γ_2, which is the disturbance adaptation gain, $\frac{1}{\gamma_2} = 20$ and $\frac{1}{\gamma_2} = 100$. Just for clarifications, Figure 4.40 shows the actual self-aligning moment torque disturbance and the friction torque separate and also added together from the model that is used for validation. The signal in green is the combination of self-aligning moment torque and friction torque, which the controller estimates and compensates for. Figure 4.41 shows the ABS control output. The jump in the torque at the zero angular velocity crossing 4.41 is due to the static friction (breakaway friction) torque that the controller has to overcome when we reverse the steering direction. Figure 4.42 shows the virtual control errors.

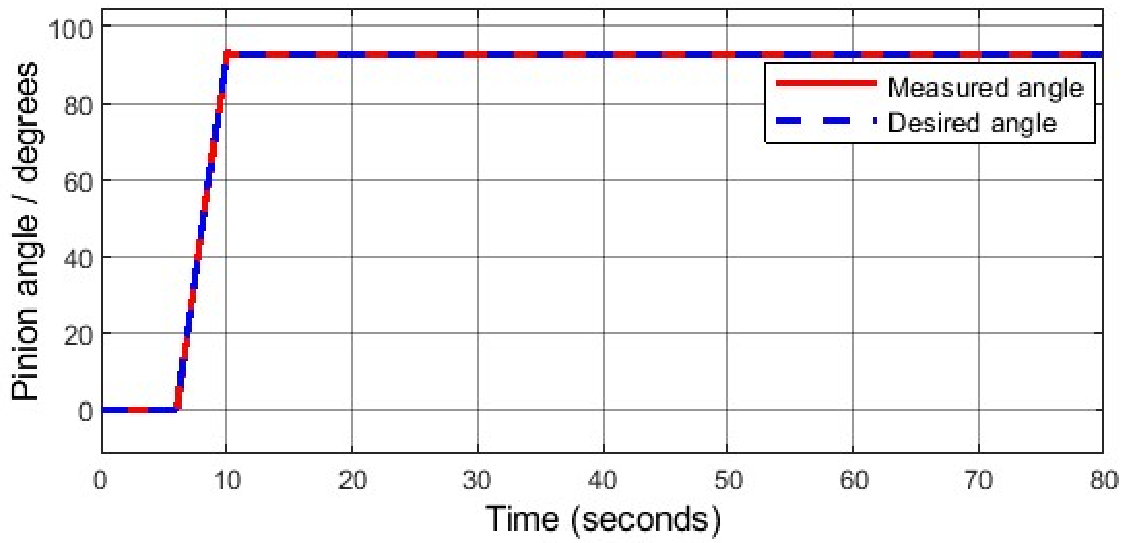

Figure 0.30 ABS SAC response for ramping up to a constant angle

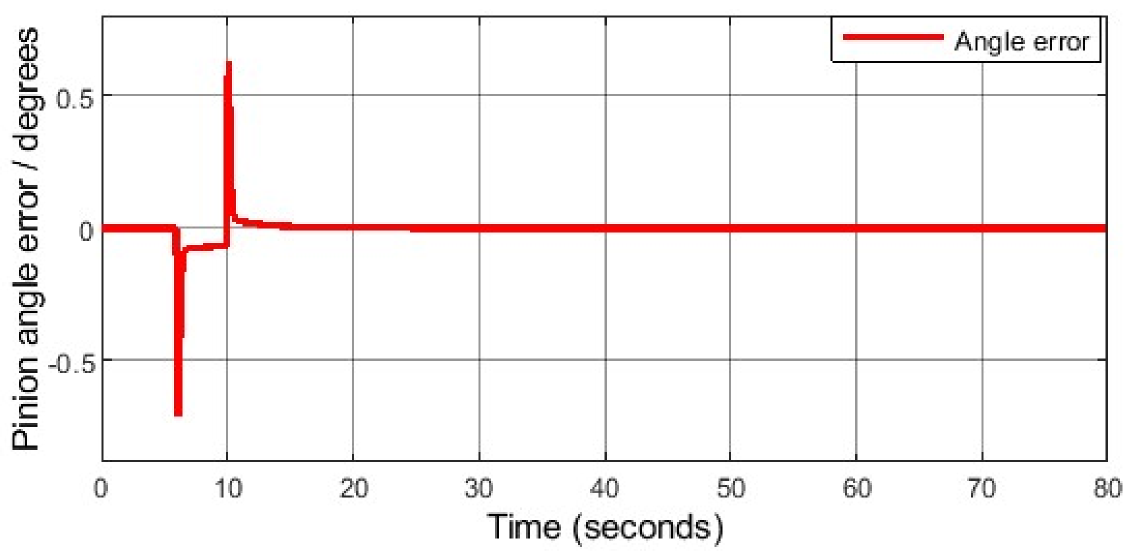

Figure 0.31 Steering angle error corresponding to the senario in Figure 4.31.

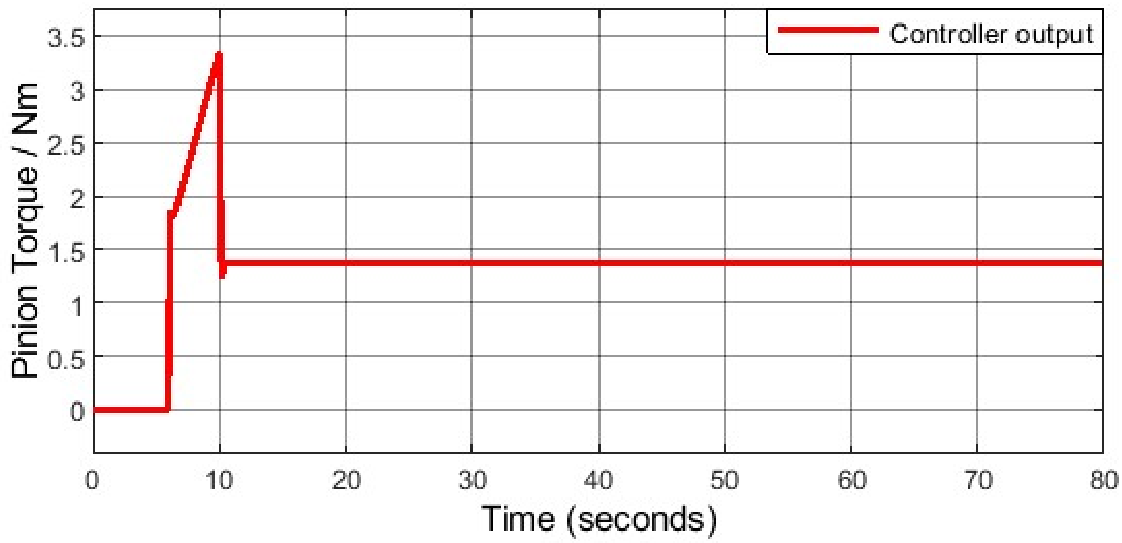

Figure 0.32 ABS SAC output corresponding to the senario in Figure 4.31.

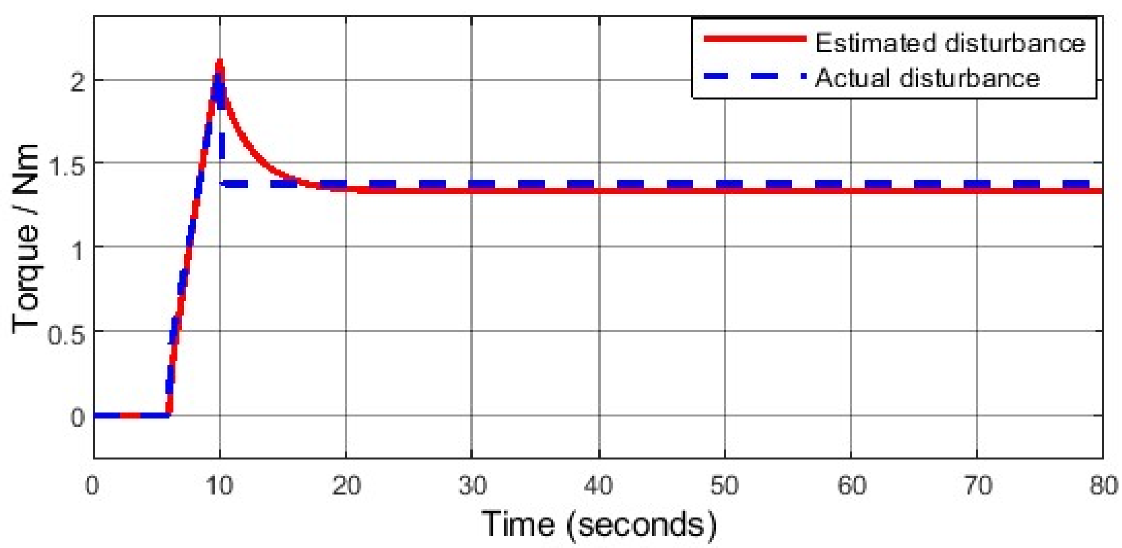

Figure 0.33 Estimated disturbance compared to actual disturbance with $\frac{1}{\gamma_2} = 20$.

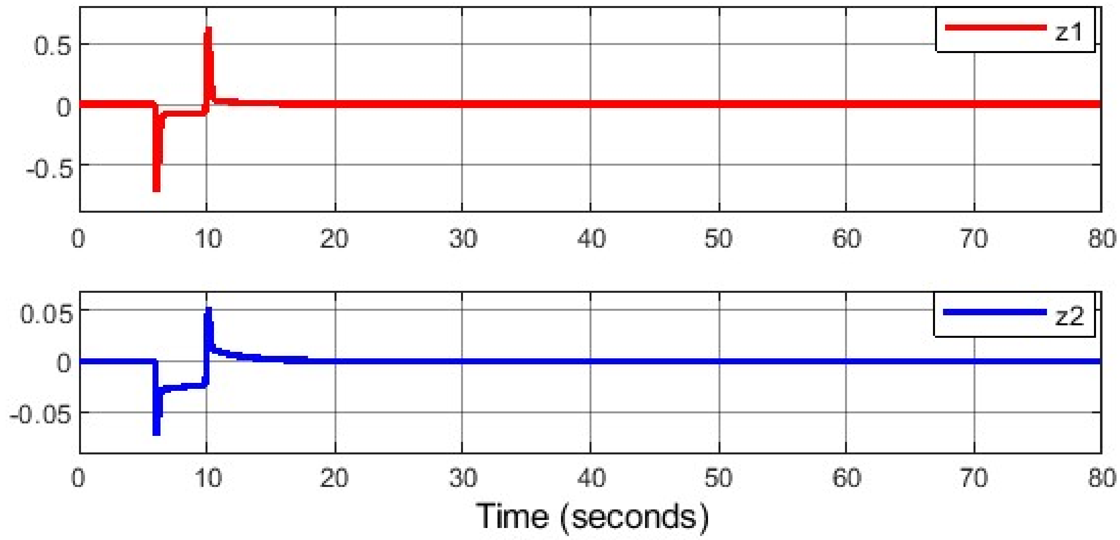

Figure 0.34 Virtual control errors $z_1 = x_1 - y_r$, $z_2 = x_2 - \alpha_1 - \dot{y}_r$.

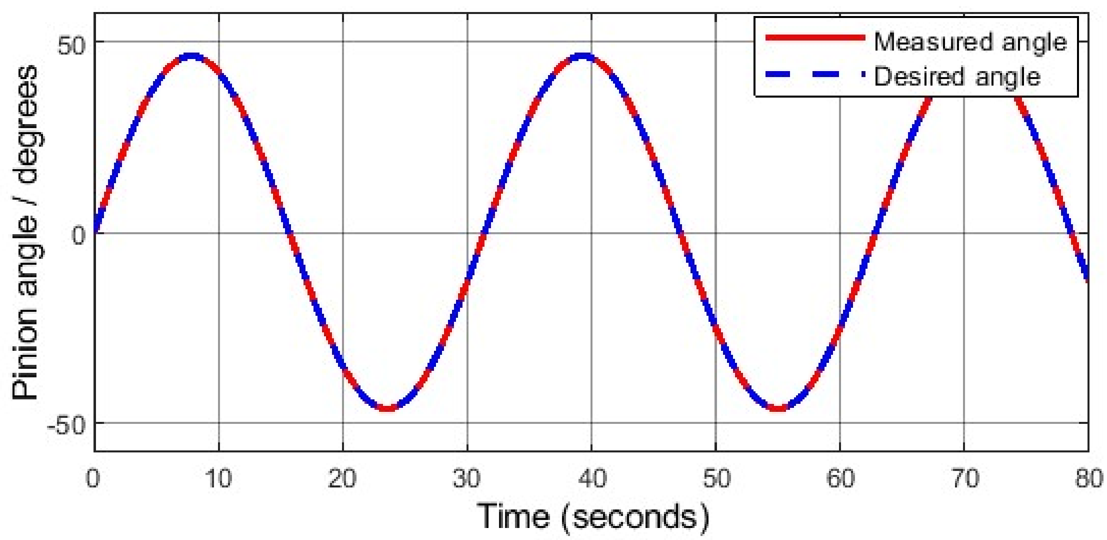

Figure 0.35 ABS SAC response to a sinusoidal steering angle request.

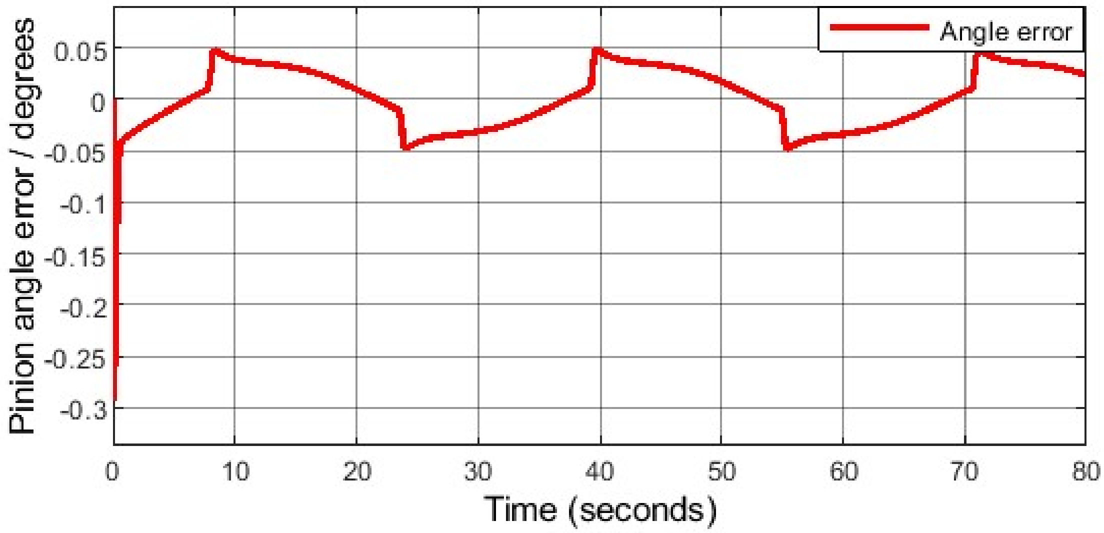

Figure 0.36 Steering angle error corresponding to the senario in Figure 4.36.

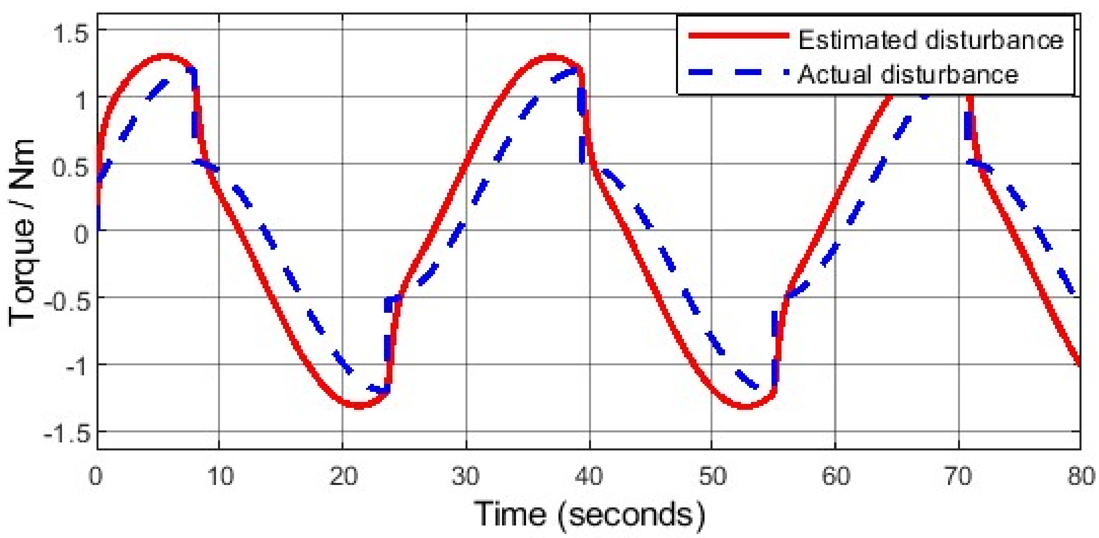

Figure 0.37 Estimated disturbance compared to actual disturbance with $\frac{1}{\gamma_2} = 20$

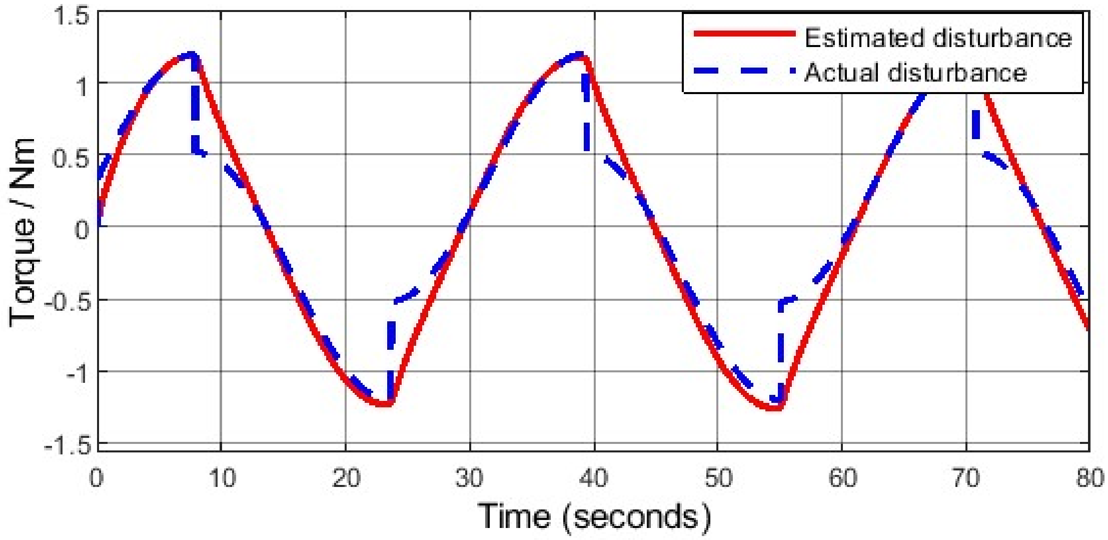

Figure 0.38 Estimated disturbance compared to actual disturbance with $\frac{1}{\gamma_2} = 100$.

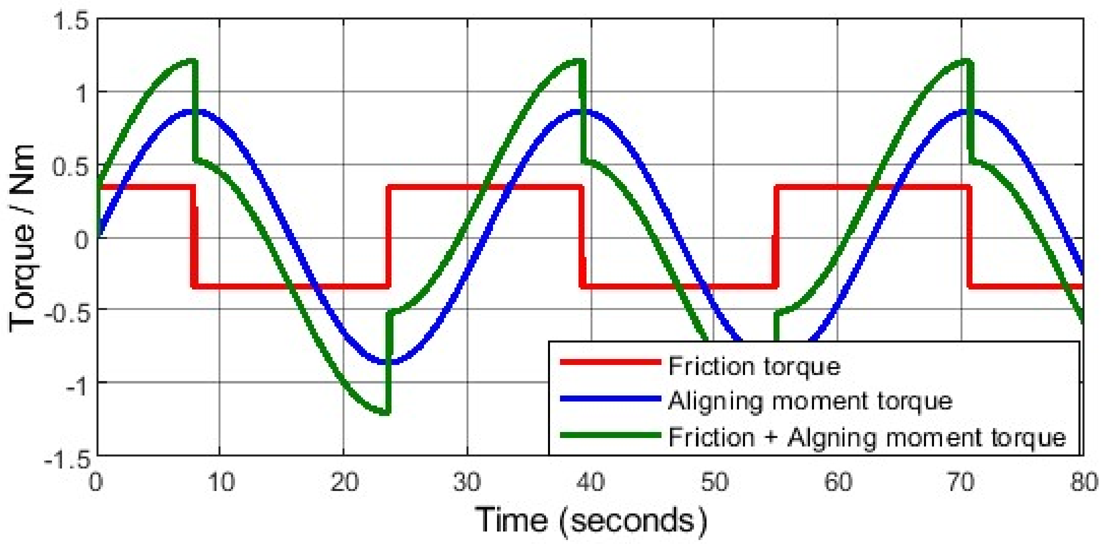

Figure 0.39 Comparison of separate and combined disturbances from the model.

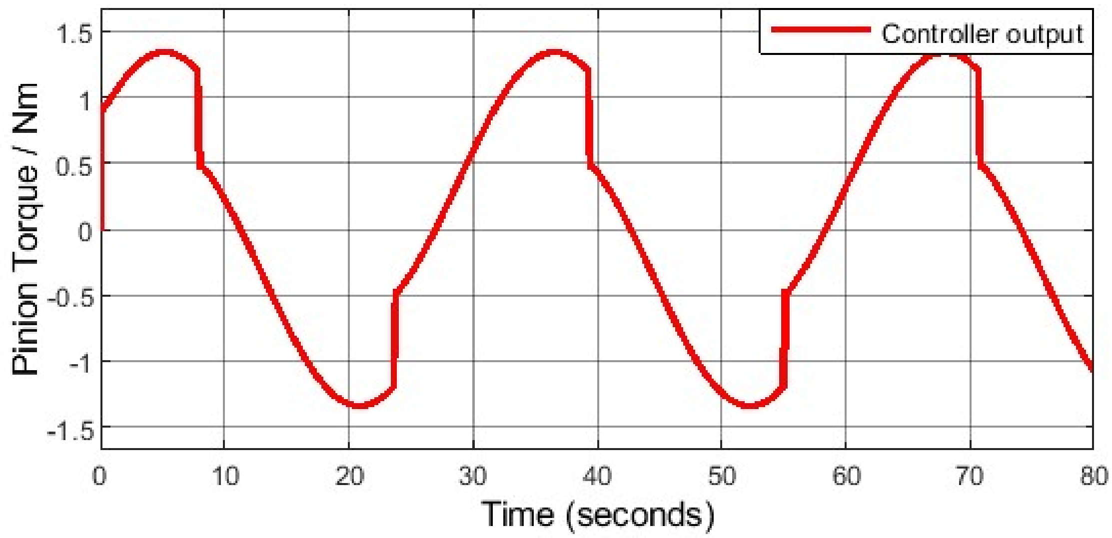

Figure 0.40 ABS SAC output corresponding to the senario in Figure 4.40.

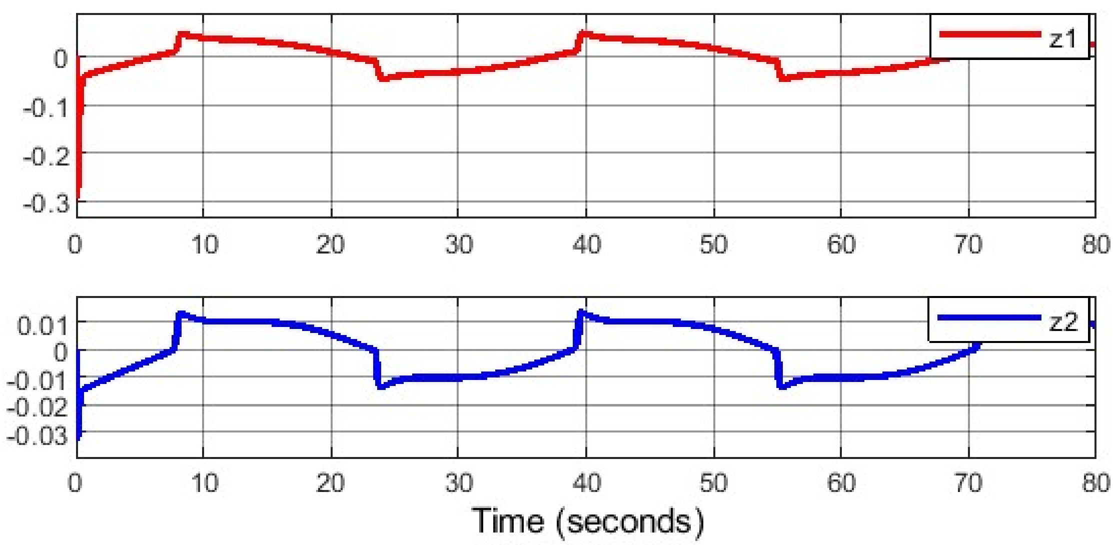

Figure 0.41 Virtual control errors $z_1 = x_1 - y_r$, $z_2 = x_2 - \alpha_1 - \dot{y}_r$

CHAPTER FIVE

LATERAL TRAJECTORY TRACKING CONTROL

¶
¶
¶

5.1 Introduction

Trajectory tracking control is the most basic and important function in autonomous vehicles. The Trajectory Tracking Controller (TTC) controls the motion of the vehicle in both lateral and longitudinal directions. Based on surrounding sensors, the environmental model generates an optimal and safe trajectory for the vehicle to follow in both lateral and longitudinal direction. The longitudinal TTC controls the longitudinal position and longitudinal speed of the vehicle and the lateral TTC controls the lateral position, lateral speed, and the heading of the vehicle while controlling it to follow the curvature of the road. The focus of this dissertation is on the lateral TTC development. The lateral TTC takes in the lateral deviation and the heading angle deviation of the vehicle from the intended trajectory and the road curvature to compute the steering angle required to correct the deviations from the desired trajectory and follow the curvature of the road. The required steering angle is then controlled by the SAC as explained in chapter 4, which computes the torque required to achieve the desired steering angle.

Researchers investigated many control methods for TTC. A review of the state of the art and challenges faced in developing path following control is discussed in [49]. The review explored the different vehicle models used, the control methods employed, and the performance criteria used to evaluate the controller's performance. In [50], an adaptive finite time trajectory tracking control for autonomous vehicles is developed. But cornering stiffness is the only vehicle parameter that is estimated online using recursive least squares but the rest of the vehicle inertial parameters (mass, moment of inertia, and center of gravity location) are assumed known and constant. In [51], a comparison of controllers for vehicle lane keeping is done using H_∞, adaptive, PID and fuzzy control. In [52], a lane keeping with adaptation to driver style is developed. But the adaptation is in the driver style, not in the vehicle parameters. In [53], two adaptive control methods are compared to control wheeled mobile robot, universal adaptive stabilization-based method and adaptive proportional method. The adaptation in both methods is in the controller's gains, not in the model parameters. This method is based on a geometrical model that does not need vehicle parameters. Geometry-based models are widely used in trajectory tracking control but they have limitations. The most famous geometry-based methods are Stanly [54],[55] and pure pursuit [56]-[57]. Geometry based methods are based on a kinematic model, which does not take into account the dynamic forces on the vehicle. Controllers developed based on such models can perform very well at low speeds and mild curvatures but they fail at high speeds and high curvatures because they ignore lateral forces. Neural Networks and vision-based methods have been gaining more interest recently [58],[59]. For vision-based methods, the controller performance is highly affected by external environmental factors, such as weather conditions and time of the day, which leads to inconsistent behavior of the controller, for example the performance in the bright sun is different than the performance when it's cloudy. In addition, vision-based methods need computational power. Integral sliding mode control and radial basis function neural network were investigated in [60]. Model Predictive Control (MPC) was investigated in [61]-[69]. MPC finds the numerical solution to a constrained optimal control problem over a finite time horizon. Even though MPC is an efficient control method, it may raise computational complexity needs because it computes a numerical solution at every time step. The Linear Quadratic Gaussian (LQG) was investigated in [70]. LQG is a combination of the Linear Quadratic Regulator (LQR) and Kalman Filter. LQR is a special case of MPC. By removing the constraints on the inputs and the states, and allowing the time horizon to go to infinity, the MPC problem becomes LQR problem, and it has an analytical solution which does not require as much computational power as MPC does, but the limitation of the LQR is that it only works in the linear tire region since it is a linear control method.

In this chapter, lateral TTCs are developed using two approaches, non-adaptive back stepping, or simply backstepping, and adaptive backstepping (ABS). Detailed derivations of both methods are presented in the next two sections of this chapter.

5.2 Backstepping (BS) TTC Derivation

To use the bicycle model for trajectory tracking control, the error dynamics with respect to the reference trajectory are added to the model in (3.2) and the errors are considered as state variables, hence the model is redefined by adding the errors as two additional states, as shown below:

ε_y : lateral deviation, defined as the lateral distance between the CG of the vehicle and the desired trajectory.

ε_ψ : Heading angle deviation, defined as the orientation error of the vehicle with respect to the reference trajectory.

The heading angle error dynamics is defined as,

$$\dot{\varepsilon}_\psi = \dot{\psi}_{desired} - \dot{\psi} \tag{5.1}$$

With the vehicle traveling with constant velocity v on a road with constant radius or slowly changing radius R, it follows that the rate of change of the heading of the vehicle must equal to the angular velocity of the vehicle and since the angular velocity of the vehicle is $\frac{v}{R}$, it follows,

$$\dot{\psi}_{desired} = v / R \tag{5.2}$$

$$\dot{\varepsilon}_{\psi} = (v / R) - \dot{\psi} \tag{5.3}$$

Since the curvature of the road κ is $1/R$, (5.3) becomes,

$$\dot{\varepsilon}_{\psi} = v\kappa - \dot{\psi} \tag{5.4}$$

The lateral error dynamics is defined as,

$$\dot{\varepsilon}_{y} = -v\beta + v\varepsilon_{\psi} \tag{5.5}$$

The resulting state space equation after adding the error dynamics is,

$$\begin{bmatrix} \dot{\beta} \\ \ddot{\psi} \\ \dot{\varepsilon}_{\psi} \\ \dot{\varepsilon}_{y} \end{bmatrix} = \begin{bmatrix} \frac{a_{11}}{v} & \frac{a_{12}}{v^2} - 1 & 0 & 0 \\ a_{21} & \frac{a_{22}}{v} & 0 & 0 \\ 0 & -1 & 0 & 0 \\ -v & 0 & v & 0 \end{bmatrix} \begin{bmatrix} \beta \\ \dot{\psi} \\ \varepsilon_{\psi} \\ \varepsilon_{y} \end{bmatrix} + \begin{bmatrix} \frac{b_1}{v} \\ b_2 \\ 0 \\ 0 \end{bmatrix} \delta + \begin{bmatrix} 0 \\ 0 \\ v\kappa \\ 0 \end{bmatrix} \tag{5.6}$$

Since this controller is designed to operate in the linear region of the tire where the slip angle is small, we can neglect the slip angle for the design of the feedback controller and further simplify the model, however the steady state slip angle is used to calculate the reference heading as discussed in the following section.

The simplified model is given by,

$$\begin{bmatrix} \dot{\varepsilon}_y \\ \dot{\varepsilon}_\psi \\ \ddot{\psi} \end{bmatrix} = \begin{bmatrix} 0 & v & 0 \\ 0 & 0 & -1 \\ 0 & 0 & \frac{a_{22}}{v} \end{bmatrix} \begin{bmatrix} \varepsilon_y \\ \varepsilon_\psi \\ \dot{\psi} \end{bmatrix} + \begin{bmatrix} 0 \\ 0 \\ b_2 \end{bmatrix} \delta + \begin{bmatrix} 0 \\ v\kappa \\ 0 \end{bmatrix} \tag{5.7}$$

In order to implement a backstepping controller for a system, it has to be affine, also called strict feedback form. The above system was transformed to the strict feedback form by change of variables, as shown below:

$$x_3 = -\dot{\psi}\,,\quad x_2 = v\varepsilon_\psi\,,\quad x_1 = \varepsilon_y\,,\quad u = b_2\delta\,,\quad \theta_1 = v\kappa,\quad \theta_2 = -\frac{a_{22}}{v}$$

That results in the strict feedback form of the model, as shown below:

$$\begin{aligned} \dot{x}_1 &= x_2 \\ \dot{x}_2 &= x_3 + \theta_1 \\ \dot{x}_3 &= \theta_2 x_3 + u \end{aligned} \tag{5.8}$$

For the transformed system we are going to design a backstepping controller to regulate the lateral error and the heading angle error and follow the curvature of the of road.

Step 1: To begin with, stabilize the first subsystem $\dot{x}_1 = x_2$ (lateral deviation error) using the stabilizing function α_1.

Treating x_2 as the virtual control of the subsystem $\dot{x}_1 = x_2$, we need to find a stabilizing function α_1 which is the desired value of x_2 that drives x_1 to zero, $x_1 \to 0$ as $t \to \infty$.

We define the change of variables or error variables as,

$$z_1 = x_1 \tag{5.9}$$

$$z_2 = x_2 - \alpha_1 \tag{5.10}$$

Taking the derivative of z_1 yields

$$\dot{z}_1 = \dot{x}_1 = x_2 = z_2 + \alpha_1 \tag{5.11}$$

We choose the following Lyapunov function to stabilize the error subsystem in (5.11),

$$V_1(z_1) = \frac{1}{2} z_1^{\,2} \tag{5.12}$$

which yields the derivative,

$$\dot{V}_1(z_1) = z_1\dot{z}_1 = z_1\left(z_2 + \alpha_1\right) = z_1 z_2 + z_1 \underbrace{\alpha_1}_{-c_1 z_1} \tag{5.13}$$

If $z_2 = 0$ in (5.13) (we will show in step 2 that $z_2 \to 0$), then choosing $\alpha_1 = -c_1 z_1$ with $c_1 \succ 0$ makes (5.13) negative definite $(\dot{V}_1 = z_1 z_2 + z_1\alpha_1 \prec 0, \forall z_1 \neq 0)$ and the origin $z_1 = 0$ is globally asymptotically stable, achieving $x_1 \to 0$ as $t \to \infty$. Substituting $\alpha_1 = -c_1 z_1$ in (5.11) and (5.13) yields respectively,

$$\dot{z}_1 = z_2 - c_1 z_1 \tag{5.14}$$

$$\dot{V} = z_1 z_2 - c_1 z_1^{\,2},\ c_1 > 0 \tag{5.15}$$

Step 2: Next, stabilize the second subsystem $\dot{x}_2 = x_3 + \theta_1$ using the stabilizing function α_2 .

Treating x_3 (yaw rate) as the virtual control for the second subsystem $\dot{x}_2 = x_3 + \theta_1$, we need to determine its stabilizing function α_2 .

We define the third error variable z_3 as the difference between x_3 and its stabilizing function α_2 ,

$$z_3 = x_3 - \alpha_2 \tag{5.16}$$

To proceed, we need to find the derivative of the second error variable in (5.10),

$$\dot{z}_2 = z_3 + \alpha_2 + \theta_1 - \dot{\alpha}_1 \tag{5.17}$$

To stabilize the (z_1, z_2) -error system, we choose the composite Lyapunov function candidate V_2 as,

$$V_2(z_1, z_2) = V_1 + \frac{1}{2} z_2^{\ 2} \tag{5.18}$$

which yields the derivative,

$$\begin{aligned} \dot{V}_2 &= \dot{V}_1 + z_2 \dot{z}_2 \\ &= -c_1 z_1^{\ 2} + z_2 z_3 + z_2 (\underbrace{z_1 + \alpha_2 + \theta_1 - \dot{\alpha}_1}_{-c_2 z_2}) \end{aligned} \tag{5.19}$$

Clearly, if $z_3 = 0$ in (5.19) (we will prove that $z_3 \to 0$ in step 3 below) and choosing α_2 to make the term $z_1 + \alpha_2 + \theta_1 - \dot{\alpha}_1 = -c_2 z_2$ with $c_2 \succ 0$ makes (5.19) negative definite.

$$\alpha_2 = -z_1 - c_2 z_2 + \dot{\alpha}_1 - \theta_1 \tag{5.20}$$

Substituting (5.20) in (5.17) and (5.19) yields respectively,

$$\dot{z}_2 = -z_1 - c_2 z_2 + z_3 \tag{5.21}$$

$$\dot{V}_2 = z_2 z_3 - c_1 z_1^{\ 2} - c_2 z_2^{\ 2} \tag{5.22}$$

The error system given by (5.14) and (5.21) can be expressed as,

$$\begin{bmatrix} \dot{z}_1 \\ \dot{z}_2 \end{bmatrix} = \underbrace{\begin{bmatrix} -c_1 & 1 \\ -1 & -c_2 \end{bmatrix}}_{A_{2z}} \begin{bmatrix} z_1 \\ z_2 \end{bmatrix} + \begin{bmatrix} 0 \\ z_3 \end{bmatrix} \tag{5.23}$$

where A_{2z} is a skew-symmetric Hurwitz matrix rendering $z_1 \to 0$ and $z_2 \to 0$ asymptotically for $z_3 = 0$.

Step 3: Next, stabilize the complete system using a backstepping control law u_{bs}.

To proceed, we need to take the derivative of (5.16) which yields,

$$\dot{z}_3 = \theta_2 x_3 + u - \dot{\alpha}_2 \tag{5.24}$$

Then we choose a composite Lyapunov function candidate to stabilize the (z_1, z_2, z_3) error system as,

$$V_3(z_1, z_2, z_3) = V_2 + \frac{1}{2} z_3^{\ 2} \tag{5.25}$$

Taking the derivative yields,

$$\begin{aligned} \dot{V}_3 &= z_2 z_3 - c_1 z_1^{\ 2} - c_2 z_2^{\ 2} + z_3 \left(\theta_2 x_3 + u - \dot{\alpha}_2 \right) \\ &= -c_1 z_1^{\ 2} - c_2 z_2^{\ 2} + z_3 \left(\underbrace{z_2 + \theta_2 x_3 + u - \dot{\alpha}_2}_{-c_3 z_3} \right) \end{aligned} \tag{5.26}$$

Choosing u_{bs} to be the backstepping control law that makes the term

$\left(z_2 + \theta_2 x_3 + u - \dot{\alpha}_2 \right) = -c_3 z_3$ in (5.26) yields,

$$u_{bs} = -z_2 - c_3 z_3 - \theta_2 x_3 + \dot{\alpha}_2 \tag{5.27}$$

Substituting (5.27) in (5.24) and (5.26) respectively yields,

$$\dot{z}_3 = -z_2 - c_3 z_3 \tag{5.28}$$

$$\dot{V}_3 = -c_1 z_1^{\ 2} - c_2 z_2^{\ 2} - c_3 z_3^{\ 2}, \quad c_1 \succ 0, c_2 \succ 0, c_3 \succ 0 \tag{5.29}$$

From (5.25) and (5.29), the global uniform boundness of z_1, z_2, and z_3 is guaranteed by Lasalle-Yoshizawa theorem [12], as stated in chapter 4. and it follows that $z_1, z_2, z_3 \to 0$ as $t \to \infty$, x_1 is also bounded since $x_1 = z_1$ and it follows that $\lim_{t \to \infty} x_1 = 0$. The boundness of x_2 follows from the boundness of α_1 and z_2 since $x_2 = \alpha_1 + z_2$. The boundness of x_3 follows from the boundness of α_2 and z_3 since $x_3 = \alpha_2 + z_3$. Given those facts it follows that $u_{bs}(t)$ in (5.27) is also bounded.

The complete error system can be expressed as,

$$\begin{bmatrix} \dot{z}_1 \\ \dot{z}_2 \\ \dot{z}_3 \end{bmatrix} = \underbrace{\begin{bmatrix} -c_1 & 1 & 0 \\ -1 & -c_2 & 1 \\ 0 & -1 & -c_3 \end{bmatrix}}_{\mathbf{A}_{ss}} \begin{bmatrix} z_1 \\ z_2 \\ z_3 \end{bmatrix} = \mathbf{A}_{ss}\mathbf{z} \tag{5.30}$$

where $\mathbf{A}_{ss}$ is a skew symmetric Hurwitz matrix for all $c_1 \succ 0, c_2 \succ 0, c_3 \succ 0$ rendering $z_1 \to 0, z_2 \to 0$ and $z_3 \to 0$ asymptotically and u_{bs} is bounded.

Converting the control law in (5.27) to the x-domain yields,

$$\begin{aligned} u_{bs} = &-\left(c_1 + c_3 + c_1c_2c_3\right)x_1 - \left(c_1c_2 + c_1c_3 + c_2c_3 + 2\right)x_2 \\ &-\left(c_1 + c_2 + c_3 + \theta_2\right)x_3 - \left(c_1 + c_2 + c_3\right)\theta_1 - \dot{\theta}_1 \end{aligned} \tag{5.31}$$

which yields the closed loop system as below,

$$\begin{aligned} \begin{bmatrix} \dot{x}_1 \\ \dot{x}_2 \\ \dot{x}_3 \end{bmatrix} = &\begin{bmatrix} 0 & 1 & 0 \\ 0 & 0 & 1 \\ c_1 + c_3 + c_1c_2c_3 & c_1c_2 + c_1c_3 + c_2c_3 + 2 & c_1 + c_2 + c_3 \end{bmatrix} \begin{bmatrix} x_1 \\ x_2 \\ x_3 \end{bmatrix} \\ &+ \begin{bmatrix} 0 \\ \theta_1 \\ -\left(c_1 + c_2 + c_3\right)\theta_1 - \dot{\theta}_1 \end{bmatrix} \end{aligned} \tag{5.32}$$

The parameters $c_1, c_2, and\, c_3$ are design parameters called the Lyapunov coefficients. The choice of these parameters dramatically affects the controller performance. They can be tuned to add damping and improve the controller tracking and regulation performance.

5.2.1 Feedforward Derivation from Vehicle Steady Dynamics

Curvature compensation is needed for curved roads. we need to calculate the steering wheel angle required to negotiate a curve with radius R. We can use the bicycle model, as given in (3.2), to compute the steering wheel angle and side slip angle at steady state cornering when the vehicle is traveling at a constant speed on a curve with constant radius R. When all derivative terms die out and substituting $\dot{\psi}$ by $\dot{\psi}_{desired} = v\kappa$,we have,

$$\begin{bmatrix} 0 \\ 0 \end{bmatrix} = \begin{bmatrix} \frac{a_{11}}{v} & \frac{a_{12}}{v^2} - 1 \\ a_{21} & \frac{a_{22}}{v} \end{bmatrix} \begin{bmatrix} \beta \\ v\kappa \end{bmatrix} + \begin{bmatrix} \frac{b_1}{v} \\ b_2 \end{bmatrix} \delta \tag{5.33}$$

As can be seen, we end up with two algebraic equations with two unknowns, δ and β. After solving the equations, we have

$$\delta_{ss} = \left(\frac{\frac{a_{12} - v^2}{a_{11}} - a_{22}}{b_2 - \frac{a_{21} b_1}{a_{11}}} \right) \kappa \tag{5.34}$$

Since δ_{ss} is the steering angle required to negotiate a curve κ, it will be added to the feedback control law to compensate for the road curvature.

$$\beta_{ss} = -\frac{b_1}{a_{11}} \delta_{ss} - \frac{a_{12} - v^2}{a_{11}} \kappa \tag{5.35}$$

β_{ss} is the steady state side slip angle and it should be considered as the reference heading of the vehicle, because at steady state cornering when the radius of the road and the vehicle speed are constant, the slip angles at the tires are completely determined, and it follows that the slip angle of the vehicle is automatically determined. This can be seen by considering the lateral error dynamics, as given by,

$$\dot{\varepsilon}_y = -v\beta + v\varepsilon_\psi \tag{5.36}$$

At steady state when $\dot{\varepsilon}_y$ is zero, we have,

$$0 = -v\beta_{ss} + v\varepsilon_{\psi_{ss}} \tag{5.37}$$

It follows that the vehicle steady state slip angle is,

$$\beta_{ss} = \varepsilon_{\psi_{ss}} \tag{5.38}$$

This means that we don't necessarily want the heading angle error ε_ψ to be zero, we want it to be equal to the steady state side slip angle, so we want $\varepsilon_{\psi_{ss}} - \beta_{ss} = 0$.

5.2.2 Simulation Results of BS TTC

The BS TTC was cascaded with the VG sliding mode angle controller and they were validated together by simulation in Matlab. The BS TTC outputs a desired angle that is required to drive the lateral deviation and heading angle deviation to zero and follow the curvature of the road. The desired steering angle is sent to the VG sliding mode steering angle controller, which in turns calculates the steering torque required to achieve the desired angle and actuates the EPS. The EPS model developed in chapter 3 was used as an actuator for the simulation. Figures 5.1-5.4 demonstrates the cascaded controller response to a sinusoidal curvature of 100 m radius (0.01 m^{-1} curvature) to emulate sucsessive curves or sucsessive lane changes maneuvers. Figure 5.1 demonstrates the BS TTC response and Figure 5.2 demonstrates the VG sliding mode steering angle response. Figures 5.3 and 5.4 are the heading angle error and the lateral deviation from the center of the trajectory, respectively. The errors did not converge to zero because the reference trajectory is continuously changing. Figures 5.5-5.8

demonstrate the cascaded controller response to a scenario of ramping up to a constant curvature of 1000 m radius (($0.001\ m^{-1}$ curvature). Figure 5.5 demonstrates the TTC response and Figure 5.6 demonstrates the steering angle controller response. Figures 5.7 and 5.8 are the heading angle error and the lateral deviation from the desired trajectory, respectively. In the transitioning period from 6 to 10 seconds, there were some transients in the errors but they settled down and converged to zero at steady state when we reached the final constant value of the curvature. It can be noticed that at steady state when the reference curvature went to a constant value, the errors converged to zero.

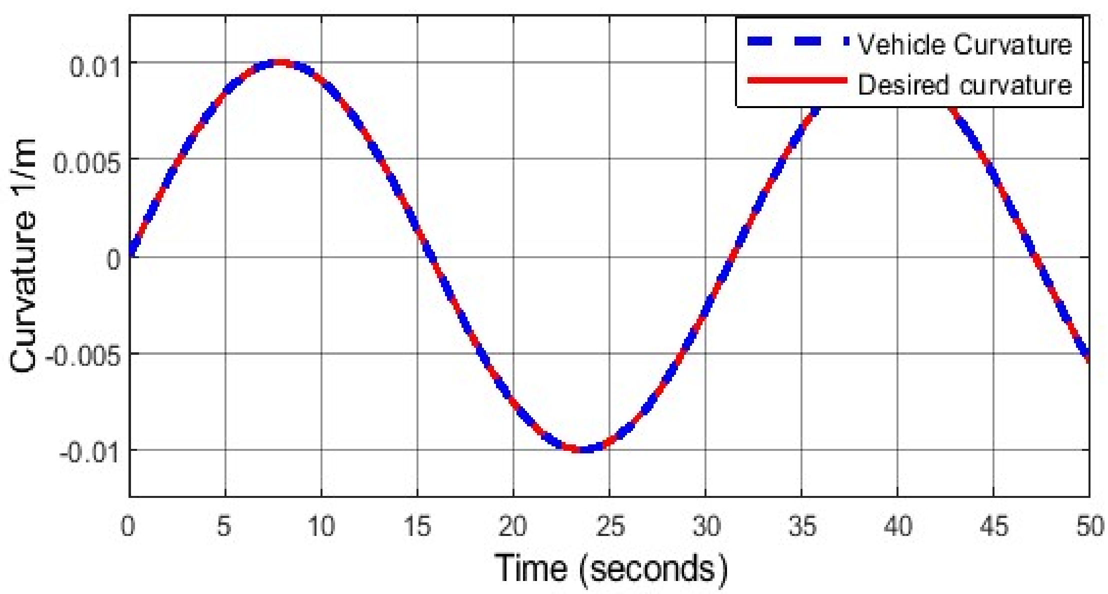

Figure 0.1 BS trajectory tracking controller response for a sinusoidal curvature.

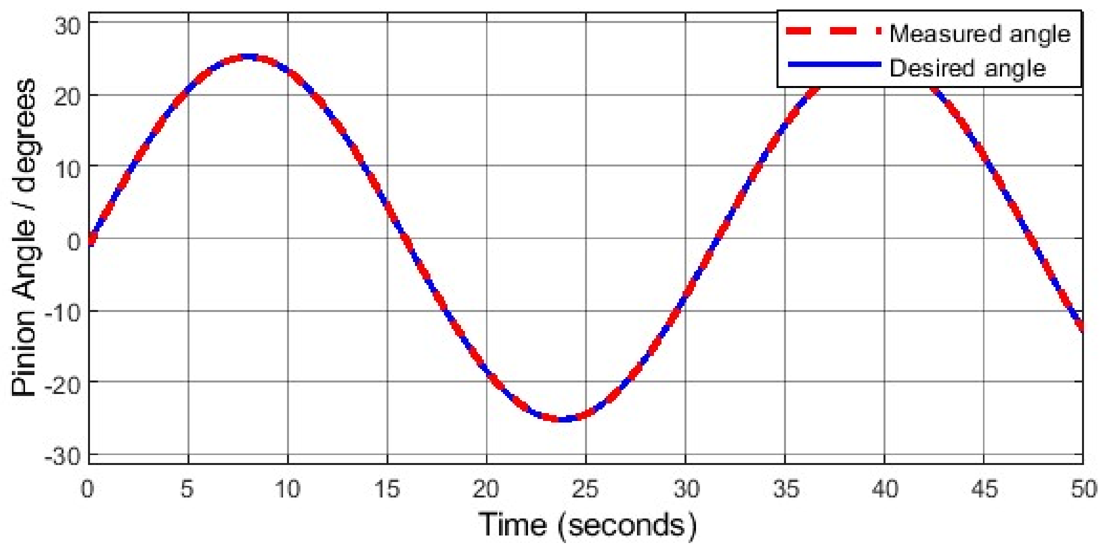

Figure 0.2 SMC SAC response corresponding to the senario in Figure 5.1.

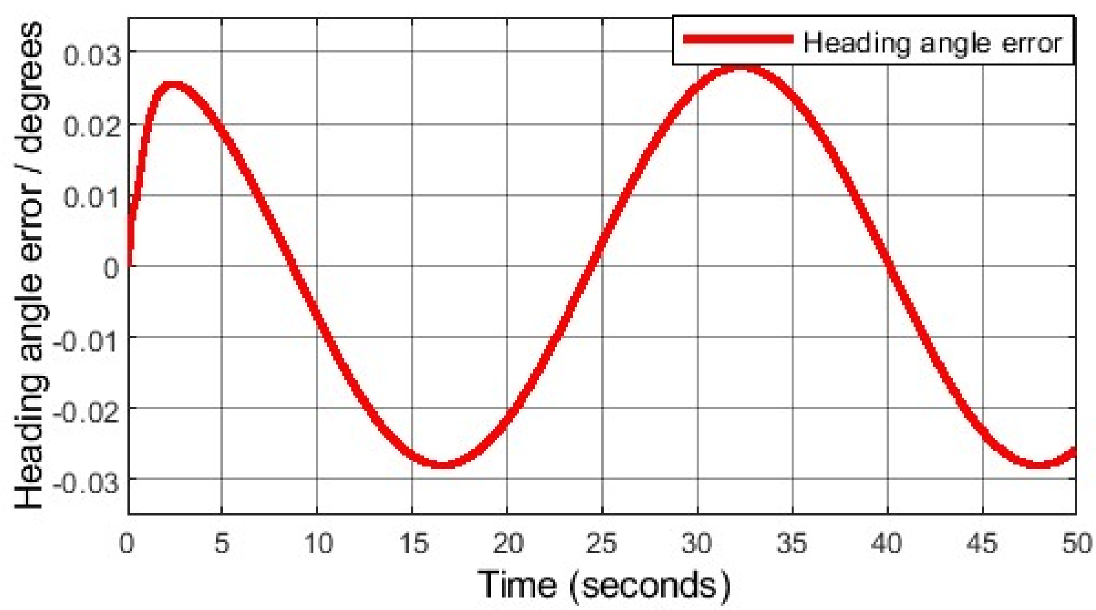

Figure 0.3 Heading angle error.

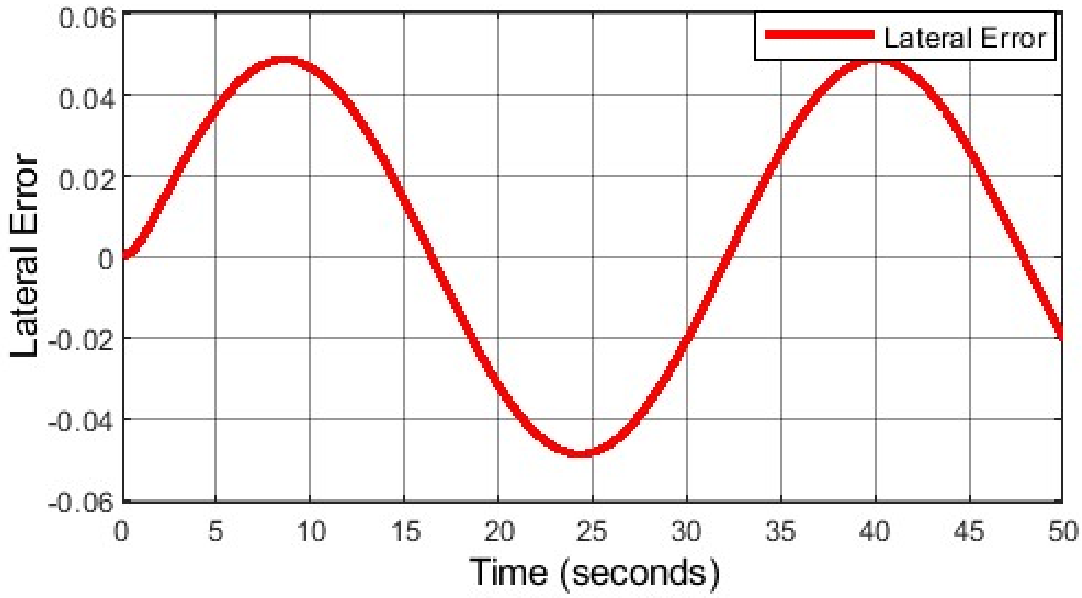

Figure 0.4 Lateral error.

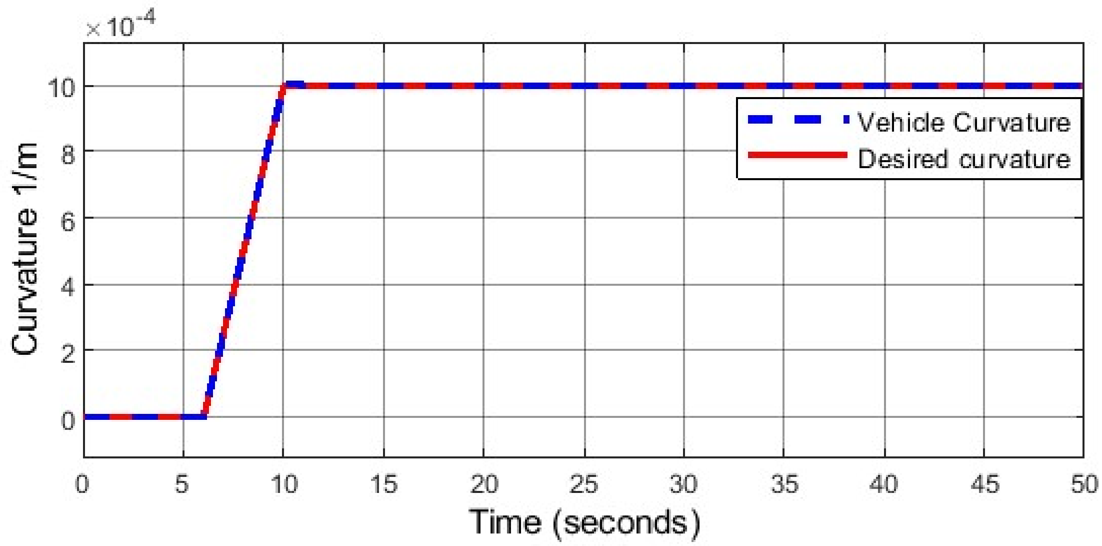

Figure 0.5 BS trajectory tracking controller response for ramping up to a constant curvature.

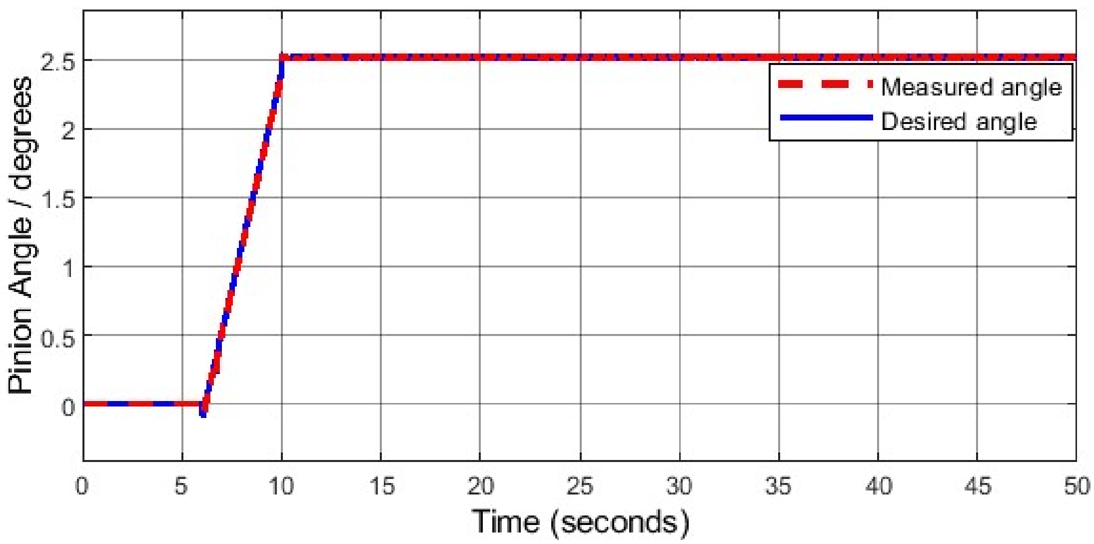

Figure 0.6 SMC SAC response corresponding to the senario in Figure 5.1.

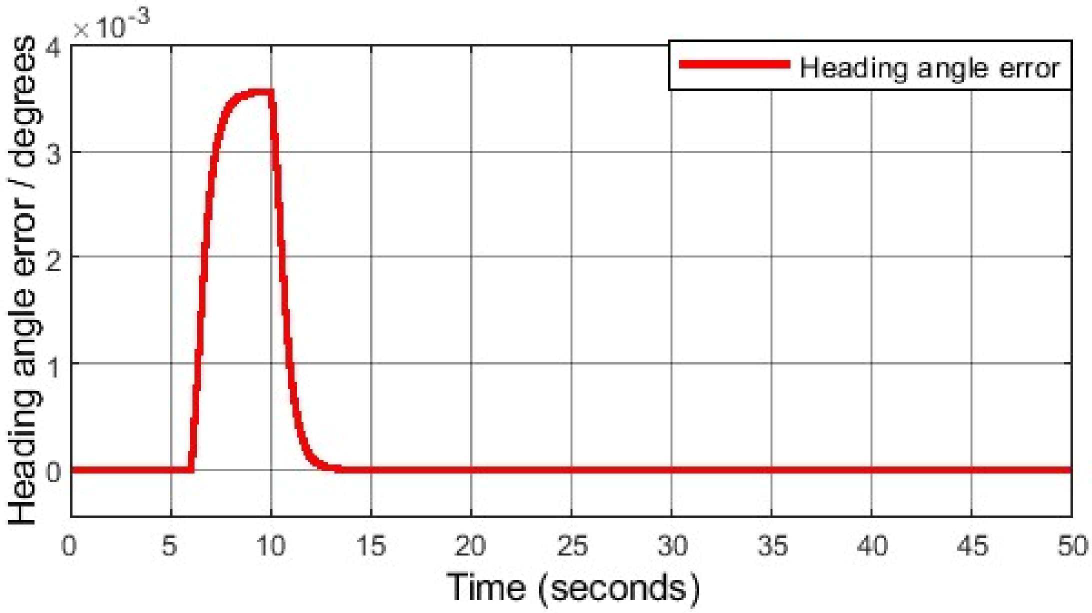

Figure 0.7 Heading angle error.

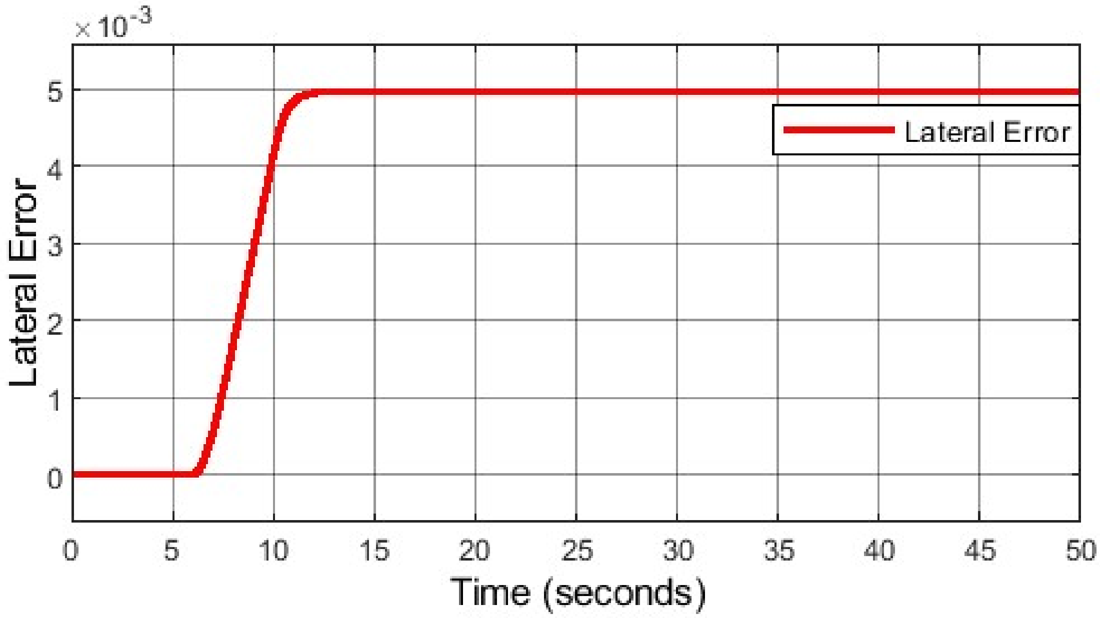

Figure 0.8 Lateral error.

5.3 Adaptive Backstepping (ABS) TTC Derivation

In the previous section, we designed a non-adaptive BS controller for vehicle trajectory tracking. The assumption in the controller design was that the vehicle Inertial parameters (center of gravity location, moment of inertia, and sprung mass) and the tire cornering stiffness are constant and previously known, and the controller proved excellent behavior based on this assumption. These parameters are usually determined experimentally by the manufacturer under certain conditions, usually empty vehicle with known load distribution, and then they are published as constant values, but in reality, they are not constant and can vary significantly in road vehicles, for example the load distribution can change with the number of passengers and seating arrangement. For the same tire, the inflation pressure and the load can significantly affect the cornering stiffness. The cornering stiffness can also change from tire to tire based on the tire type, it can also change with the tire size and width, number of piles and cord angles, it can also change when the tire wears out. The variation of these plant parameters can deteriorate the closed-loop behavior of the non-adaptive BS TTC, because it does not have the learning behavior to adapt itself to these variations. This can result in inconsistent behavior in the control performance, because it was initially tuned for different parameters. We should not overlook the variations of the plant parameters and their consequences because they might cause unstable behavior in the controller if they are too far from the parameters that the controller was initially tuned for. In this section, we are going to derive an ABS control law to overcome the problem of parameter variation. The difference of the ABS controller design from the non-adaptive BS controller designed in the previous section is that in the ABS, we assume no knowledge of the vehicle inertial parameters and cornering stiffeness. Adaptive laws are developed using Lyapunov stability theory to estimate them online; whereas in the BS design, these vehicle parameters are assumed to be previously known and constant.

The ABS controller consists of two parts, a "static" feedback part similar to the feedback control law in the BS controller, and an additional dynamic part that employs a form of nonlinear integral feedback. The purpose of the dynamic part of the feedback law is parameter estimation. The static part of the control law is continuously adapted to the new parameter estimate coming from the dynamic part.

Road curvature is a very important signal that must be accurately known for the controller to follow the planned trajectory. It is usually measured by cameras, or by fusing the camera with other vision sensors. The quality of vision sensors' measurements is usually affected by environmental factors, such as the weather and the time of the day, and that can affect the behavior of the control system. In the ABS design, an adaptive law is developed to estimate the road curvature online. This estimate can replace the measurement from the camera or can potentially be fused with the camera measurement to come up with a better estimate.

In adaptive backstepping basic form, the design employs over-parameterization, which means more than one estimate per unknown parameter. This means that the dynamic part of the controller is not of minimal order. To overcome this problem, a special design procedure is developed in [12] called the "tuning functions procedure". There is a special case where the terms containing the unknown parameters are in the span of the control, which means they appear in the same equation where the control u appears, such as the θ_2 in (5.8). In this case, the parameter θ_2 can be directly cancelled by

u, and this is called the "matching condition". In this case the adaptive design is straight forward because of the matching condition. Another special case is when the term containing the unknown parameters appears in the system one integrator before the control does, such as the parameter θ_1 in (5.8). In this case, we can follow a design procedure called the "extended matching design" [12], which is a transition between over-parametrized and minimal order designs. In the extended matching design, we can avoid over-parameterization without the tuning functions procedure, as explained in detail in steps 2 and 3 of the adaptive controller design in this section.

Given the transformed system in (5.8), repeated below,

$$\begin{aligned} \dot{x}_1 &= x_2 \\ \dot{x}_2 &= x_3 + \theta_1 \\ \dot{x}_3 &= \theta_2 x_3 + u \end{aligned}$$

Our control objective is to regulate the lateral error and the heading angle error and follow the curvature of the of road while stabilizing the vehicle by controlling the yaw rate to prevent excessive steering. We assume that θ_1, θ_2, and b_2 are unknown parameters and we are going to develop adaptive law to estimate them along with the backstepping feedback control law.

Step 1: We start by stabilizing the first subsystem $\dot{x}_1 = x_2$ using the stabilizing function α_1.

We treat x_2 as the virtual control of the subsystem $\dot{x}_1 = x_2$, and then we construct a stabilizing function α_1 for it which is the desired value of x_2 that drives x_1 to zero as time goes to infinity, $x_1 \to 0$ as $t \to \infty$. Since there will be an error between the virtual control x_2 and the stabilizing function α_1, we construct a new state space equation by change of variables, and we call it the "error system". The states of this error system are the differences between the real states and the stabilizing functions, and the control objective is to stabilize all the error states asymptotically.

The first state x_1 which corresponds to the lateral error needs to be driven to zero, so we consider it as the first state z_1 of the error system as below,

$$z_1 = x_1 \tag{5.39}$$

We consider the error between the second state x_2 and its stabilizing function α_1 as the second state in the error system as,

$$z_2 = x_2 - \alpha_1 \tag{5.40}$$

Then we take the derivative of z_1,

$$\dot{z}_1 = \dot{x}_1 = x_2 = z_2 + \alpha_1 \tag{5.41}$$

Then we stabilize the first error system by a Lyapunov function candidate as below,

$$V_1(z_1) = \frac{1}{2} z_1^2 \tag{5.42}$$

$$\dot{V}_1 = z_1 \dot{z}_1 = z_1 \left(z_2 + \alpha_1 \right) = z_1 z_2 + z_1 \alpha_1. \tag{5.43}$$

Setting the stabilizing function α_1 in (5.43) as $\alpha_1 = -c_1 z_1$ with $c_1 \succ 0$ and substituting it in (5.41) and (5.43) yields, respectively,

$$\dot{z}_1 = z_2 - c_1 z_1 \tag{5.44}$$

$$\dot{V}_1 = z_1 z_2 - c_1 z_1^2, \ \forall z_1 \neq 0 \tag{5.45}$$

From (5.45), clearly, if $z_2 = 0$ (we will prove in step 2 below that $z_2 \to 0$), then $\dot{V}_1 = c_1 z_1{}^2 \prec 0, \ \forall z_1 \neq 0$, and z_1 is guaranteed to converge to zero, whereby achieving global asymptotic stability: $z_1 \to 0 \, as \, t \to \infty$.

Step 2: Next, we stabilize the second subsystem $\dot{x}_2 = x_3 - \theta_1$ using the stabilizing function α_2.

We treat x_3 as the intermediate or virtual control, and then we design its stabilizing function α_2 which is the desired value of x_3 that drives x_2 to zero as time goes to infinity, $x_2 \to 0$ as $t \to \infty$.

We consider the error between the third state x_3 and its stabilizing function α_2 as the third state variable in the error system as

$$z_3 = x_3 - \alpha_2 \tag{5.46}$$

To continue, we find the derivative of (5.40), which yields,

$$\dot{z}_2 = z_3 + \alpha_2 - \theta_1 - \dot{\alpha}_1 \tag{5.47}$$

To stabilize the (z_1, z_2)-error system, a composite Lyapunov function candidate is chosen to include both z_1 and z_2. But since θ_1 is unknown and we need to estimate it, then we need to add a third term to the Lyapunov function to include the estimation error. The task in this step then is to develop an adaptive update law to obtain an estimate of θ_1 and to find the stabilizing function α_2. Denote $\hat{\theta}_1$ to be the estimate of θ_1 and $\tilde{\theta}_1 = \theta_1 - \hat{\theta}_1$ to be the estimation error.

The composite Lyapunov function is chosen as,

$$V_2(V_1, z_2, \tilde{\theta}_1) = V_1(z_1) + \frac{1}{2} z_2^{\,2} + \frac{1}{2} \lambda_1 \tilde{\theta}_1^{\,2} \tag{5.48}$$

Taking the derivative of (5.48) yields,

$$\begin{aligned}
\dot{V}_2 &= \dot{V}_1 + z_2 \dot{z}_2 + \lambda_1 \tilde{\theta}_1 \dot{\tilde{\theta}}_1 \\
&= z_1 z_2 - c_1 z_1^{\,2} + z_2 (z_3 + \alpha_2 - \theta_1 - \dot{\alpha}_1) + \lambda_1 \tilde{\theta}_1 \dot{\hat{\theta}}_1 \\
&= -c_1 z_1^{\,2} + z_2 z_3 + z_2 (z_1 + \alpha_2 - \theta_1 - \dot{\alpha}_1) + \lambda_1 \tilde{\theta}_1 \dot{\hat{\theta}}_1
\end{aligned} \tag{5.49}$$

The objective here is to find α_2 and an update law $\dot{\hat{\theta}}_1$ that makes $\dot{V}_1$ negative definite.

First, we will find α_2, and then we will find the update law $\dot{\hat{\theta}}_1$. By inspection, choosing α_2 in (5.49) to make the term $z_1 + \alpha_2 - \theta_1 - \dot{\alpha}_1 = -c_2 z_2$ makes the third term in the equation negative definite and that yields,

$$\alpha_2 = -z_1 - c_2 z_2 + \dot{\alpha}_1 + \theta_1 \tag{5.50}$$

Since (5.50) contains θ_1 and θ_1 is unknown, we cannot substitute the virtual control law (5.50) in (5.49), instead we replace θ_1 by its estimate $\hat{\theta}_1$, so (5.50) becomes,

$$\alpha_2 = -z_1 - c_2 z_2 + \dot{\alpha}_1 + \hat{\theta}_1 \tag{5.51}$$

Then substitute (5.51) in (5.49) to yield,

$$\begin{aligned}
\dot{V}_2 &= -c_1 z_1^{\,2} + z_2 z_3 + z_2 (z_1 - z_1 - c_2 z_2 + \dot{\alpha}_1 + \hat{\theta}_1 - \theta_1 - \dot{\alpha}_1) - \lambda_1 \tilde{\theta}_1 \dot{\hat{\theta}}_1 \\
&= -c_1 z_1^{\,2} + z_2 z_3 + z_2 (-c_2 z_2 + \hat{\theta}_1 - \theta_1) - \lambda_1 \tilde{\theta}_1 \dot{\hat{\theta}}_1 \\
&= -c_1 z_1^{\,2} + z_2 z_3 - c_2 z_2^{\,2} - \tilde{\theta}_1 z_2 - \lambda_1 \tilde{\theta}_1 \dot{\hat{\theta}}_1 \\
&= -c_1 z_1^{\,2} + z_2 z_3 - c_2 z_2^{\,2} - \tilde{\theta}_1 (\lambda_1 \dot{\hat{\theta}}_1 + z_2)
\end{aligned} \tag{5.52}$$

θ_1 is going to appear again in step 3 in $\dot{\alpha}_2$, and we can't use the same estimate we got in step 2, so we have to estimate it again in step 3. To avoid this overparameterization (having multiple estimates for more than one parameter), which is undesirable because it increases the dynamic order of the resulting adaptive controller, we postpone the choice of the update law for $\hat{\theta}_1$ until the next step to avoid over-parametrization, because it is going to appear again in the next step, and that's what we call the extended matching design.

Step 3: The next step is to develop a backstepping control law for u.

To proceed, we need to convert (5.51) to the x-domain, which yields,

$$\alpha_2 = -\left(1 + c_1 c_2\right) x_1 - \left(c_1 + c_2\right) x_2 + \hat{\theta}_1 \tag{5.53}$$

Taking the derivative of (5.53) yields,

$$\dot{\alpha}_2 = \frac{\partial \alpha_2}{\partial x_1}\dot{x}_1 + \frac{\partial \alpha_2}{\partial x_2}\dot{x}_2 + \frac{\partial \alpha_2}{\partial \hat{\theta}_1}\dot{\hat{\theta}}_1 \tag{5.54}$$

Next, we need to find the derivative of z_3, which yields,

$$\begin{aligned}
\dot{z}_3 &= \dot{x}_3 - \dot{\alpha}_2 \\
&= \theta_2 x_3 + b_2 u - \dot{\alpha}_2 \\
&= \theta_2 x_3 + b_2 u - \frac{\partial \alpha_2}{\partial x_1}\dot{x}_1 - \frac{\partial \alpha_2}{\partial x_2}\dot{x}_2 - \frac{\partial \alpha_2}{\partial \hat{\theta}_1}\dot{\hat{\theta}}_1 \\
&= \theta_2 x_3 + b_2 u - \frac{\partial \alpha_2}{\partial x_1}x_2 - \frac{\partial \alpha_2}{\partial x_2}(x_3 + \theta_1) - \frac{\partial \alpha_2}{\partial \hat{\theta}_1}\dot{\hat{\theta}}_1 \\
&= \theta_2 x_3 + b_2 u - \frac{\partial \alpha_2}{\partial x_1}x_2 - \frac{\partial \alpha_2}{\partial x_2}(x_3 + \tilde{\theta}_1 + \hat{\theta}_1) - \frac{\partial \alpha_2}{\partial \hat{\theta}_1}\dot{\hat{\theta}}_1 \\
&= \theta_2 x_3 + b_2 u - \frac{\partial \alpha_2}{\partial x_1}x_2 - \frac{\partial \alpha_2}{\partial x_2}x_3 - \frac{\partial \alpha_2}{\partial x_2}\tilde{\theta}_1 - \frac{\partial \alpha_2}{\partial x_2}\hat{\theta}_1 - \frac{\partial \alpha_2}{\partial \hat{\theta}_1}\dot{\hat{\theta}}_1
\end{aligned} \tag{5.55}$$

Since θ_2 is unknown, we need to develop an update law to obtain an estimate $\hat{\theta}_2$ for it. Define the estimation error as $\tilde{\theta}_2 = \theta_2 - \hat{\theta}_2$ which is the difference between the real value of θ_2 and the estimate $\hat{\theta}_2$. Also, b_2 is unknown and we need to develop update law to estimate it. Denote b_2^{-1} by p, $\hat{p}$ is an estimate of p, and $\tilde{p} = p - \hat{p}$ is the estimation error.

Next, we construct a composite Lyapunov function V_3 to stabilize the $(z_2, z_3, \tilde{\theta}_2, \tilde{p})$-error system.

$$V_3(V_2, z_3, \tilde{\theta}_2, \tilde{p}) = V_2\left(z_1, z_2, \tilde{\theta}_1\right) + \frac{1}{2}z_3^{\,2} + \frac{1}{2}\lambda_2\tilde{\theta}_2^{\,2} + \frac{1}{2}\lambda_3|b_2|\tilde{p}^2,\ \lambda_2, \lambda_3 \succ 0 \tag{5.56}$$

Taking the derivative of (5.56) yields,

$$\begin{aligned}
\dot{V}_3 &= z_2 z_3 - c_1 z_1^{\,2} - c_2 z_2^{\,2} - \tilde{\theta}_1(z_2 + \lambda_1\dot{\hat{\theta}}_1) + z_3(\theta_2 x_3 + b_2 u - \dot{\alpha}_2) \\
&\quad - \lambda_2\tilde{\theta}_2\dot{\hat{\theta}}_2 - |b_2|\lambda_3\tilde{p}\dot{\hat{p}} \\
&= -c_1 z_1^{\,2} - c_2 z_2^{\,2} - \tilde{\theta}_1(z_2 + \lambda_1\dot{\hat{\theta}}_1) + \\
&\quad z_3(z_2 + \theta_2 x_3 + b_2 u - \frac{\partial\alpha_2}{\partial x_1}x_2 - \frac{\partial\alpha_2}{\partial x_2}x_3 - \frac{\partial\alpha_2}{\partial x_2}\tilde{\theta}_1 - \frac{\partial\alpha_2}{\partial\hat{\theta}_1}\dot{\hat{\theta}}_1) \\
&\quad - \lambda_2\tilde{\theta}_2\dot{\hat{\theta}}_2 - |b_2|\lambda_3\tilde{p}\dot{\hat{p}} \\
&= -c_1 z_1^{\,2} - c_2 z_2^{\,2} - \tilde{\theta}_1(z_2 + \lambda_1\dot{\hat{\theta}}_1 - \frac{\partial\alpha_2}{\partial x_2}z_3) \\
&\quad + z_3(z_2 + \theta_2 x_3 + b_2 u - \frac{\partial\alpha_2}{\partial x_1}x_2 - \frac{\partial\alpha_2}{\partial x_2}x_3 - \frac{\partial\alpha_2}{\partial\hat{\theta}_1}\dot{\hat{\theta}}_1) \\
&\quad - \lambda_2\tilde{\theta}_2\dot{\hat{\theta}}_2 - |b_2|\lambda_3\tilde{p}\dot{\hat{p}}
\end{aligned} \tag{5.57}$$

Next, we are going to eliminate $\tilde{\theta}_1$ from (5.57) by the choice of the adaptive law $\dot{\hat{\theta}}_1$. This is the step that we postponed in step 2 to avoid overparameterization, and this is what we call “extended matching design”.

In (5.57), all the terms containing $\tilde{\theta}_1$ have been grouped together. To eliminate them, the update law is chosen as $\dot{\hat{\theta}}_1 = -\frac{1}{\lambda_1}(z_2 + \frac{\partial\alpha_2}{\partial x_2}z_3)$.

Now $\dot{V}_3$ becomes,

$$\dot{V}_3 = -c_1 z_1^2 - c_2 z_2^2 + z_3(z_2 + \theta_2 x_3 + b_2 u - \frac{\partial \alpha_2}{\partial x_1} x_2 - \frac{\partial \alpha_2}{\partial x_2} x_3 - \frac{\partial \alpha_2}{\partial \hat{\theta}_1} \dot{\hat{\theta}}) \\ - \lambda_2 \tilde{\theta}_2 \dot{\hat{\theta}}_2 - |b_2| \lambda_3 \tilde{p} \dot{\hat{p}} \tag{5.58}$$

Next, we need to find the backstepping control law u and the adaptive laws for $\dot{\hat{\theta}}_2$, $\dot{\hat{p}}$ that make (5.58) negative definite.

Choosing u to make the term $z_2 + \theta_2 x_3 + b_2 u - \frac{\partial \alpha_2}{\partial x_1} x_2 - \frac{\partial \alpha_2}{\partial x_2} x_3 - \frac{\partial \alpha_2}{\partial \hat{\theta}_1} \dot{\hat{\theta}}_1 = -c_3 z_3,\ c_3 \succ 0$ makes the third term in (5.58) negative definite, and that results in the backstepping control law u to be,

$$u = b_2^{-1}(-z_2 - c_3 z_3 - \theta_2 x_3 + \frac{\partial \alpha_2}{\partial x_1} x_2 + \frac{\partial \alpha_2}{\partial x_2} x_3 + \frac{\partial \alpha_2}{\partial \hat{\theta}_1} \dot{\hat{\theta}}_1) \tag{5.59}$$

Since we don't know θ_2 and b_2 in (5.58), we can't substitute it directly in (5.58). Instead, we need to substitute their estimates first, so (5.59) becomes,

$$u = \hat{p}\underbrace{(-z_2 - c_3 z_3 - \hat{\theta}_2 x_3 + \frac{\partial \alpha_2}{\partial x_1} x_2 + \frac{\partial \alpha_2}{\partial x_2} x_3 + \frac{\partial \alpha_2}{\partial \hat{\theta}_1} \dot{\hat{\theta}}_1)}_{\bar{u}} \tag{5.60}$$

$$u = \hat{p}\bar{u} \Rightarrow b_2 u = b_2 \hat{p} \bar{u} \tag{5.61}$$

We have with $\hat{p} = p - \tilde{p}$,

$$b_2 u = \bar{u} - b_2 \tilde{p} \bar{u} \tag{5.62}$$

Then we substitute (5.62) in (5.58), which yields,

$$
\begin{aligned}
\dot{V}_3 &= -c_1 z_1^{\,2} - c_2 z_2^{\,2} + z_3(z_2 + \theta_2 x_3 + \bar{u} - b_2 \tilde{p}\bar{u} - \frac{\partial \alpha_2}{\partial x_1} x_2 - \frac{\partial \alpha_2}{\partial x_2} x_3 - \frac{\partial \alpha_2}{\partial \hat{\theta}_1}\dot{\hat{\theta}}_1) \\
&\quad - \lambda_2 \tilde{\theta}_2 \dot{\hat{\theta}}_2 - |b_2| \lambda_3 \tilde{p}\dot{\hat{p}} \\
&= -c_1 z_1^{\,2} - c_2 z_2^{\,2} + z_3(z_2 + \theta_2 x_3 + \bar{u} - \frac{\partial \alpha_2}{\partial x_1} x_2 - \frac{\partial \alpha_2}{\partial x_2} x_3 - \frac{\partial \alpha_2}{\partial \hat{\theta}_1}\dot{\hat{\theta}}_1) \\
&\quad - \lambda_2 \tilde{\theta}_2 \dot{\hat{\theta}}_2 - b_2 \tilde{p}\bar{u} z_3 - |b_2| \lambda_3 \tilde{p}\dot{\hat{p}} \\
&= -c_1 z_1^{\,2} - c_2 z_2^{\,2} + z_3(z_2 + \theta_2 x_3 + -z_2 - c_3 z_3 - \hat{\theta}_2 x_3 + \frac{\partial \alpha_2}{\partial x_1} x_2 + \frac{\partial \alpha_2}{\partial x_2} x_3 \\
&\quad + \frac{\partial \alpha_2}{\partial \hat{\theta}_1}\dot{\hat{\theta}}_1 - \frac{\partial \alpha_2}{\partial x_1} x_2 - \frac{\partial \alpha_2}{\partial x_2} x_3 - \frac{\partial \alpha_2}{\partial \hat{\theta}_1}\dot{\hat{\theta}}_1) - \lambda_2 \tilde{\theta}_2 \dot{\hat{\theta}}_2 - b_2 \tilde{p}\bar{u} z_3 - |b_2| \lambda_3 \tilde{p}\dot{\hat{p}} \\
&= -c_1 z_1^{\,2} - c_2 z_2^{\,2} + z_3(\theta_2 x_3 + -c_3 z_3 - \hat{\theta}_2 x_3) - \lambda_2 \tilde{\theta}_2 \dot{\hat{\theta}}_2 - b_2 \tilde{p}\bar{u} z_3 - |b_2| \lambda_3 \tilde{p}\dot{\hat{p}} \\
&= -c_1 z_1^{\,2} - c_2 z_2^{\,2} - c_3 z^2_3 + \theta_2 x_3 z_3 - z_3 \hat{\theta}_2 x_3 - \lambda_2 \tilde{\theta}_2 \dot{\hat{\theta}}_2 - b_2 \tilde{p}\bar{u} z_3 - |b_2| \lambda_3 \tilde{p}\dot{\hat{p}} \\
&= -c_1 z_1^{\,2} - c_2 z_2^{\,2} - c_3 z^2_3 + x_3 z_3 \tilde{\theta}_2 - \lambda_2 \tilde{\theta}_2 \dot{\hat{\theta}}_2 - b_2 \tilde{p}\bar{u} z_3 - |b_2| \lambda_3 \tilde{p}\dot{\hat{p}} \\
&= -c_1 z_1^{\,2} - c_2 z_2^{\,2} - c_3 z^2_3 + \tilde{\theta}_2 (x_3 z_3 - \lambda_2 \dot{\hat{\theta}}_2) - |b_2| \lambda_3 \tilde{p}(\dot{\hat{p}} + \frac{1}{\lambda_3} sign(b_2)\bar{u} z_3)
\end{aligned}
\tag{5.63}
$$

We can eliminate $\tilde{\theta}_2$ by choosing the update law $\dot{\hat{\theta}}_2 = \frac{1}{\lambda_2} x_3 z_3$, and eliminate $\tilde{p}$ by choosing the update law for $\dot{\hat{p}}$ to be $\dot{\hat{p}} = -\frac{1}{\lambda_3} sign(b_2)\bar{u} z_3$.

Then $\dot{V}_3$ becomes,

$$
\dot{V}_3 = -c_1 z_1^{\,2} - c_2 z_2^{\,2} - c_3 z_3^{\,2},\ c_1 \succ 0, c_2 \succ 0, c_3 \succ 0 \tag{5.64}
$$

From (5.56) and (5.64), the Lasalle-Yoshizawa theorem [12], stated in chapter 3, guarantees the global boundness of $z_1, z_2, z_3, \hat{\theta}_1, \hat{\theta}_2, \hat{p}$, and it follows that $z_1, z_2, z_3 \to 0$ as $t \to \infty$, x_1 is also bounded since $x_1 = z_1$ and it follows that $\lim_{t \to \infty} x_1 = 0$, x_2 boundness follows from the boundness of α_1 and z_2 since $x_2 = \alpha_1 + z_2$. The boundness of x_3

follows from the boundness of α_2 and z_3 since $x_3 = \alpha_2 + z_3$. Given those facts with (5.62), it follows that $u(t)$ in (5.60) is also bounded.

Next, we need to find the backstepping control law u in the x-domain, which yields,

$$u = \hat{p}\begin{pmatrix} -(c_1 + c_3 + c_1c_2c_3)x_1 - (c_1c_2 + c_1c_3 + c_2c_3 + 2)x_2 \\ -(c_1 + c_2 + c_3 + \hat{\theta}_2)x_3 + c_3\hat{\theta}_1 + \dot{\hat{\theta}}_1 \end{pmatrix} \tag{5.65}$$

Finally, we need to convert the update laws $\dot{\hat{\theta}}_1, \dot{\hat{\theta}}_2, \dot{\hat{p}}$ to the x-domain,

$$\dot{\hat{\theta}}_1 = -\frac{1}{\lambda_1}\left(c_1x_1 + x_2 - (c_1 + c_2)(x_3 - \alpha_2)\right) \tag{5.66}$$

$$\dot{\hat{\theta}}_2 = \frac{1}{\lambda_2}x_3(x_3 - \alpha_2) \tag{5.67}$$

$$\dot{\hat{p}} = -\frac{1}{\lambda_3}sign(b_2)\bar{u}(x_3 - \alpha_2) \tag{5.68}$$

where,

$$\alpha_2 = -(1 + c_1c_2)x_1 - (c_1 + c_2)x_2 + \hat{\theta}_1$$

$$\begin{aligned}\bar{u} = &-(c_1 + c_3 + c_1c_2c_3)x_1 - (c_1c_2 + c_1c_3 + c_2c_3 + 2)x_2 \\ &-(c_1 + c_2 + c_3 + \hat{\theta}_2)x_3 + c_3\hat{\theta}_1 + \dot{\hat{\theta}}\end{aligned}$$

The parameters $c_1, c_2, and\, c_3$ are the tuning parameters for the controller performance. the choice of those parameters dramatically affects the controller behavior. For example, they can be tuned to eliminate steady state error, add damping and reduce rise time. The parameters $\lambda_1, \lambda_2, and\, \lambda_3$ are the adaptation gains, they can be tuned to control the rate of convergence of the estimated parameters. λ_1 is the adaptation gain for $\theta_1 = v\kappa$. After estimating θ_1, we divide it by vehicle velocity v to extract the road curvature value κ to be used in the feedforward. λ_2 and λ_3 are the adaptation gains for the lumped parameters $\theta_2 = a_{22} / v = \left(-C_r l_r^2 + C_f l_f^2\right) / vI_z$ and $p = b_2^{-1} = \left(C_f l_f / I_z\right)^{-1}$, respectively.

5.3.1 Dynamic Feedforward Transfer Function Estimation

Curvature compensation is needed for curved roads. Given the road curvature, we need to convert this curvature to steering angle command and add it to the feedback control law. A commonly known geometrical relationship between curvature and steering angle that can be used for curvature compensation is $\delta = \tan^{-1}\left(\frac{L}{R}\right) = \tan^{-1}\left(L\kappa\right)$, L is the wheel base (constant and known), and R is the radius of the road. This kinematic relationship works only at low speeds (about 2.5 mps/9 kph and below) but will fail at high speeds when lateral forces and slip angles develop. The approach we develop in dissertation to account for high speeds is to find the relationship between curvature and angle by estimating the dynamics of the transfer function from vehicle curvature to steering angle and then use this transfer function in the controller to compensate for curvature.

To do the estimation, a signal generator was used to send sine wave angle commands at different vehicle speeds to the steering angle controller in the test vehicle, and then we calculated the curvature that the vehicle actually took based on the commanded steering angle, we measured the yaw rate and the vehicle speed and then we calculated the vehicle curvature by dividing yaw rate by vehicle speed $\rho = \dot{\psi} / v$. For the same angle, the curvature will be different at different speeds, so the coefficients will also be different depending on speed, so we need to create look up tables based on speed for all the coefficients.

It is important to distinguish here between the road curvature denoted by κ and the actual curvature that the vehicle took denoted by ρ. ρ does not necessarily equal to κ, but this is our control objective as we want the vehicle curvature to follow the road curvature. The transfer function will be used in the controller as the feedforward part. It will take the road curvature as input to compute the feedforward steering angle that is required to negotiate that given road curvature.

The Recursive Least Squares Estimation (RLSE) algorithm was used to estimate the coefficients of the transfer function knowing only the front wheel steering angle and the vehicle curvature.

$$\frac{y_{rlse}}{u_{rlse}} = \frac{\rho}{\delta} = \frac{b_1 z + b_2}{z^2 + a_1 z + a_2} \tag{5.69}$$

We need to estimate the vector $\hat{\boldsymbol{\theta}}_k = \begin{bmatrix} a_1 & a_2 & b_1 & b_2 \end{bmatrix}'$ knowing only the vector of inputs and outputs given by:

$$\mathbf{H}_k = \begin{bmatrix} -y_{rlse_{k-1}} & -y_{rlse_{k-2}} & u_{rlse_{k-1}} & u_{rlse_{k-2}} \end{bmatrix} \tag{5.70}$$

where a_1, a_2, b_1, b_2 are the second order transfer function coefficients. The standard RLSE equations below are used for the estimation.

$$\begin{aligned}
\mathbf{H}_k &= \begin{bmatrix} -y_{rlse_{k-1}} & -y_{rlse_{k-2}} & u_{rlse_{k-1}} & u_{rlse_{k-2}} & 1 \end{bmatrix} \\
\mathbf{K}_k &= \mathbf{P}_{k-1}\mathbf{H}_k^T \left(\mathbf{H}_k \mathbf{P}_{k-1} \mathbf{H}_k^T + \lambda_{rlse} \right)^{-1} \\
\hat{\boldsymbol{\theta}}_k &= \hat{\boldsymbol{\theta}}_{k-1} + \mathbf{K}_k \left(y_k - \mathbf{H}_k \hat{\boldsymbol{\theta}}_{k-1} \right) \\
\mathbf{P}_k &= \left(\mathbf{I}_3 - \mathbf{K}_k \mathbf{H}_k \right) \mathbf{P}_{k-1} / \lambda_{rlse}
\end{aligned}$$

where, $\mathbf{P}_k$ is the covariance matrix and λ_{rlse} is the forgetting factor used to tune the rate of convergence of the estimated parameters. A typical value for it is in the range 0.9 to 1. The value that was used is 0.98.

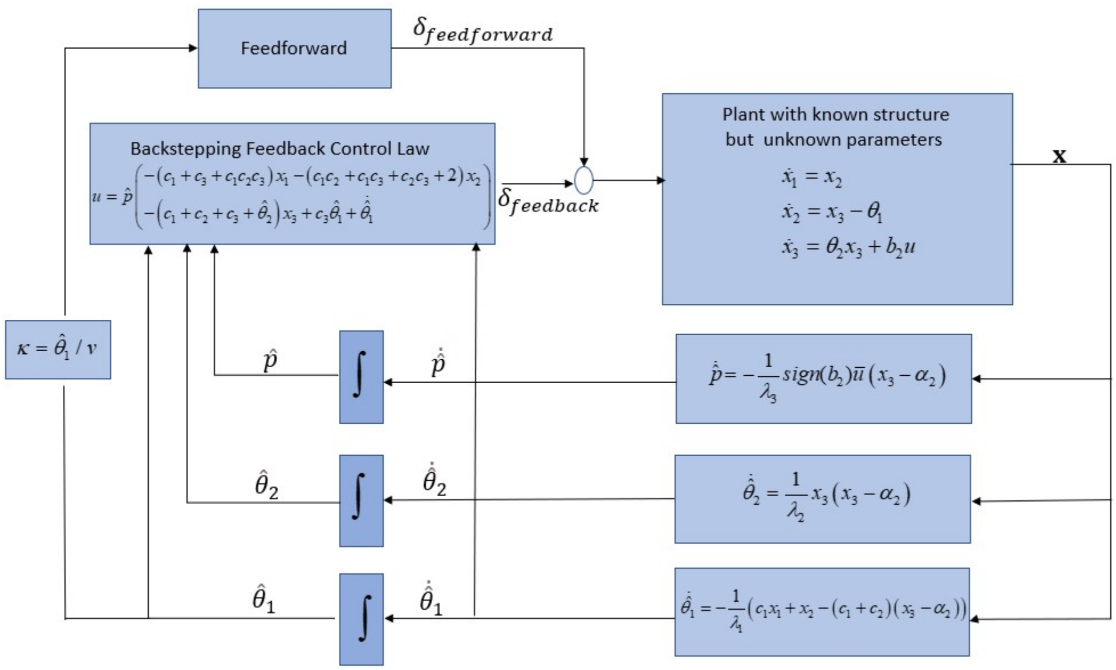

Figure 0.9 ABS trajectory tracking controller closed loop system

5.3.2 Simulation Results of ABS TTC

The simulations were conducted in Matlab by generating an artificial trajectory for the vehicle to follow, and then one scenario was conducted in Matlab and Carsim. The Lyapunov coefficients c_1, c_2, and c_3 were tuned to achieve the desired performance.

c_1 was tuned to reduce the steady state errors, c_2 was tuned to control the damping in the errors, and c_3 was tuned to control the yaw rate of the vehicle to prevent excessive steering and eliminate oscillations. A signal generator was used to generate an artificial trajectory for the vehicle to follow. In Figures 5.10 - 5.15, the trajectory starts with zero curvature and then ramps up to a constant radius curve of 333m, which corresponds to 0.003 m^{-1} in curvature unit, at 20 m/s (72 kph). Figure 5.10 shows excellent tracking of the vehicle curvature to the desired curvature. Figure 5.11 shows the estimated road curvature convergence to the actual road curvature. Fast and accurate convergence was achieved with very minor overshoot at 4s at the point when we transitioned to the final value of the curve. Figure 5.12 shows the asymptotic convergence of the virtual control errors (z_1, z_2, z_3) to zero. In the transitioning period from 0 to 4 seconds, there were some transients in the errors but they settled down and converged to zero at steady state when we reached the final constant value of the curvature. Figure 5.13 shows the heading angle error and the lateral error, both converged to zero at steady state. Figure 5.14 shows the yaw rate of the vehicle, which did not exceed the desired value $\dot{\psi}_{desired} = v\kappa = (20)(0.003) = 0.06$ radians/s.

Figure 5.15 shows the results of computing the feedforward steering angle that is required to negotiate the estimated road curvature from the transfer function. Figures 5.16-5.21 demonstrate the controller response to a sine wave with a sharper curve than the previous scenario (200 m radius curve/0.005 m^{-1}) but at lower speed (15 mps /54 kph). Figures 5.16 and 5.17 show tracking and estimation of the road curvature, respectively. Figure 5.18 shows the virtual control errors (differences between the states that we treated as virtual controls and their stabilizing functions). Since the reference signal is constantly changing, the virtual control errors will also keep changing to keep up with the changing reference signal and will not converge to a constant value. Similarly, the heading angle error and the lateral error in Figure 5.19 will not converge to a constant value. Figure 5.20 shows the yaw rate of the vehicle, which did not exceed the desired value, $\dot{\psi}_{desired} = v\kappa = (15)(0.005) = 0.075$ radians/s. Figure 5.21 shows the results of computing the feedforward steering angle that is required to negotiate the estimated road curvature from the transfer function. In both of the scenarios, the controller parameters were chosen to be $c_1 = 20, c_2 = 20, c_3 = 5$, and adaptation gains were chosen to be $\lambda_1 = 10, \lambda_2 = 1, \lambda_3 = 1$.

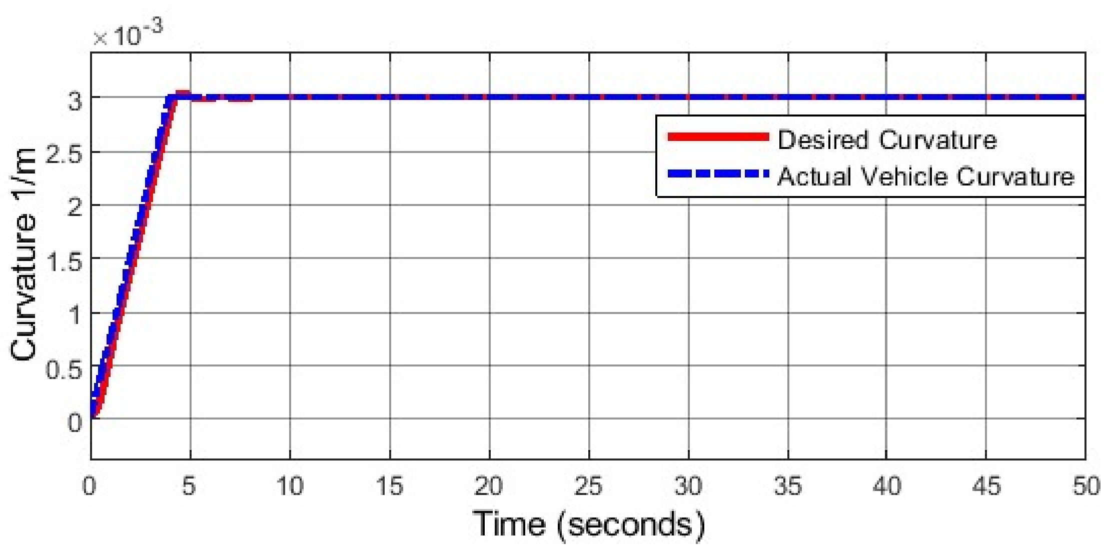

Figure 0.9 Desired curvature vs. vehicle actual curvature

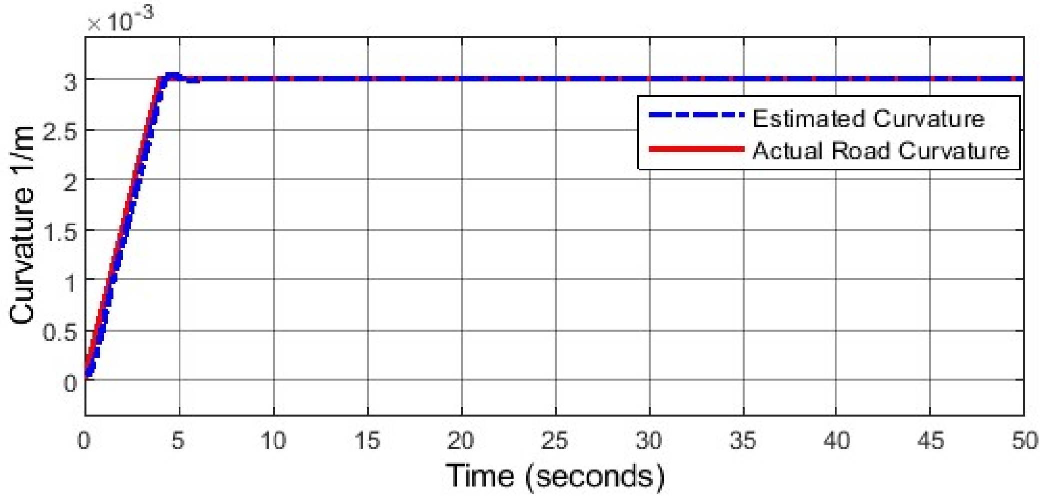

Figure 0.10 Estimated vs actual road curvature

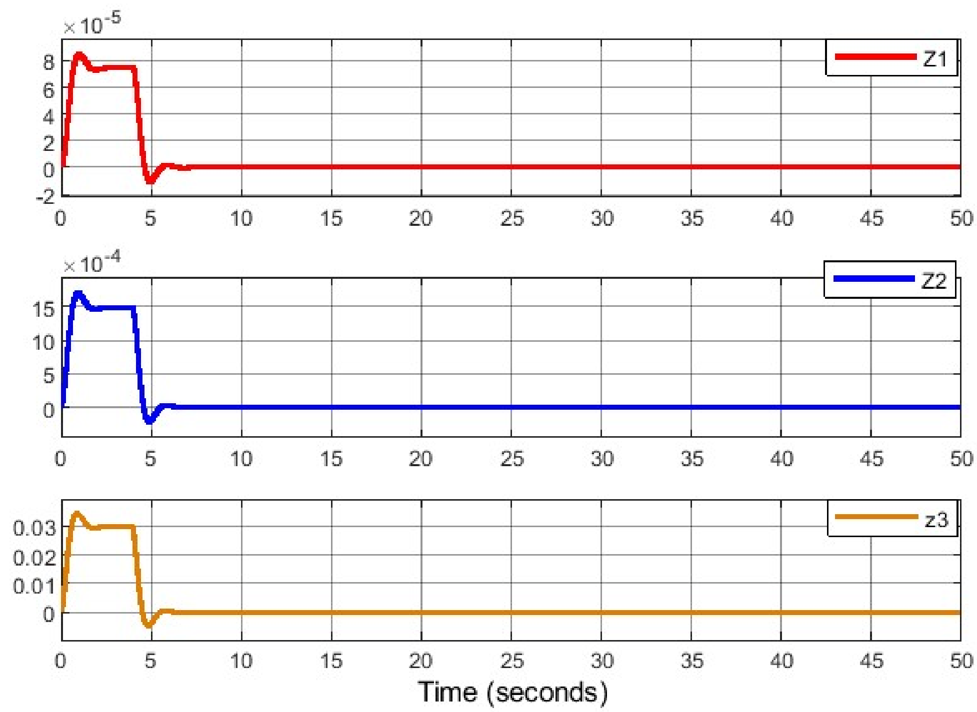

Figure 0.11 Virtual controls errors

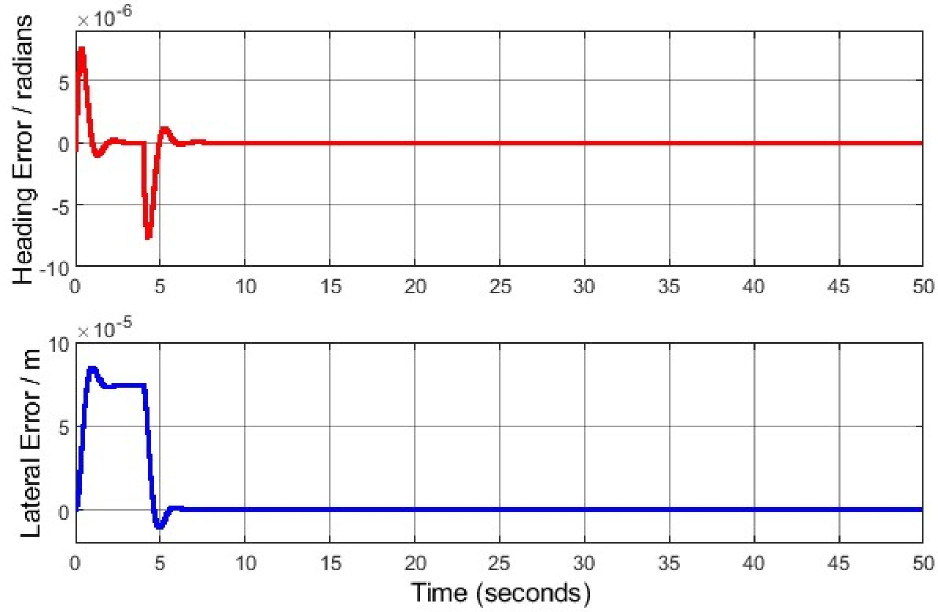

Figure 0.12 Errors with respect to the reference trajectory

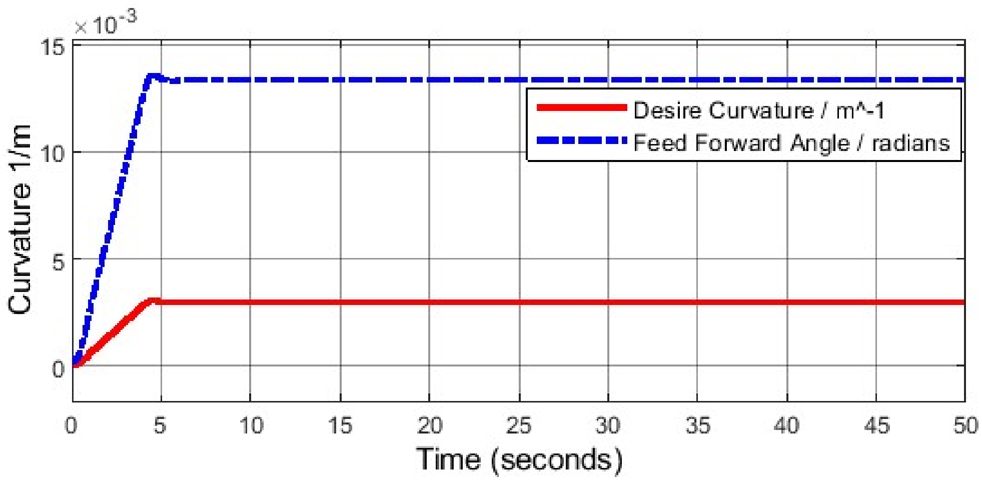

Figure 0.13 Feedforward steering angle vs. road curvature

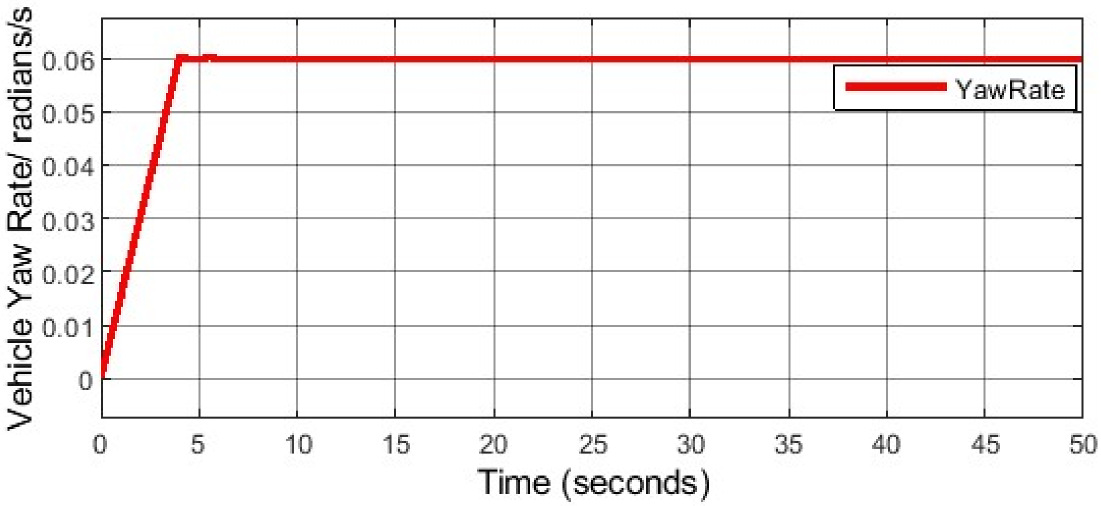

Figure 0.14 Vehicle yaw rate

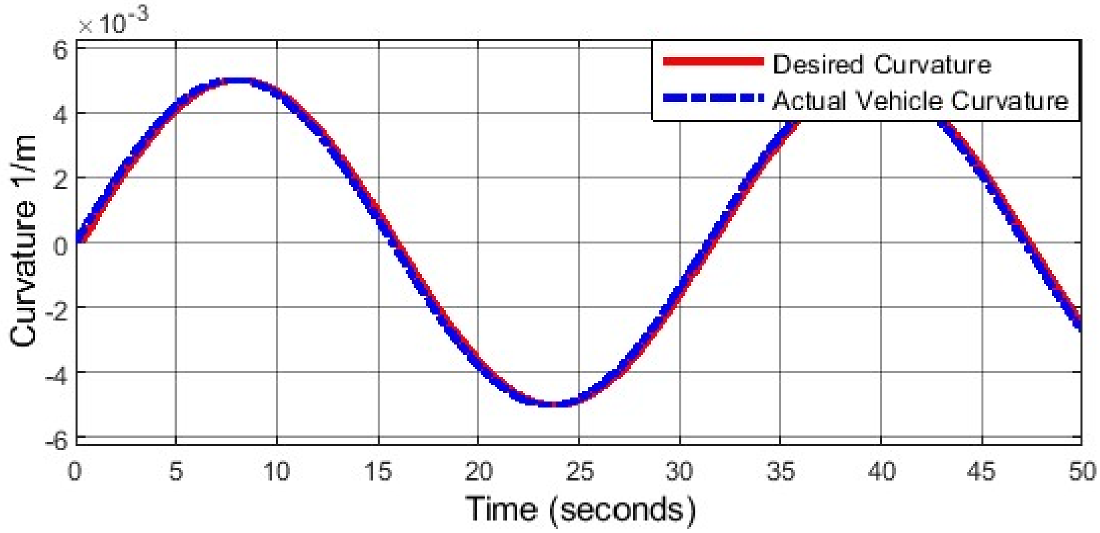

Figure 0.15 Desired curvature vs. vehicle actual curvature

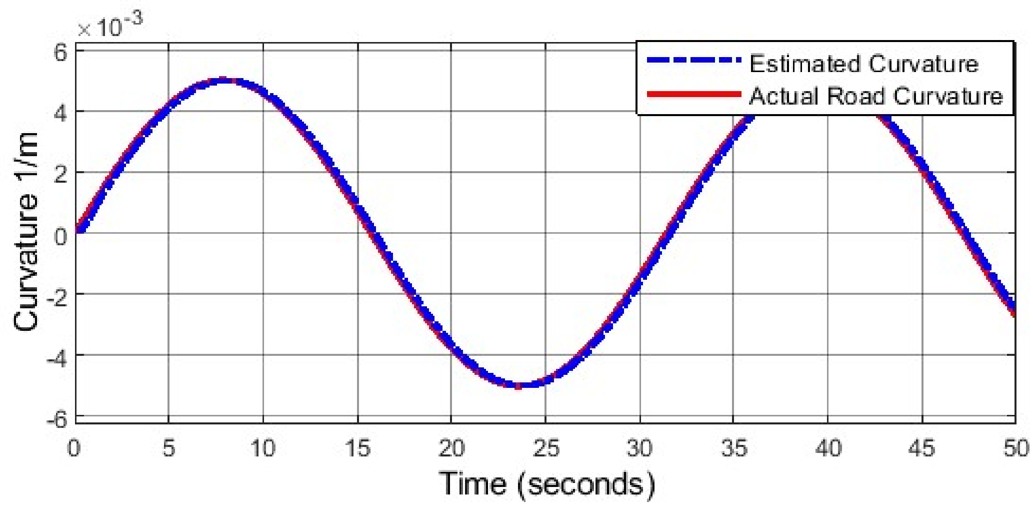

Figure 0.16 Estimated vs actual road curvature

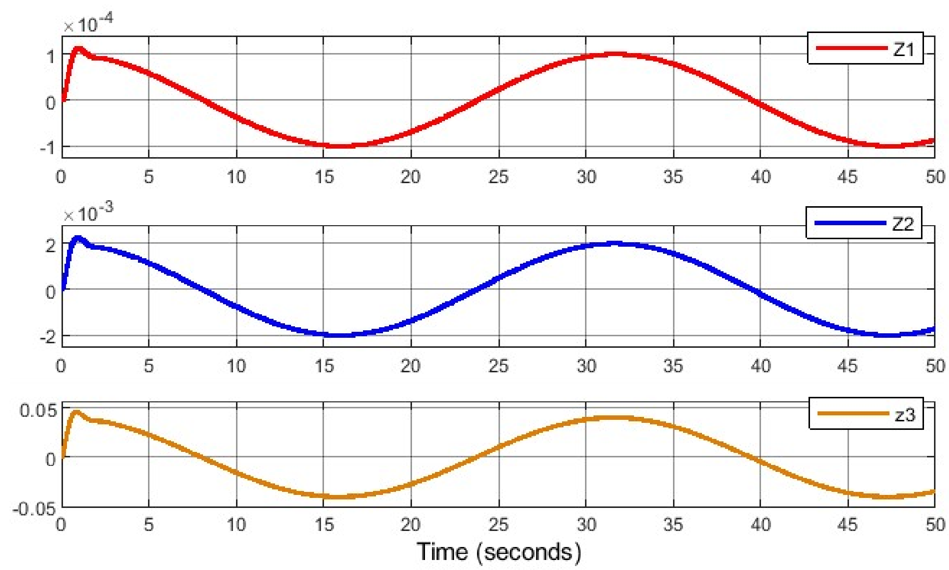

Figure 0.17 Virtual controls errors

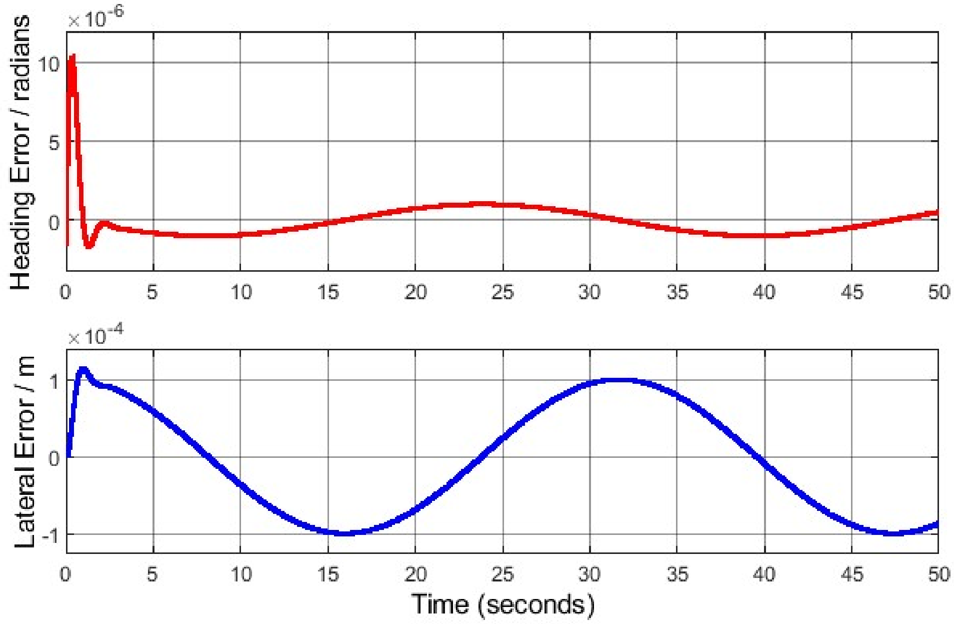

Figure 0.18 Errors with respect to reference trajectory

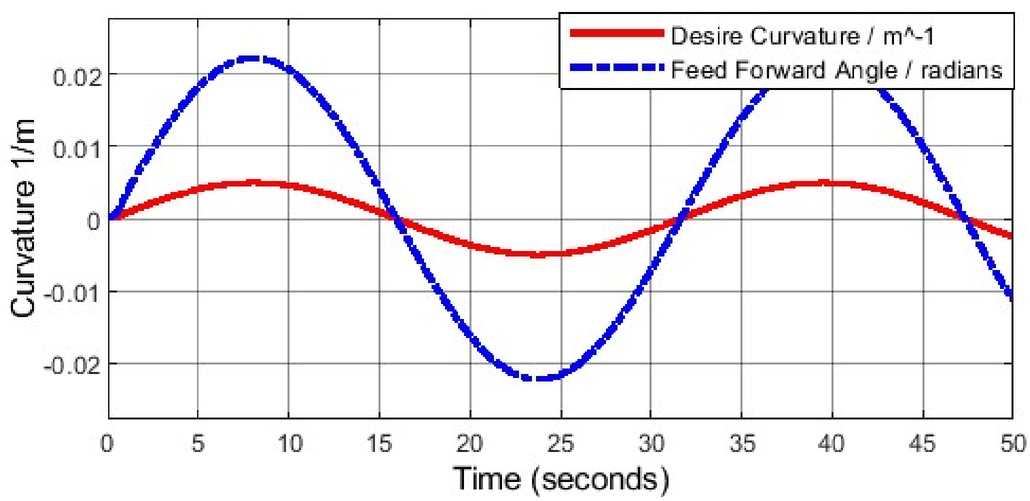

Figure 0.19 Feedforward steering angle vs. road curvature

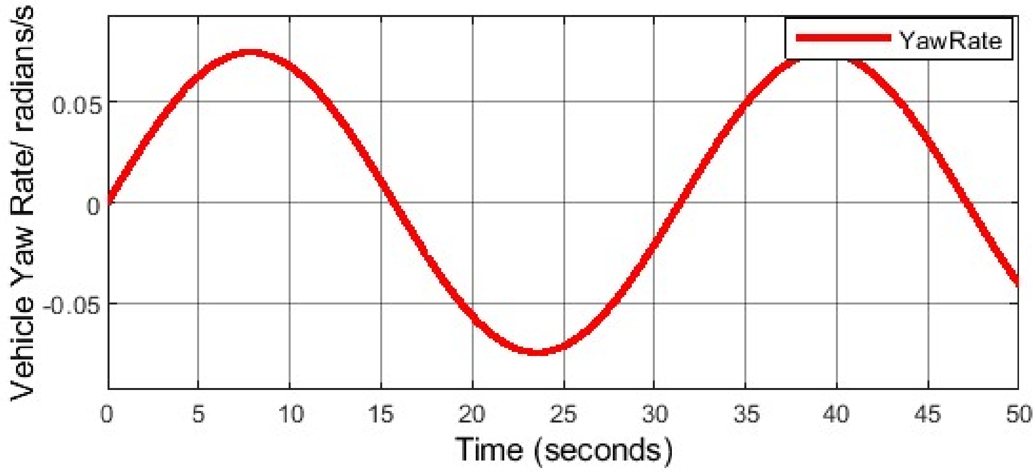

Figure 0.20 Vehicle yaw rate

The ABS TTC was also tested and validated in Carsim software environment. CarSim is a very usefull software tool for simulating the dynamic behavior of vehicles in a virtual environment. Simulink models that have the model-based controllers design can be easily connected to Carsim for testing and validation. As shown in Figure 5.22. The road was chosen to start on a straight section and then to transitions to a 200 m radius curved section and then to transitions back to a straight section again to cover curve entry and curve exit scenarios in addition to straight and curved road.

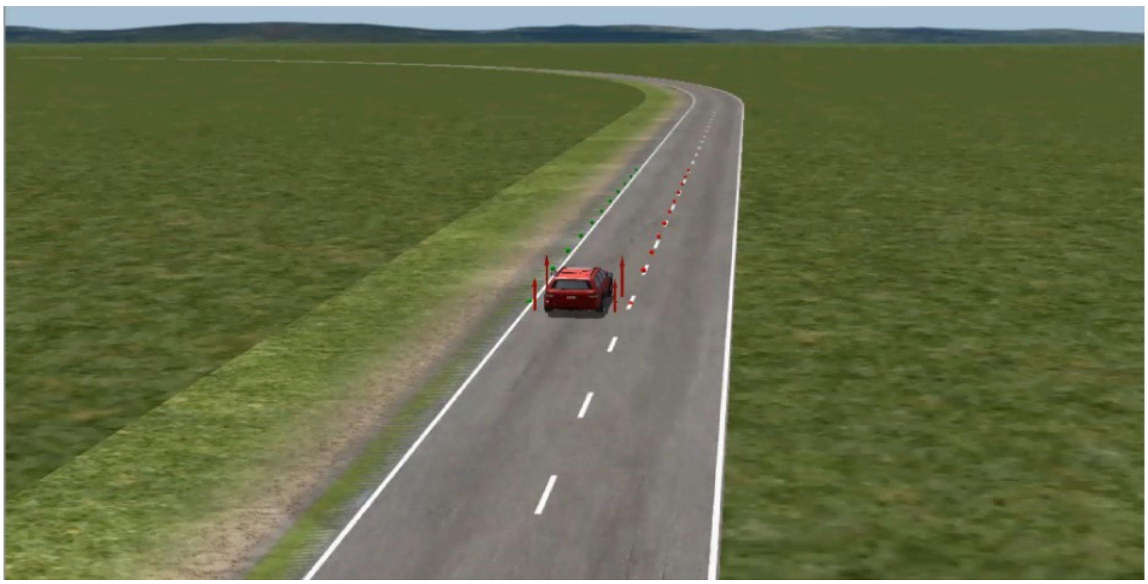

Figure 0.21 The Carsim scenario used for simulation.

CHAPTER SIX

CONCLUSION AND FUTURE WORK

Two control strategies were developed to control the electric power steering angle under parameter uncertainties, modeling inaccuracies, and disturbances. The first one is sliding mode control (SMC), which is a simple approach to robust control, and the second one is adaptive backstepping control. Both methods proved excellent tracking of the EPS angle in the presence of model uncertainty and disturbances. The only drawback of the SMC approach is the chattering phenomenon produced because of the discontinuous part of the control law. To overcome this problem, a VG SMC was developed, which reduced the chattering significantly and that was proved by experimental results on a test vehicle on the road. Also, experimental results proved that the SMC was able to overcome the asymmetrical hysteresis behavior caused by friction and backlash which is usually challenging to overcome with other methods.

To compare the two methods in general, adaptive control does not require a priori information about the model parameters because of its learning behavior, while robust control requires reasonable a priori estimate about the model parameters bounds. An adaptive controller improves its behavior through the parameter adaptation process, while a robust controller tries to keep consistent behavior. The high control activity of a robust controller makes it superior to adaptive control in dealing with disturbances and fast varying parameters. Conversely, adaptive control is superior in dealing with constant and slowly varying parameters because of its learning behavior as outlined in [12]. My future work will be aimed toward developing a SAC to control the EPS angle by combining the desirable features of both methods to lead to robust adaptive control.

Two control strategies were developed for TTC, non-adaptive backstepping and adaptive backstepping. Non-adaptive backstepping showed excellent results assuming that the vehicle inertial parameters are known and constant, but in real world applications, these parameters are not constant and can vary significantly in road vehicles. Parameter variation cannot guarantee consistent controller behavior. Adaptive backstepping proved excellent performance with no a priori information about the model parameters because of the learning behavior of adaptive control, where it improves its behavior by adjusting the model parameters, and that keeps a consistent control behavior even when the parameters are varying. The adaptive controller resulted in a very good estimate of the road curvature, which can potentially be fused with the road curvature measured by vision sensors to come up with a more stable and accurate estimate.

Three approaches were developed to estimate the self-aligning moment. The first one is model based, which depends on the knowledge of lateral and normal forces, tire slip angle, and some parameters of the tires that the vehicle is equipped with. The drawback of this method is that because it depends on tire parameters, changing the tires in the vehicle means that these parameters are not valid anymore. To overcome this problem, two other methods were developed to estimate the self-aligning moment with no required information about the tire parameters. Both methods treat the self-aligning moment as disturbance. In addition, the static friction is treated as disturbance and estimated with the self aligning moment. The first method is a sliding mode observer, which is a modular design separate from the controller design. The second one is a

Lyapunov based method, which is embedded in the backstepping controller design. The backstepping method proved a reasonably good estimate, but the sliding mode observer resulted in a more accurate estimate, also the modularity of the sliding mode observer makes the estimate usable by other control modules.

A real-time estimation algorithm for road bank angle disturbance and vehicle side slip angle is developed using inexpensive on-board vehicle sensors. The algorithm utilizes a combination of yaw rate and lateral acceleration measurements from IMU and a vehicle model that describes the vehicle lateral motion in terms of side slip angle and yaw rate. The developed algorithm was evaluated by experimental tests on a test vehicle on a test track with previously known bank angles. The results of the side slip angle and yaw rate angle were compared with the estimate from a GPS/INS system installed in the vehicle. The experimental results show that the algorithm provides estimates with reasonable accuracy for the vehicle side slip angle and road bank angle in various driving maneuvers. The estimated vehicle side slip angle was used to compute the tire slip angle for the self- aligning moment model-based estimation. In addition, both road bank angle and side slip angle estimates can potentially be used in vehicle stability control systems, such as yaw stability control and rollover prevention. Currently, I am investigating adding the vehicle roll dynamics and the side wind dynamics to the model to estimate them as well. The roll angle results from suspension deflection and it is considered as a state, while the bank angle is the road inclination, which is considered as disturbance. It is important for the estimation algorithm to distinguish between the two angles as the control system needs to compensate for them differently.

REFERENCES

[1] Jean-Jacques Slotine , Weiping Li , " Applied Nonlinear Control " ISBN 0-13-040890-5.

[2] Bartolini, G., Ferrara, A., Usai, E.: Chattering avoidance by second-order sliding mode control. IEEE Trans. Autom. Control 43(2), 241–246 (1998).

[3] Bartolini, G., Pisano, A., Punta, E., Usai, E.: A survey of applications of second-order sliding mode control to mechanical systems. IEEE Trans. Autom. Control 76(9/10), 875–892 (2003).

[4] Boiko, I., Fridman, L., Pisano, A., Usai, E.: Analysis of chattering in systems with second-order sliding modes. IEEE Trans. Autom. Control 52(11), 2085–2102 (2007).

[5] Chalanga, A., Kamal, S., Fridman, L.M., Bandyopadhyay, B., Moreno, J.A.: Implementation of super-twisting control: super-twisting and higher order sliding-mode observer-based approaches. IEEE Trans. Ind. Electron. 63(6), 3677–3685 (2016).

[6] Levant, A.: Sliding order and sliding accuracy in sliding mode control. Int. J. Control 58(6), 1247–1263 (1993).

[7] Levant, A.: Chattering analysis. IEEE Trans. Autom. Control 55(6), 1380–1389 (2010).

[8] Levant, A.: Robust exact differentiation via sliding mode technique. Automatica 34(3), 379– 384 (1998).

[9] Levant, A.: Higher order sliding modes, differentiation and output-feedback control. Int. J. Control 76(9/10), 924–941 (2003).

[10] Levant, A.: Homogeneity approach to high-order sliding mode design. Automatica 41(5), 823– 830 (2005).

[11] Levant, A.: Quasi-continuous high-order sliding-mode controllers. IEEE Trans. Autom. Control 50(11), 1812–1816 (2005).

[12] Krstic, M., Kanellakopoulos, I., Kokotovic, P.V.: Nonlinear and Adaptive Control Design. Wiley, New York (1995).

[13] Ioannou, P., Kokotovic, P.: An asymptotic error analysis of identifiers and adaptive observers in the presence of parasitics. IEEE Transactions on Automatic Control 27, 921–927 (1982).

[14] Praly, L.: Towards a globally stable direct adaptive control scheme for not necessarily minimum phase systems. IEEE Transactions on Automatic Control 29, 946–949 (1984).

[15] Praly, L.: Lyapunov design of stabilizing controllers for cascaded systems. IEEE Transactions on Automatic Control 36, 1177–1181 (1991).

[16] Praly, L., d'Andrea Novel, B., Coron, J.M.: Lyapunov design of stabilizing controllers. In: Proceedings of the 28th IEEE Conference on Decision and Control, vol. 2, pp. 1047–1052 (1989).

[17] Praly, L.: Towards an adaptive regulator: Lyapunov design with a growth condition. In: Proceedings of the 30th IEEE Conference on Decision and Control, vol. 2, pp. 1094–1099 (1991).

[18] Pomet, J.B., Praly, L.: Adaptive nonlinear regulation: estimation from the lyapunov equation. IEEE Transactions on Automatic Control 37, 729–740 (1992).

[19] Tao, G., Ioannou, P.A.: Model reference adaptive control for plants with unknown relative degree. IEEE Transactions on Automatic Control 38, 976–982 (1993).

[20] Rajamani, R., 2011. Vehicle dynamics and control. Springer Science & Business Media.

[21] Boucher, C. and Noyer, J.C., 2018. A general framework for 3-D parameters estimation of roads using GPS, OSM and DEM data. Sensors, 18(1), p.41.

[22] Ryu, J. and Gerdes, J.C., 2004, June. Estimation of vehicle roll and road bank angle. In Proceedings of the 2004 American control conference (Vol. 3, pp. 2110-2115). IEEE.

[23] Hahn, J.O., Rajamani, R., You, S.H. and Lee, K.I., 2004. Real-time identification of road-bank angle using differential GPS. IEEE Transactions on Control Systems Technology, 12(4), pp.589-599.

[24] Ryu, J., 2005. State and parameter estimation for vehicle dynamics control using GPS. Stanford University.

[25] Brown, L.S. and Bevly, D.M., 2015. Roll and Bank Estimation Using GPS/INS and Suspension Deflections. Electronics, 4(1), pp.118-149.

[26] Kim, K.W., Lee, S.B., Park, C.S. and Yi, K., 2015. Estimation of lateral disturbance under parameter uncertainties. International Journal of Automotive Technology, 16(3), pp.427-433.

[27] Acosta, M., Alatorre, A., Kanarachos, S., Victorino, A. and Charara, A., 2017. Estimation of tire forces, road grade, and road bank angle using tire model-less approaches and Fuzzy Logic. IFAC-PapersOnLine, 50(1), pp.14836-14842.

[28] Jiang, K., Victorino, A.C. and Charara, A., 2015, September. Adaptive estimation of vehicle dynamics through RLS and Kalman filter approaches. In 2015 IEEE 18th International Conference on Intelligent Transportation Systems (pp. 1741-1746). IEEE.

[29] Zhou, Shiying, Minghui Zheng, Fu Zhang, and Masayoshi Tomizuka. "Synthesized disturbance observer for vehicle lateral disturbance rejection." In 2018 Annual American Control Conference (ACC), pp. 398-403. IEEE, 2018.

[30] Boada, B.L., Garcia-Pozuelo, D., Boada, M.J.L. and Diaz, V., 2016. A constrained dual Kalman filter based on pdf truncation for estimation of vehicle parameters and road bank angle: Analysis and experimental validation. IEEE Transactions on Intelligent Transportation Systems, 18(4), pp.1006-1016.

[31] Fnadi, M., Plumet, F. and Amar, F.B., 2019, July. Road bank and road grade angles estimation for a double steering off-road mobile robot. In IFToMM World Congress on Mechanism and Machine Science (pp. 1771-1780). Springer, Cham.

[32] Kim, J., Lee, H. and Choi, S., 2012. A robust road bank angle estimation based on a proportional–integral H∞ filter. Proceedings of the Institution of Mechanical Engineers, Part D: Journal of automobile engineering, 226(6), pp.779-794.

[33] Rubin, D., Gutman, P.O., Oshman, Y. and Jodorkovsky, M., 2016, July. State and disturbance estimation for a road vehicle via IMM filtering. In 2016 American Control Conference (ACC) (pp. 2403-2408). IEEE.

[34] Khasawneh, L. and Das, M., 2021, May. Modeling, Parameter Identification, and Steering Angle Control of Electric Power Steering for Trajectory Following in Autonomous Vehicles. In 2021 IEEE International Conference on Electro Information Technology (EIT) (pp. 260-267). IEEE.

[35] Lee, D. and Yi, K., 2017, May. Disturbance adaptive steering wheel torque control for enhanced path tracking of autonomous vehicles. In 2017 American Control Conference (ACC) (pp. 2321-2326). IEEE.

[36] Sun, Z., Zheng, J., Man, Z., Wang, H. and Lu, R., 2018. Sliding mode-based active disturbance rejection control for vehicle steer-by-wire systems. IET Cyber-Physical Systems: Theory & Applications, 3(1), pp.1-10.

[37] Yu, J.Y., Kim, W., Son, Y.S. and Chung, C.C., 2015. Sliding mode control for an electric power steering system in an autonomous lane keeping system. Journal of Institute of Control, Robotics and Systems, 21(2), pp.95-101.

[38] Chen, T., Cai, Y., Chen, L., Xu, X. and Sun, X., 2021. Trajectory tracking control of steer-by-wire autonomous ground vehicle considering the complete failure of vehicle steering motor. Simulation Modelling Practice and Theory, 109, p.102235.

[39] Deng, B., Shao, K. and Zhao, H., 2020. Adaptive second order recursive terminal sliding mode control for a four-wheel independent steer-by-wire system. IEEE Access, 8, pp.75936-75945.

[40] Nam, H., Choi, W. and Ahn, C., 2019. Model predictive control for evasive steering of an autonomous vehicle. International journal of automotive technology, 20(5), pp.1033-1042.

[41] Kim, W., Son, Y.S. and Chung, C.C., 2015. Torque-overlay-based robust steering wheel angle control of electrical power steering for a lane-keeping system of automated vehicles. IEEE Transactions on Vehicular Technology, 65(6), pp.4379-4392.

[42] Yih, P. and Gerdes, J.C., 2005. Modification of vehicle handling characteristics via steer-by-wire. IEEE transactions on control systems technology, 13(6), pp.965-976.

[43] Jeong, Y.W., Kim, J.S., Kang, C.M. and Chung, C.C., 2017, September. Backstepping control design for the second-order electric power steering system using augmented observer. In 2017 56th Annual Conference of the Society of Instrument and Control Engineers of Japan (SICE) (pp. 79-84). IEEE.

[44] Xiong, L., Jiang, Y. and Fu, Z., 2018. Steering angle control of autonomous vehicles based on active disturbance rejection control. IFAC-PapersOnLine, 51(31), pp.796-800.

[45] Han, J., 2009. From PID to active disturbance rejection control. IEEE transactions on Industrial Electronics, 56(3), pp.900-906.

[46] He, Z., Nie, L., Yin, Z. and Huang, S., 2020. A two-layer controller for lateral path tracking control of autonomous vehicles. Sensors, 20(13), p.3689.

[47] Cetin, A.E., Adli, M.A., Barkana, D.E. and Kucuk, H., 2012. Adaptive on-line parameter identification of a steer-by-wire system. Mechatronics, 22(2), pp.152-166.

[48] Leng, B., Jiang, Y., Yu, Y., Xiong, L. and Yu, Z., 2021. Distributed drive electric autonomous vehicle steering angle control based on active disturbance rejection control. Proceedings of the Institution of Mechanical Engineers, Part D: Journal of Automobile Engineering, 235(1), pp.128-142.

[49] Noor Hafizah Amer, Hairi Zamzuri, Khisbullah Hudha, Zulkiffli Abdul Kadir, " Modelling and Control Strategies in Path Tracking Control for Autonomous Ground Vehicles: A Review of State of the Art and Challenges", J Intell Robot Syst (2017) 86:225–254, Springer, DOI 10.1007/s10846-016-0442-0.

[50] T. Zhang, J. Xue, X. Jiao and Z. Wang, "Adaptive Finite Time Trajectory Tracking Control of Autonomous Vehicles," 2020 4th CAA International Conference on Vehicular Control and Intelligence (CVCI), 2020, pp. 684-688, doi: 10.1109/CVCI51460.2020.9338572.

[51] Salim Chaib, Mariana S. Netto, Said Mammar, " H_∞ , Adaptive, PID and fuzzy control: a comparison of controllers for vehicle lane keeping" June 14-17,2004.

[52] J. J. Rath, C. Sentouh and J. Popieul, "A Lane Keeping Assist Design: Adaptation to Driving Style Based on Aggressiveness," 2019 American Control Conference (ACC), 2019, pp. 5316-5321, doi: 10.23919/ACC.2019.8814323.

[53] Khatib, E.I.A., Al-Masri, W.M.F., Mukhopadhyay, S., Jaradat, M.A., Abdel-Hafez, M.: A comparison of adaptive trajectory tracking controllers for wheeled mobile robots. In: 2015 10th International Symposium on Mechatronics and its Applications (ISMA), 8-10 Dec. 2015, pp. 1–6 (2015).

[54] S. Thrun et al., ''Stanley: The robot that won the DARPA grand challenge,'' J. Field Robot., vol. 23, no. 9, pp. 661–692, Sep. 2006.

[55] G. M. Hoffmann, C. J. Tomlin, M. Montemerlo, and S. Thrun, ''Autonomous automobile trajectory tracking for off-road driving: Controller design, experimental validation and racing,'' in Proc. Amer. Control Conf., Jul. 2007, pp. 2296–2301.

[56] O. Amidi and C. E. Thorpe, ''Integrated mobile robot control,'' Mobile Robots, vol. 1388, pp. 504–524, Mar. 1991.

[57] M.-W. Park, S.-W. Lee, and W.-Y. Han, ''Development of lateral control system for autonomous vehicle based on adaptive pure pursuit algorithm,'' in Proc. 14th Int. Conf. Control, Automat. Syst. (ICCAS), Oct. 2014, pp. 1443–1447.

[58] M. Elbanhawi, M. Simic, and R. Jazar, ''Receding horizon lateral vehicle control for pure pursuit path tracking,'' J. Vib. Control, vol. 24, no. 3, pp. 619–642, Feb. 2018.

[59] Rochan, R.M., Alagammai, A.K., Sujatha, J.: Computer vision based novel steering angle calculation for autonomous vehicles. In: Second IEEE International Conference on Robotic Computing (2018).

[60] Eraqi, H.M., Moustafa, M.N., Honer, J.: End-to-end deep learning for steering autonomous vehicles considering temporal dependencies. In: 31st Conference on Neural Information Processing Systems (NIPS), Machine Learning for Intelligent Transportation Systems Workshop, Long Beach, CA, USA (2017).

[61] C. Hu et al., "MME-EKF-Based Path-Tracking Control of Autonomous Vehicles Considering Input Saturation," in IEEE Transactions on Vehicular Technology, vol. 68, no. 6, pp. 5246-5259, June 2019, doi: 10.1109/TVT.2019.2907696.

[62] H. Guo, D. Cao, H. Chen, Z. Sun, and Y. Hu, ‘‘Model predictive path following control for autonomous cars considering a measurable disturbance: Implementation, testing, and verification,’’ Mech. Syst. Signal Process., vol. 118, pp. 41–60, Mar. 2019.

[63] Q. Cui, R. Ding, B. Zhou, and X. Wu, ‘‘Path-tracking of an autonomous vehicle via model predictive control and nonlinear filtering,’’ Proc. Inst. Mech. Eng. D, J. Automobile Eng., vol. 232, no. 9, pp. 1237–1252, 2017.

[64] J. Ji, A. Khajepour, W. W. Melek, and Y. Huang, ‘‘Path planning and tracking for vehicle collision avoidance based on model predictive control with multiconstraints,’’ IEEE Trans. Ultrason. Eng., vol. 66, no. 2, pp. 952–964, Feb. 2017.

[65] B. Chen, B. Luan and K. Lee, "Design of lane keeping system using adaptive model predictive control," 2014 IEEE International Conference on Automation Science and Engineering (CASE), 2014, pp. 922-926, doi: 10.1109/CoASE.2014.6899436.

[66] Xu, Y.; Tang, W.; Chen, B.; Qiu, L.; Yang, R. A Model Predictive Control with Preview-Follower Theory Algorithm for Trajectory Tracking Control in Autonomous Vehicles. Symmetry 2021, 13, 381. https://doi.org/10.3390/sym13030381.

[67] K. Zhang, Q. Sun and Y. Shi, "Trajectory Tracking Control of Autonomous Ground Vehicles Using Adaptive Learning MPC," in IEEE Transactions on Neural Networks and Learning Systems, doi: 10.1109/TNNLS.2020.3048305.

[68] Hu, J., Xiong, S., Zha, J. et al. Lane Detection and Trajectory Tracking Control of Autonomous Vehicle Based on Model Predictive Control. Int.J Automot. Technol. 21, 285–295 (2020).

[69] Z. Luan, J. Zhang, W. Zhao and C. Wang, "Trajectory Tracking Control of Autonomous Vehicle with Random Network Delay," in IEEE Transactions on Vehicular Technology, vol. 69, no. 8, pp. 8140-8150, Aug. 2020, doi: 10.1109/TVT.2020.2995408.

[70] KIBEOM LEE 1, SEUNGMIN JEON1, HEEGWON KIM2, AND DONGSUK KUM 1, (Member, IEEE), ‘‘Optimal Path Tracking Control of Autonomous Vehicle: Adaptive Full-State Linear Quadratic Gaussian (LQG) Control,” Aug. 2019.

LIST OF PUBLICATIONS

- Khasawneh, Lubna, and M. Das. "Modeling, Parameter Identification, and Steering Angle Control of Electric Power Steering for Trajectory Following in Autonomous Vehicles." In 2021 IEEE International Conference on Electro Information Technology (EIT), pp. 260-267. IEEE, 2021.

- Khasawneh, Lubna, and M. Das. "Lateral Trajectory Tracking Control using Backstepping Method for Autonomous Vehicles." In *2021 IEEE International Midwest Symposium on Circuits and Systems (MWSCAS)*, pp. 1013-1016. IEEE, 2021.
- Khasawneh, L. and Das, M. (2022). Adaptive Steering Angle Controller for Autonomous Vehicles in the Presence of Parameter Uncertainty and Disturbances. *International Journal of Automotive Technology*

- Khasawneh, L. and Das, M. (2022). Real Time Estimation of Road Bank Disturbance and Vehicle Side Slip Angle. *International Journal of Intelligent Transportation Systems Research*